The Thesis Committee for Matthew Craig Reichenbach
Certifies that this is the approved version of the following thesis:

Evaluating Vehicular-Induced Vibrations of Typical Highway Bridges for Energy Harvesting Applications

APPROVED BY
SUPERVISING COMMITTEE:

Supervisor:

Sharon L. Wood

Todd A. Helwig

Evaluating Vehicular-Induced Vibrations of Typical Highway Bridges for Energy Harvesting Applications

by

Matthew Craig Reichenbach, B.S.

Thesis

Presented to the Faculty of the Graduate School of

The University of Texas at Austin

in Partial Fulfillment

of the Requirements

for the Degree of

Master of Science in Engineering

The University of Texas at Austin

May 2012

Dedication

To my family and friends

Acknowledgements

First, I'd like to extend appreciation to the National Institute of Standards and Technology for providing the funding to make this project possible. I would also like to thank my advisors, Dr. Sharon Wood and Dr. Todd Helwig for all of their guidance throughout this project. Dr. Wood was a great resource for technical issues over the course of the research, but more importantly she was a wonderful mentor to me. Dr. Helwig was terrific as my second reader and a wonderful professor.

To my fellow students on the project, Jeremiah Fasl, Vasilis Samaras, and Ali Abu Yosef, I owe you a great deal. You welcomed me to our little research family, and helped me immensely along the way. I could thank you for hundreds of things, but I'm unfortunately limited to one page. Let me sum up by saying that this research and thesis would have been impossible without your guidance, expertise, and friendship. I always felt comfortable asking you questions, whether it be technical or personal in nature. I could not have asked for three better partners.

Additionally, I want to acknowledge Barbara Howard for helping us with trip logistics and supplies purchases and the remainder of the NIST project team, including Eric Dierks, Jason Weaver, Rich Lindenberg, Dr. Dean Niekirk, Dr. Praveen Pasupathy, Dr. Rich Crawford, and Dr. Kris Wood. To Prof. Steve Kurtz, your passion led me to structural engineering so I am forever grateful for that.

I want to thank the students at FSEL for making my two years in Texas more than enjoyable. And finally, I want to thank Raymell Rice for his inspiration and dedication over the last four years.

May 4, 2012

Abstract

Evaluating Vehicular-Induced Vibrations of Typical Highway Bridges for Energy Harvesting Applications

Matthew Craig Reichenbach, M.S.E.

The University of Texas at Austin, 2012

Supervisor: Sharon L. Wood

Highway bridges are vital links in any transportation network. Identifying the possible safety problems in the approximately 600,000 bridges across the U.S. is generally accomplished through labor-intensive, visual inspections. Wireless monitoring technology seeks to improve current practices by supplementing the visual inspections with real-time evaluation of bridges. To be economically feasible, wireless sensor networks should be able to (a) operate independent of the power grid, and (b) achieve a service life of at least ten years. Novel energy harvesting approaches have been investigated to fulfill these two criteria. In particular, the feasibility of a vibration energy harvester as a long-term power source was assessed. The goal of the research was to process measured acceleration data and analyze the vibrational response of typical highway bridges under truck loads. The effects of ambient temperature, truck traffic patterns, and harvester position on the power content of the vibrations were explored, as well as the effects of linear and nonlinear harvesters. This thesis presents the results of evaluating the response of five steel bridges in Texas and Oregon for energy harvesting applications.

Table of Contents

List of Tables

List of Figures

CHAPTER 1
Introduction

1.1 Overview of Project

Highway bridges are vital links in any transportation network, providing the public with routes for daily commutes and businesses with the infrastructure needed to supply goods and services. Maintenance of these structures is a high priority for owners. By preserving the structural integrity of a bridge, the benefits are twofold. First and foremost, public safety is ensured. And secondly, expenditures are minimized because retrofit and/or replacement of deteriorating bridges are a costly investment. For example, the direct cost of replacing the I-35 steel truss bridge in Minneapolis, Minnesota after its collapse in August 2007 was $400 million including demolition of the old bridge, cleanup, and other related activities (Olson, 2008). The impact on displaced commuters and detours was estimated to be an additional $400,000 per day (Minnesota Department of Transportation, 2008).

Identifying possible safety problems in the approximately 600,000 bridges across the United States is generally accomplished through labor-intensive, visual inspections. Although more cost-effective than complete replacement, the funding and time required for inspection are limited resources, especially with so many bridges nearing the end of their service life. The age distribution of bridges in the US (Figure 1.1) reveals that many of the nation's bridges are beyond 50 years in age. The Federal Highway Administration (2010) reports that 146,633 bridges of the 600,000 (24%) are structurally deficient, which means they have been closed or restricted to lighter vehicles because of at least one deteriorating structural component.

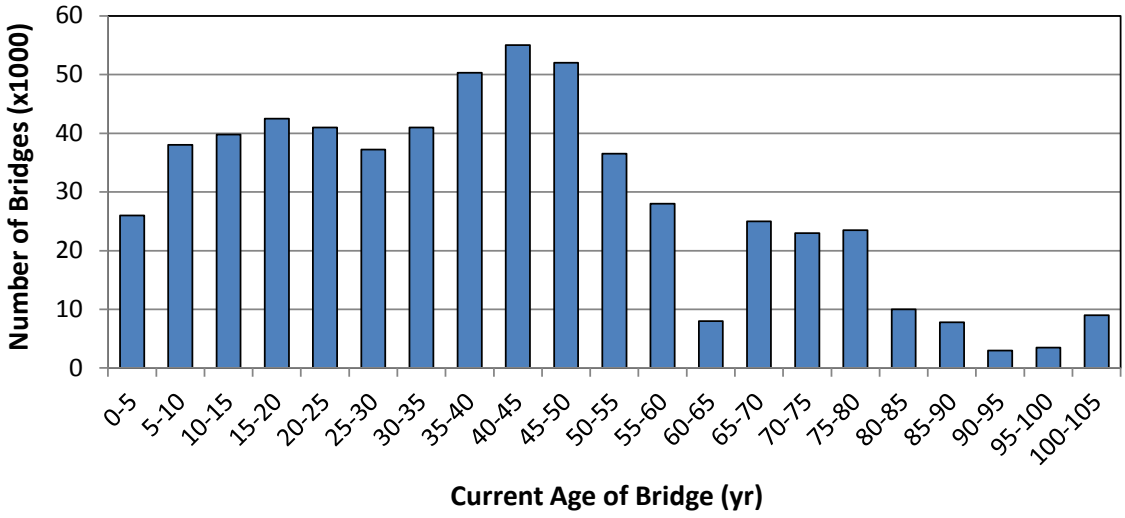

Figure 1.1 Age distribution of bridges in the United States (National Bridge Inventory, 2008).

Currently, any highway bridge that spans at least 20 feet is scheduled for visual inspection at least once every two years, regardless of age or condition. Although a quick, visual inspection suffices for newer, undamaged structures, a more detailed inspection is required for others. Fracture-critical bridges, in particular, must be observed thoroughly for growth of existing cracks and location of new ones. Fracture-critical bridges are non-redundant structures that will likely collapse in event that one of its structural components fails. A steel bridge with only two longitudinal I-girders is the most common type of fracture-critical bridges.

For fracture-critical bridge inspections, a crew is mobilized to the site to investigate critical locations of the bridge for defects, namely fatigue cracks in the steel components and corrosion in the concrete components. Traffic is often slowed and redirected during these inspections, as the crew accesses the structural members via a snooper truck as shown by Figure 1.2.

Figure 1.2 Detailed visual inspection of a fracture-critical bridge.

In recent years, bills have been presented in the legislature aimed to increase the frequency of inspection for fracture-critical bridges. Seemingly at their capacity already, state Departments of Transportation (DOTs) would struggle to obtain the resources necessary to achieve an annual inspection calendar for its bridges, especially for larger states with many bridges such as Texas. Real-time monitoring of civil infrastructure, if economically feasible, can provide some relief to DOTs.

Sensor networks have been used in the past by engineers and bridge owners to continually observe the current conditions and performance of bridges. As the name implies, structural health monitoring consists of monitoring the "health" of a structure through field instrumentation. Data acquired from sensors can be used to assess the current status of a bridge. For example, strain gages provide information on stress levels in a bridge cross-section, accelerometers describe the dynamic response to vehicular-induced excitation forces, and crack propagation gages measure the growth of a crack. Data can then be processed and presented in a format that is meaningful to a bridge

owner. The owner, in turn, can make informed decisions about the current performance of the bridge. This process is shown schematically in Figure 1.3.

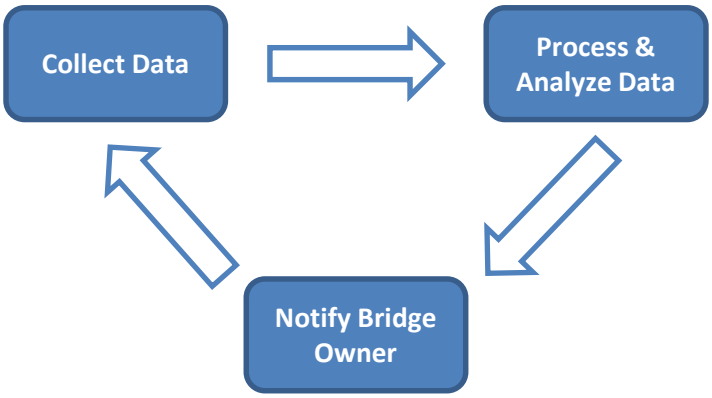

Figure 1.3 Schematic of continuous bridge monitoring and owner interaction.

Wired systems have traditionally been used, in which each sensor is physically connected back to the data acquisition system. In larger civil structures such as long-span bridges, this is a major issue. The direct costs or installing and maintaining potentially thousands of feet of wire are high. If a wireless system is utilized, the instrumentation can be done quickly and with reduced costs.

The goal of the research outlined in this thesis is the development of a rugged, low-power wireless sensor network for long-term monitoring. A wireless sensor network is a system that may include up to five-tiers, including sensors, nodes, routers, gateways, and remote access. A schematic of a WSN configuration is shown in Figure 1.4. WSN nodes collect raw data from sensors (strain gage, thermocouple, etc.), process the data, and then transmit the data along the length of the bridge. Router nodes can be configured to receive data from nearby nodes and pass the data on to the gateway(s), creating a more efficient and reliable transmission mesh. A programmable gateway receives the data and performs additional processing. Data processing at this level serves two purposes. First, streaming continuous, raw data across the wireless network significantly increases the power demand of the system. And second, the owner is generally only concerned with

processed results. Once information is gathered at the gateway, an owner can then securely access the real-time results at a remote desktop.

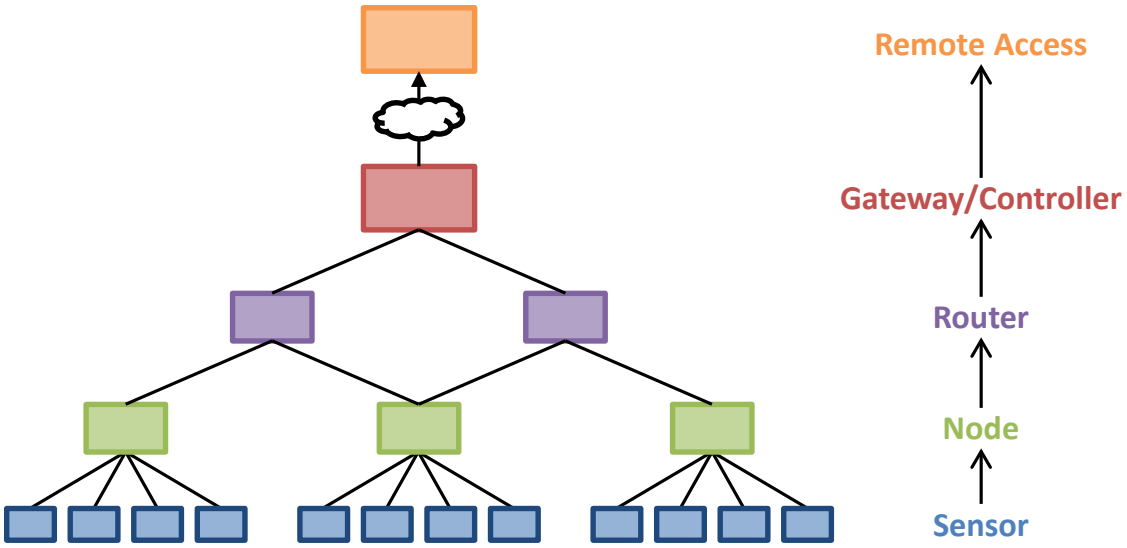

Figure 1.4 Schematic of a wireless sensor network configuration.

1.1.1 Project Description

In 2008, the National Institute of Standards and Technology (NIST) awarded several research projects through the Technology Innovation Program (TIP) to develop infrastructure monitoring and improve inspection practices for civil infrastructure. In particular, NIST-TIP supplied funding to the University of Texas at Austin for a five-year project entitled, “Development of Rapid, Reliable and Economic Methods for Inspection and Monitoring of Highway Bridges.” Fracture-critical, steel bridges were identified as the structure most in need of a wireless monitoring system. The scope of the project has been limited to evaluating fracture-critical bridges; however, the knowledge and information gained from this research is applicable to several types of civil infrastructure.

The project is a multi-discipline, joint venture between the University of Texas at Austin (UT), National Instruments (NI), and Wiss, Janney, Elstner Associates (WJE). Within the University of Texas team, students and faculty within the Departments of Civil, Architectural, and Environmental Engineering, Electrical and Computer

Engineering, and Mechanical Engineering are actively involved. The structural engineering team, based at the Ferguson Structural Engineering Laboratory (FSEL), serves as overall project managers, and is mainly responsible for the instrumentation and data acquisition of bridges, evaluation and analysis of measured response, and reliability testing of sensors. The mechanical engineering team leads the energy harvesting studies of the project. National Instruments (Austin, TX) is developing the wireless systems used for bridge monitoring, and Wiss, Janney, Elstner Associates (Northbrook, IL) is providing expert insight on field instrumentation activities and interactions with potential clients of a real-time, continuous monitoring system.

1.1.2 Advantages of a Wireless System

There are a few limitations to the current practice of biennial, visual inspections. First, accumulation of damage and crack growth is only assessed at discrete points in time. Vital information about the health of a bridge can be lost in the time between inspection cycles. Second, visual inspections are not necessarily comprehensive. There is a high degree of variability in the rating system set by the National Bridge Inspection Program, and cursory inspections are prone to miss problematic locations and/or defects on the bridge (Moore et al., 2001). Lastly, fixed intervals of inspection for all bridges, independent of age or condition, can sometimes be wasteful of resources. Heavily damaged bridges that have been in service for several years should require more attention from the DOT than a newly constructed bridge.

The following are foreseen benefits of an integrated, long-term wireless sensor network. It must be noted that the proposed system is not intended to replace visual inspections, but rather complement them. A bridge owner can receive real-time, quantitative evaluation of the infrastructure. This will permit better allocation of resources because bridges can be prioritized based on current conditions. Accumulation of damage can be detected between inspections, so that maintenance crews can be

mobilized to sites more efficiently. So in general, the owner can manage time and resources better with the aid of a wireless sensor network (Fasl, 2011).

1.2 RESEARCH OBJECTIVES

1.2.1 Motivation for Energy Harvesting

For any given bridge, the direct costs of a wireless sensor network can be higher than the current practice of biennial visual inspections. In order for a wireless sensor network to be economically feasible, the life-cycle costs must be minimized. A ten-year service life of this wireless system is envisioned, which means minimal maintenance of the system for a ten-year period following installation. Therefore, the sensors and wireless hardware must be rugged enough to withstand environmental impacts, reliable enough to provide good data, and be supplied sufficient power to run for ten years.

Using the power grid as a source of energy for the wireless sensor network is often impractical and expensive. As a result, energy harvesting techniques are investigated as potential power sources. Researchers in the Mechanical Engineering Department at UT have explored three alternatives for energy harvesting at a bridge site: solar, wind, and vibration.

Solar panels are a well-studied technology and offer high power densities. If correctly sized, one solar panel can potentially power an entire WSN (nodes, routers, and gateways). However, there are some installation downsides for solar panels on large civil structures. If sensors stretch the entire length of a long-span bridge, cabling from the solar panel to each node is necessary to supply power, thereby defeating the benefit of utilizing wireless technology. Also, mounting a solar panel to a bridge presents certain challenges. Because anchoring to a deck barrier is not always practical, a girder mount will likely be necessary. Providing the required height above the deck to maximize sun exposure can be difficult and is unique for all bridges.

Harvesting wind energy, either ambient or vehicular-induced, provides significantly less power than a solar panel, but is a more localized system. One wind harvester could be connected locally to a close cross frame or stiffener and potentially power one or more wireless nodes in the area. As a result, the length of wire is minimized. However, McEvoy (2011) concluded that power output of a wind harvester is highly dependent on the depth of a bridge girder. Because the blade usually cannot extend below the bottom flange due to traffic underneath the bridge, there are restrictions to the capacity of such a technology.

Vibration energy of a bridge can be harvested from vehicular-induced excitations. Like wind energy harvesting, the power density for vibration harvesters is orders of magnitude less than solar panels. Roundy et al. (2003) concluded that, in normal conditions, the power density of a solar panel is roughly 60 times that of a vibration energy harvester. However, the localized nature of the system is suitable for a bridge environment. Most vibration harvesters described in the literature are small enough to sit on the bottom flange of a bridge girder. The small amount of wire from the harvester to a node is desirable from an installation standpoint. The major disadvantage to harvesting vibration energy is the variability in the dynamic response of bridge components. Some bridges do not vibrate with sufficient amplitude and others do not experience enough daily truck traffic to make vibration energy harvesting a feasible power solution. The focus of this thesis is strictly vibration energy harvesting and characterizing the dynamic response of bridges so that the efficiency of this technology is maximized.

1.2.2 Power Requirement of Wireless Node

National Instruments has expanded the field of wireless monitoring by introducing a wireless sensor network platform to the market in recent years. With the research project focus on lower-power, rugged, and reliable systems, the UT FSEL team adopted the WSN platform for its bridge instrumentation for the NIST project. The development of the wireless strain node, NI WSN-3214, is of particular interest for

structural health monitoring and this research. The power requirements of the programmable WSN-3214 node are the baseline for which all vibration energy studies in this thesis are compared. Figure 1.5 shows the NI programmable wireless node, which is commercially available.

Figure 1.5 NI Wireless Strain Node (WSN-3214) (National Instruments, 2011).

The power requirements of the wireless node are highly dependent on its expected activity. Weaver et. al (2011) examined the power usage of a WSN strain node based on “always on”, “deep sleep”, and “turn off” modes of activity for different sampling rates (Figure 1.6). The long-term average power requirement of the wireless sensor node was estimated as 0.5 mW given normal acquisition procedures. If the node is configured as a router, the power requirements increased to 200 mW. And the gateway, where the transmission of processed data occurs, requires about 5-10 W of power on average.

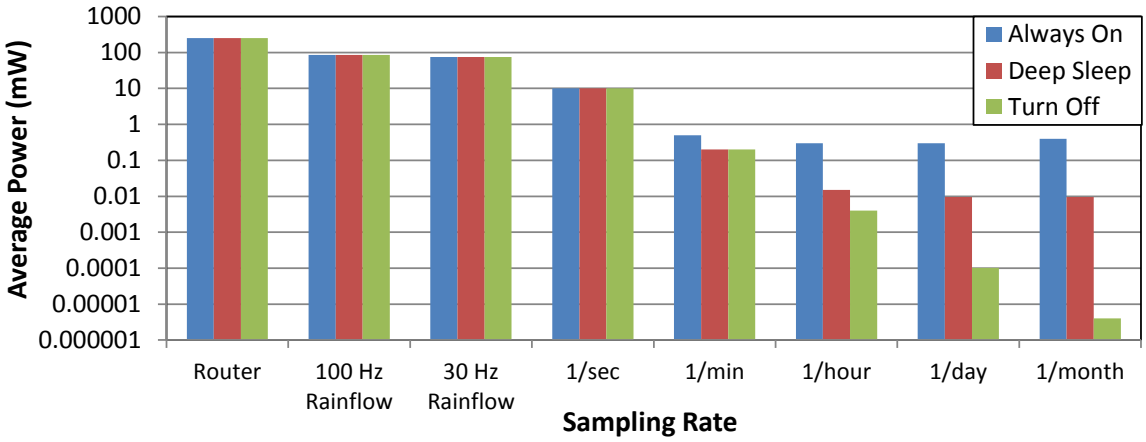

Figure 1.6 Power requirements of a WSN-3214 for different configurations. Adapted from (Weaver, Wood, & Crawford, 2011).

Based on the initial results of the research, traffic-induced vibrations have only enough energy to power a node, not a router or gateway. Consequently, the UT Mechanical Engineering team envisions an energy harvesting system with solar panels powering the gateway and vibration and/or wind harvesters powering the nodes. This is schematically presented in Figure 1.7.

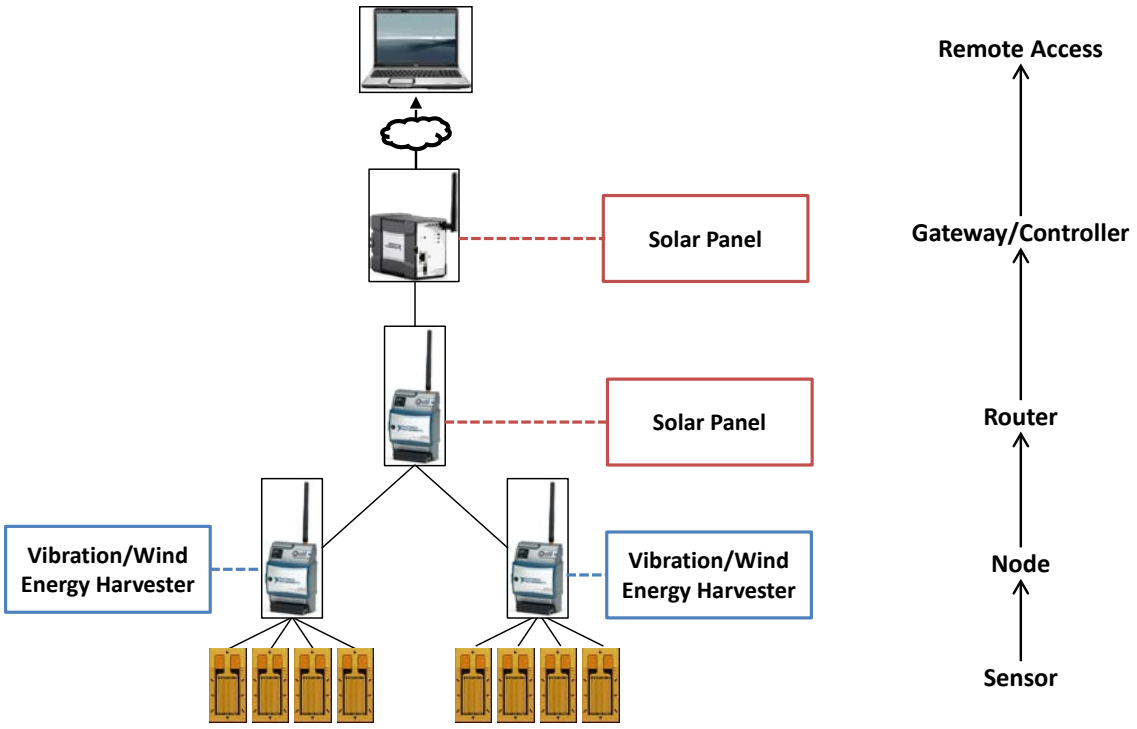

Figure 1.7 Schematic of wireless sensor network with integrated energy harvesting systems. Adapted from (Dierks, 2011).

The root of this thesis is assessing the feasibility of a vibration energy harvester in powering a wireless node. If a harvester achieves a long-term average greater than the required 0.5 mW of power, then the technology is likely feasible. This calculation, however, is not as simple as measuring the vibration energy of a bridge generated during a single truck event. There are several variables that complicate the estimation of long-term power.

1.2.3 Variability of Bridge Response

As suggested, there are several variables that present challenges in assessing the long-term power potential of a vibration energy harvester. Both the frequency content and amplitude of bridge vibrations can change depending on the ambient temperature, truck traffic, boundary conditions, and bridge geometry and configuration. Each of these factors must be quantified in order to estimate long-term harvester production.

Studies have shown that fluctuations in the ambient temperature can, in rare occasions, shift natural frequencies significantly. The truck traffic volume crossing a bridge, which is strongly correlated to time of day, affects the amplitude of bridge vibrations. The conditions of the bridge itself (age, boundary conditions, and flexibility) vary over time as well, and can affect both the modes of vibration and amplitudes. Lastly, mode shapes vary along the length of bridge. Therefore, the modes contributing to the vibrational response vary with location, and spatial effects of the response become important.

These are all characteristics unique to a bridge. Because no two bridges are identical, all variables in the dynamic response must be considered independently. As a result, vibration energy harvesting is not a viable option for all bridges. This thesis investigates these effects on five different bridges, and the feasibility of vibration energy harvesting is addressed.

1.2.4 Implications of Research

The main goal of this research is to assess the feasibility of vibration energy harvesting for bridge structures. Because every bridge has different conditions and every vibration energy harvester has different parameters, a consistent method of comparison was devised. Rather than examine the output energy of the harvester, which is typically done in the literature, the input energy of the source (i.e. the bridge) is evaluated. Obviously, the kinetic energy of a massive structure such as a bridge is enormous. The portion of that energy, however, that is imparted into the harvester is comparatively small. Therefore, the described “input energy” is not that of the global structure, but the energy that enters the localized harvester system.

By only measuring the input, energy losses due to friction and fabrication tolerances within the harvester are not directly considered. Therefore, the estimates described in this thesis are upper-bounds to the energy captured and used to power a wireless sensor node. The analysis herein serves as a benchmark when designing a

vibration energy harvester for a particular bridge. The efficiency of an energy harvester can be evaluated by comparing these analytical results and actual experimental tests of the system.

The major advantage to analysis of the input energy is the ease of computation. Energy input to the harvester can be calculated directly from acceleration data. Note that there are two ways to obtain the traffic-induced dynamic response of the bridge: through field instrumentation and through finite element (FE) modeling. Although field instrumentation was the focus of this research, FE models have shown good agreement to their corresponding field data. Samaras (2012) of the FSEL team, in particular, has modeled two of the bridges examined in this thesis with success. A more in-depth discussion of FE modeling is provided in the "Recommendations" section of Chapter 9.

As far as the field instrumentation approach, accelerometers can be positioned on a bridge at any location. The filtered signals from the sensors can be then analyzed to estimate the power delivered to the energy harvester from the bridge vibrations. This thesis presents the results of processing acceleration data at various bridges to estimate harvested power potential and assess the feasibility of a vehicular-induced vibration energy harvester.

The mechanical engineering team at UT, which is developing its own vibration energy harvesters for bridge applications, benefits from the results of this work. An understanding of the bridge response to truck traffic and which frequencies are excited, allows the optimization of the vibrational energy that can be utilized. Evaluating vibrational patterns and dominant bridge frequencies will aid in the design and implementation of a harvester. Tuning frequencies and system parameters can be optimized on a case-by-case basis to maximize the energy harvested at various types of bridges.

If the bridge vibrations are substantial enough, sensor nodes can continually recharge from the harvested energy, and the proposed real-time monitoring system can operate off the power grid. Thus, life cycle costs are reduced, making the wireless sensor

network economically feasible. State DOTs will be more inclined to implement a wireless monitoring system if the price is reasonable. In summary, processing acceleration data to assess the feasibility of a vibration energy harvester has major implications on the future of wireless monitoring systems.

1.3 ORGANIZATION OF THESIS

This thesis consists of nine chapters, with focus on the development of an analytical model to estimate the energy associated with bridge vibrations. Following this introductory chapter, Chapter 2 provides a review of vibration energy harvesting in the literature. A discussion on different types of vibration energy harvesters and conversion techniques is presented as well as an overview of the vibration harvester design from the Mechanical Engineering team at the University of Texas.

Chapter 3 summarizes the five different bridges that were instrumented and analyzed during the two-year study. The respective accelerometer instrumentation plans and data acquisition systems are described. A discussion of accelerometer sensitivity with regards to low-amplitude and low-frequency signals is also included.

Chapter 4 introduces the basics for spectral analysis, mainly Fourier transforms, and how they apply to ambient vibration sources such as bridges. Additionally, spectrogram analysis is presented, and the distinction between free and forced vibration is made. And lastly, the limitations of spectral analysis with regards to energy harvesting are evaluated.

In Chapter 5, the devised analytical model that estimates harvester input energy from acceleration data is explained. The model, which is based on the Newmark-Beta Method for numerical integration, is applicable for linear and nonlinear systems. The differences between the two approaches are identified. And the derivation of power response spectra, which are the basis of all analysis in this thesis, is detailed.

Chapter 6 presents the variables that affect the long-term dynamic behavior of a bridge. These variables (temperature, truck traffic volume, bridge configuration and

stiffness, and spatial effects) were introduced in Chapter 1, but are further explained and quantified in this chapter. The effects of frequency shifts and amplitude changes on long-term power potential of a harvester are detailed. Literature related to these effects is also summarized and verified with the results of this study.

While Chapter 6 focuses on the variables at the global bridge level, Chapter 7 describes the variables at the local harvester level that affect long-term harvester production. Damping (mechanical and electrical) and spring nonlinearity are the two key parameters examined. There is an abundance of literature on the benefits of nonlinear vibration energy harvesting. These sources are reviewed and compared to the results of this study.

Chapter 8 uses components of all the previous chapters to present the major results of this research. Long-term response spectra for all five bridges are developed and compared. From this, generalized conclusions about the feasibility of vibration energy harvesting are made.

A summary of the research conducted is provided in Chapter 9. The implications of the work to the design and optimization of a vibration energy harvester are outlined. Finally, conclusions about the feasibility of vibration energy harvesting at civil structures like bridges and recommendations for future feasibility studies are made.

CHAPTER 2

Review of Vibration Energy Harvesting

In order to understand the scope of the research, a review of the relevant literature is important. This chapter provides an overview of previous work on bridge vibrations and energy harvesting of ambient sources. It must be noted that bridge vibration analyses and energy harvester optimization have typically been considered independently of each other. Little work has been done to unite these two areas of expertise. Therefore, the motivation for the research outlined in this thesis was to evaluate the efficiency of a vibration energy harvester with a strong focus on the vibration source itself (the bridge). The harvester and the energy source are equally important, and considerable attention must be paid to both.

Also, energy conversion methods of typical vibration harvesters are briefly explained. The vibration energy harvester developed by the mechanical engineering team at UT and its key parameters are introduced in this chapter.

2.1 SPECTRAL ANALYSIS OF BRIDGE DATA

Evaluating bridge acceleration data is a well-established practice for engineers. Numerous cases of successful instrumentations and analyses have been documented in the literature. Spectral analysis is performed to examine the frequency content of the vibrations. Many different techniques within the realm of spectral analysis have been proposed to achieve reliable and accurate results. Note that Chapter 4 outlines the basics of spectral analysis in greater detail.

However, many of the past studies have not evaluated the acceleration data with respect to the potential for energy harvesting. Spectral analysis of raw acceleration data has usually been done from a damage detection perspective. In other words, changes in the frequency content of the structure due to the accumulation of damage were tracked over time. As a result, valuable information regarding the feasibility of harvesting

vibration energy at a given location on a bridge is unclear and, more often, unknown. The following are a few examples of such papers.

Alampalli et al. (1995) developed statistical methods to determine the degree of damage in steel bridges based on controlled laboratory experiments and field tests. Doebling et al. (1997) and Zhao et al. (2002) assessed the accuracy of several different spectral analysis techniques in detecting significant structural degradation. Lauzon et al. (2006) evaluated damage detection methods by conducting full scale field tests; cracks were manufactured in the bridge and frequency content was subsequently measured and compared with the undamaged structure. Mazurek et al. (1990) also studied the effects of temperature and truck mass on the frequency content.

Although these research investigations advanced the field of bridge vibration analysis, harvesting those vibrations as an energy source was never the focus. For this research, both the energy source and the harvester are important. Spectral analysis of field data is critical in determining the feasibility of bridge vibration energy harvesting, but some complementary information on the harvester itself is equally important.

2.2 TRAFFIC-INDUCED VIBRATION ENERGY HARVESTING

Vibration energy harvesting is also a well-established technology, especially for mechanical or motor-type applications where amplitudes and frequency are nearly constant. Several manufacturers produce such harvesters. Much of the literature is aimed towards optimizing and improving an existing technology. For example, Roundy et al. (2003) examined energy harvesting in context to high-amplitude and high-frequency mechanical sources. However, most of their focus is on the components of the harvester and parameter optimization, not the source of energy.

Harvesting from ambient sources such as human motions and traffic-induced bridge vibrations is a relatively new area of research. The variable nature of these vibrations poses an extra challenge to harvest the energy efficiently. Yun et al. (2008) is one example of researchers advancing the field. Significant work has been done on

devices powered by the motions of a human. The research from Galchev et al. (2011), Li et al. (2008), and Roundy (2003) had a similar theme, but instead focused on traffic-induced bridge vibrations. They studied low-level bridge vibrations as a power source for wireless sensor nodes like those described in Chapter 1. In all cases, however, little consideration is made to the energy source. Harvester parameters and energy conversion are the emphasis of the work.

Although this research advanced the field of low-amplitude, low-frequency vibration energy harvesting, the source of the energy was never the primary focus. As noted earlier, the energy source and the harvester design are equally important. Optimizing harvester parameters are critical in determining the feasibility of a vibration energy harvester, but so is understanding the source of the energy. It is still extremely important to understand the source and how it can change depending on time of day, truck traffic patterns, and temperature (Chapter 6).

2.3 ENERGY CONVERSION

Although not in direct scope of this thesis, a basic understanding of how an energy harvester can convert mechanical energy from traffic-induced bridge vibrations into useful power for a WSN is important. First and foremost, it should be recognized that the input and output energy are never the same, and that frictional losses must be considered in the design of a harvester. Efficiency is the ratio of input to output energy. The conversion type must also be considered. As laid out by Cottone (2011), there are four major types of mechanical energy conversion: electrostatic/capacitive, magnetostrictive, piezoelectric, and electromagnetic/inductive. Each has different advantages and disadvantages.

Electrostatic/capacitive conversion utilizes a variation in capacitance. This change is caused by an increase in charge or voltage due to the relative motion of the harvester and the bridge on which it sits. Electrostatic conversion produces relatively small power densities in comparison to the other three types. Magnetostrictive conversion uses the

magnetostrictive property of materials and a magnetic field to produce useful power. However, this technology is difficult to integrate into a vibration energy harvesting system and is therefore rarely employed in such an application.

Piezoelectric conversion is the process of converting mechanical strain to electric current or voltage. Many piezoelectric vibration energy harvesters consist of a cantilever beam set to the natural frequency of the source with piezoelectric material at areas of high strain. Electromagnetic conversion, on the other hand, operates using Faraday's Law of Induction. The relative movement between a magnet and a coil produces voltage. Common products such as shake flashlights and commercially-available vibration energy harvesters utilize this technology (Figure 2.1). Inductive-based harvesters are typically well-suited for low-frequency applications because of their impedance characteristics (Dierks, 2011). Much of this information was utilized in the design of the UT Austin vibration energy harvester.

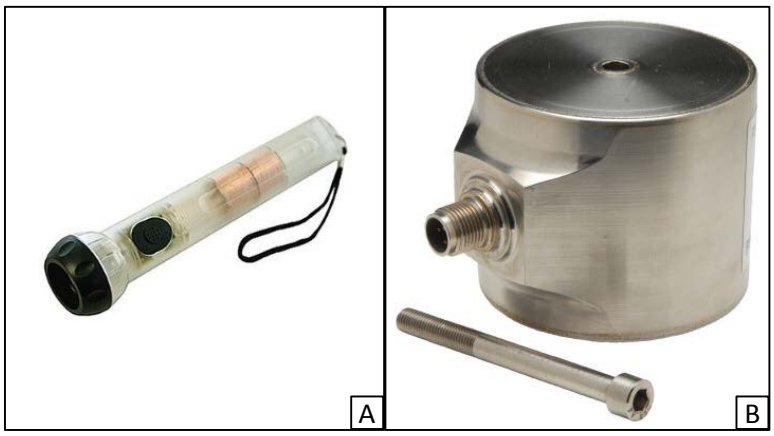

Figure 2.1 (a) Motion-activated Faraday flashlight (Infmetry, 2011); (b) Commercially-available vibration energy harvester (Perpetuum, 2011).

2.4 THE UT AUSTIN HARVESTER

The UT mechanical engineering team in the NIST-TIP project has developed a vibration energy harvester prototype (Figure 2.2). The selection of conversion type and the key parameters were based on the information gathered from the literature

summarized in Sections 2.2 and 2.3 of this chapter. The UT harvester utilizes electromagnetic inductive principles because of its improved performance at low frequencies. The geometry of the harvester, its tuning capabilities, and some of the key parameters are described in the following sections.

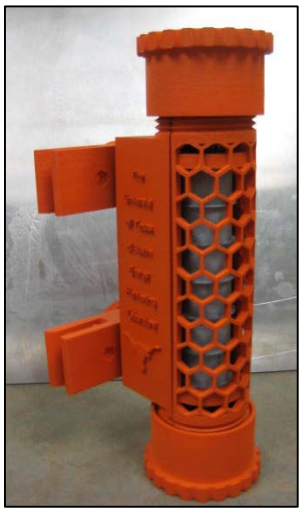

Figure 2.2 The UT Austin electromagnetic vibration energy harvester.

2.4.1 Geometry of UT Harvester

Figure 2.3 presents a general schematic of the harvester. Fundamentally, a magnet is attached to a shaft, which vibrates relative to the housing due to the traffic-induced motions of the instrumented bridge. The moving magnet has a mass and is damped by a spring of some specified stiffness. Energy from the bridge vibrations are converted to voltage by movement of the mass relative to the coils. These components are encased in a housing that is approximately 12-in tall with a 3-in diameter. Due to the intermittent nature of bridge vibrations, a Li-ion battery is integrated into the system to store energy during low-traffic times. In total, the expected weight of the system is between 10 and 15 lb. Another unique feature of the harvester is its flexible mounting capabilities. Rotating grips were incorporated so that the harvester can be mounted to different structural components such as a web stiffener, a girder flange, and/or a cross-frame depending on

the location of the sensors and the bridge type. Figure 2.4 shows the possible clamping mechanisms of the harvester schematically.

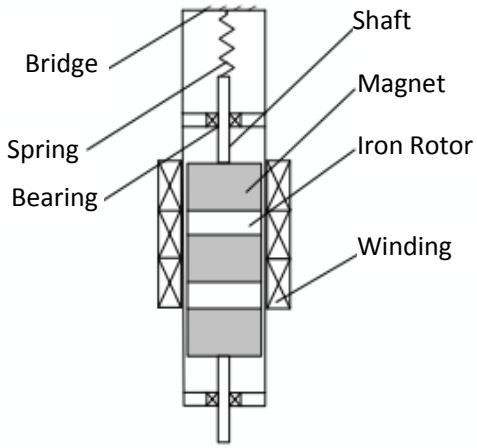

Figure 2.3 Schematic of an electromagnetic vibration energy harvester. Adapted from (Dierks, 2011).

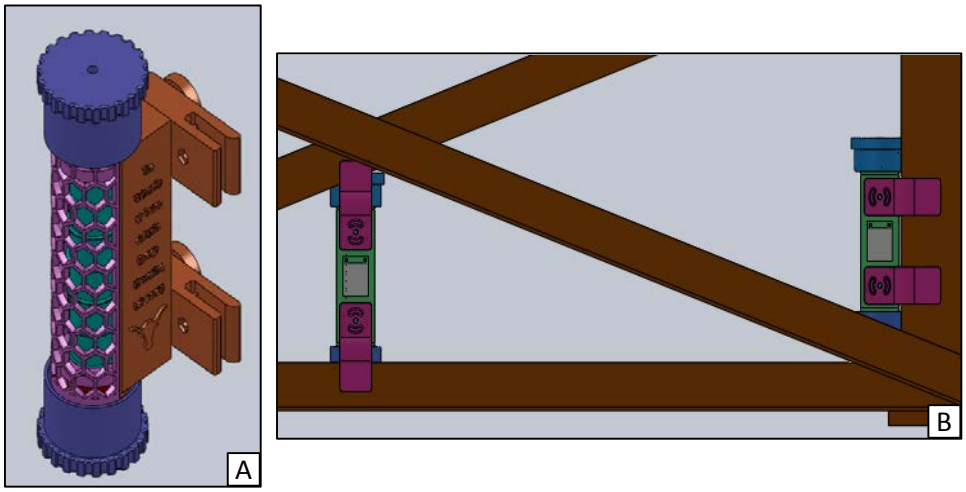

Figure 2.4 (a) Adjustable grips on the UT harvester; (b) Clamping configurations on a typical highway bridge (Dierks, 2011).

2.4.2 Tuning Capabilities of UT Harvester

The harvester is assumed to have a single fundamental frequency because it has one degree-of-freedom (vertical translation). The moving mass is attached to a spring, which has some specified stiffness. Equation 2.1 describes the relationship between fundamental frequency of the harvester (f_h in Hz), spring stiffness (k_s), and mass (m).

$$f_h = \frac{1}{2\pi}\sqrt{k_s/m} \qquad \textbf{Equation 2.1}$$

As will be discussed in subsequent chapters, the fundamental frequency of the harvester should closely match with the dominant frequencies of the vibration source (the bridge). Because every bridge has a different frequency signature, the natural frequency of the harvester should be adjustable. Based on Equation 2-1, this can be achieved by changing the mass or the stiffness of the spring. Because the moving magnet that serves as the mass is encased in the outer shell of the harvester, it is more appropriate to adjust the spring stiffness externally. Dierks (2011) has fabricated the harvester such that the spring can be stiffened or softened externally by twisting the end cap. This allows for easy adjustments to the harvester. Altering the frequency can also be done electrically. But the ease of operation for the mechanical system influenced this particular design. Also note that the spring stiffness is not necessarily linear. Discussion of the relative advantages of linear and nonlinear springs is provided in Chapter 7.

2.4.3 Key Parameters of UT Harvester

Aside from the stiffness of the system, mass and damping are the other two parameters that govern the response of the harvester. Unlike spring stiffness, the mass and damping are not easily adjusted after fabrication. The moving mass not only affects the natural frequency of the system (Equation 2-1), but also affects the power generated. The effect of mass on power output are discussed in depth in Chapter 5. All calculations throughout the thesis are presented for a unit mass (power density). In other words, the actual mass of the energy harvester is not considered in the analysis.

Damping can be classified as mechanical or electrical, and total damping is then the sum of the mechanical and electrical components (Equation 2.2).

$$\zeta_{mech} + \zeta_{elec} = \zeta_{total} \qquad \textbf{Equation 2.2}$$

Mechanical damping is related to frictional losses within the system. Frictional losses do not contribute to the total power output and are lost as heat, which lowers the efficiency of the harvester. Figure 2.3 shows that the shaft moves through a bearing. Frictional resistance must be minimized along the bearing surfaces to minimize mechanical damping. Electrical damping, on the other hand, is the relationship between the source impedance and the output impedance of a system, and is directly related to the power output of the system (Section 5.4).

Parametric studies were conducted by Dierks (2011) in the design of the UT electromagnetic harvester to optimize these values. Table 2.1 presents the results of the parametric study and the chosen values for the working prototype. Note that the mass was selected as 1.454 kg due to size constraints within the housing. And the mechanical damping was approximated by conducting frictional loss experimental studies. The parameters in Table 2.1 were used in all analyses presented in this thesis. A discussion is of the impact of damping and spring nonlinearity on the power potential of a vibration energy harvester is provided in Chapter 7.

Table 2.1 Key parameters of the UT Austin electromagnetic vibration energy harvester.

Parameter	Value	Unit
Mass	1.454	kg
Frequency	Adjustable	Hz
Mechanical Damping	0.044	-
Electrical Damping	0.0546	-
Total Damping	0.0986	-

2.5 CHAPTER SUMMARY

In this chapter, relevant literature was discussed in context to this research. It was discovered that the bridge vibration analysis and energy harvesting fields of research have yet to be fully united. Significant progress has been made in both areas, but the research has not been fully integrated. The purpose of this research is to emphasize the importance of both fields as well as tie them together. Design of the harvester and the characterization of the energy source are equally important, and this thesis addresses both.

In addition to the literature review, the four main types of energy conversion for vibration energy harvesting were examined. The UT Austin electromagnetic harvester was also introduced, and the key parameters were described. Chapter 3 provides a detailed description of all the bridges instrumented and analyzed during the two-year study.

CHAPTER 3
Field Instrumentation and Data Acquisition

Five steel bridges in Texas and Oregon were identified for monitoring vehicular-induced dynamic behavior. Of the three Texas bridges, two are located in Austin and one near San Antonio. Both Oregon bridges are located near Portland. The five bridges studied encompass a wide range of highway bridges with respect to age, type, and traffic patterns. The bridge superstructures that were monitored consisted of trapezoidal box girders, I-girders (both rolled sections and welded plate girders), and a multi-span truss which are typical for highway bridges and interchanges. One of the I-shaped bridges was comprised of a riveted, plate-girder bridge near the end of its design life. The geometry and instrumentation of these bridges is explained in this chapter. In addition, discussions of the data acquisition system and the selection of sensors at the sites are provided.

3.1 I-35N Bridge over Medina River in San Antonio, TX

The I-35N Bridge over the Medina River (Figure 3.1) is located on the southwestern edge of the San Antonio city limits near Von Ormy, Texas (Figure 3.2). It is a twin girder bridge that is classified as fracture-critical because, if the tension flange of one girder fractured, the bridge would likely collapse.

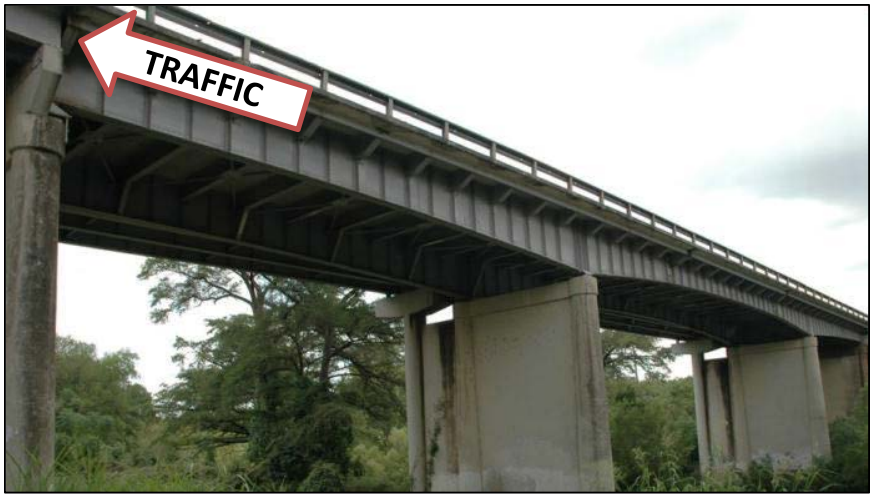

Figure 3.1 Three middle spans at I-35N Bridge over Medina River.

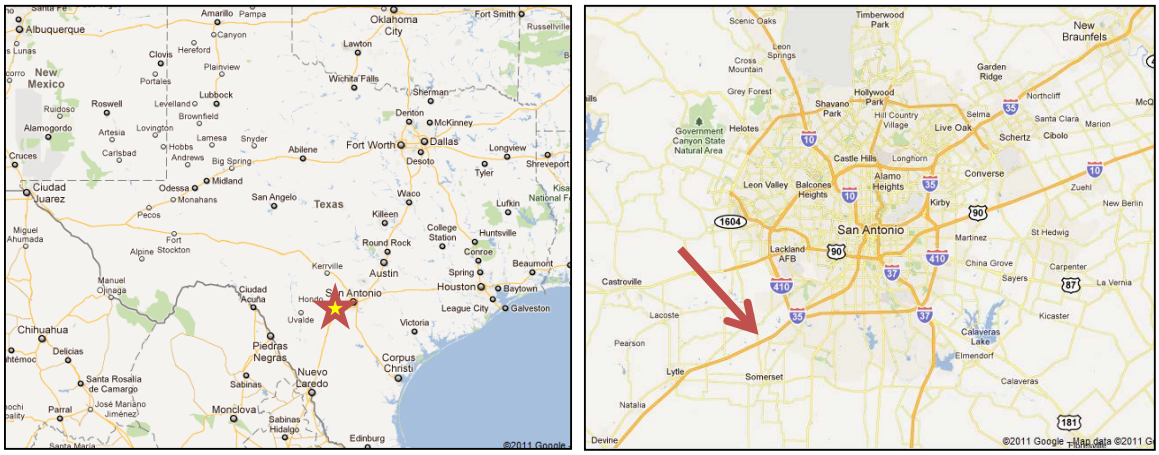

Figure 3.2 Location map of Medina River Bridge (Google Maps, 2011).

The Medina River Bridge was constructed in 1935. It initially served one lane of northbound traffic and one lane of southbound traffic. In 1974, the bridge was widened by welding cantilever brackets to the outside of the twin girders. Lane widths increased from 12 ft to 14 ft. Note that a separate structure was later constructed adjacent to the original bridge to serve as an additional third lane of traffic. The separate bridge is a plate-girder system, and is independent of the fracture-critical portion. A longitudinal gap was left between the concrete decks so that no interaction between the separate bridges exists (Figure 3.3). The additional right-lane structure was not considered in the

instrumentation, and, as a result, will not be discussed further in this thesis. As of 2005, average daily truck traffic was 4,000. An aerial view of the bridge is presented in Figure 3.4.

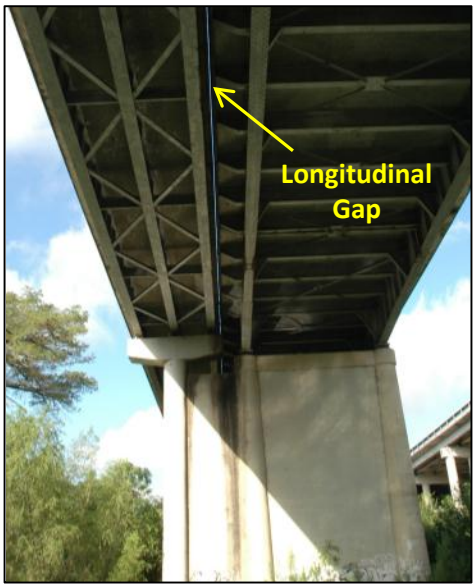

Figure 3.3 Longitudinal gap between original bridge (right) and plate girder bridge constructed in 1971 (left).

Figure 3.4 Aerial view of Medina River Bridge showing direction of traffic (Google Maps, 2011).

3.1.1 Geometry of Medina River Bridge

The Medina River Bridge has eleven spans and is 665 ft in total length. The four north spans are 50-ft long, and the four south spans are 48-ft long. Each span is simply-supported by eight I-girders. Therefore, the approach spans are not considered to be fracture-critical. Tests and monitoring were only conducted on only the three spans in the middle of the bridge.

The overall length of the three middle spans is 273 feet. The two longitudinal girders (east and west) are nominally identical, and the geometry of the spans is symmetric about the midpoint. Therefore, the north half is the mirror image of the south half. The three interior spans consist of two anchor spans (north and south), which are 73′-6″ long, and a 125-ft center span. The center span then consists of two identical overhang sections (30′-7″) and a suspended section (63′-10″). A pin and hanger assembly connects the suspended and overhang sections (Figure 3.5a). As a result, there is a deck discontinuity directly above that location (Figure 3.5b). A dimensioned elevation view of the Medina River Bridge is provided in Figure 3.6.

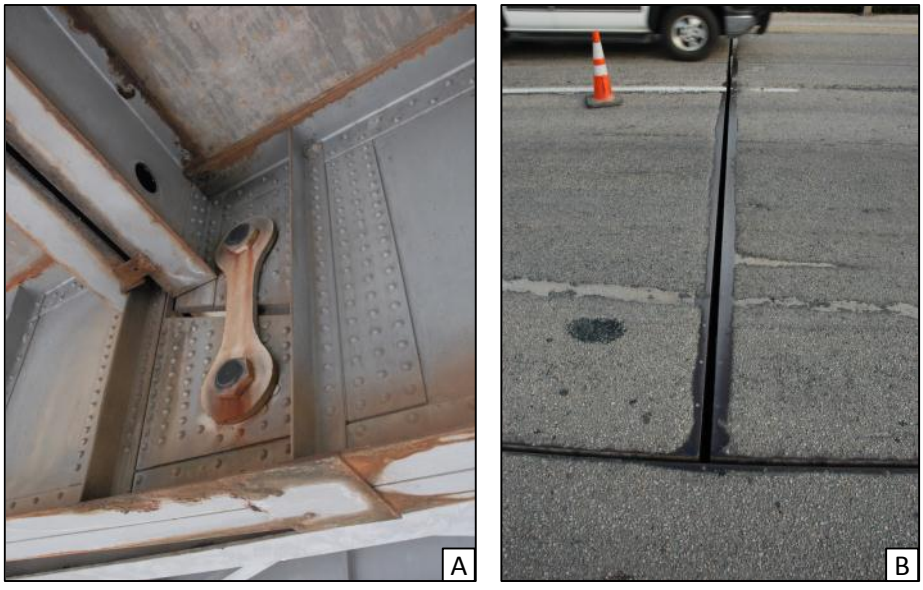

Figure 3.5 (a) Hanger detail at Medina River Bridge; (b) Road surface joint at hanger.

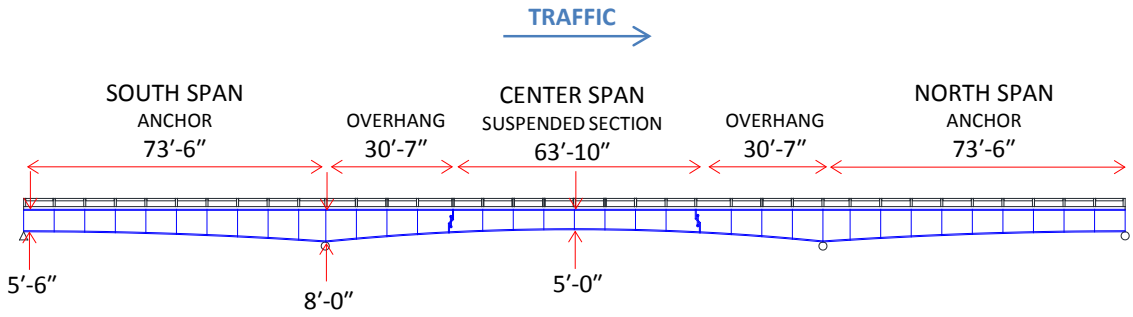

Figure 3.6 Elevation view of the Medina River Bridge.

Floor beams transfer traffic loads from the deck to the longitudinal girders and are spaced every 7′-6″ on center. Rolled W27x91 sections were used for the floor beams. In total, there are 39 floor beams in the three middle spans. The two longitudinal girders vary in depth along the length of the bridge and are spaced 23-ft apart center-to-center. The maximum depth (8 ft) occurs in the negative moment region over the interior supports, and the minimum (5 ft) occurs at midspan of the suspended section. This is also demonstrated in Figure 3.6. Rivets were used to fabricate the plate girders. As a result, the girder flanges consist of two angles riveted to the top and bottom of the web plate. Cover plates were fastened to the angle flanges over the interior supports and at the center of the suspended section to increase the moment capacity, but there is still an inherent flexibility with the design.

An X-shaped lateral bracing system that was composed of 3″x3″x5/16″ angles was used to improve the lateral stiffness of the twin girder bridge. Because of the high slenderness of the angles, the truss will behave as a “tension-only” system in which the slender compression diagonal is conservatively neglected. Figure 3.7 shows the lateral bracing system from underneath the bridge, and Figure 3.8 shows the typical intersection between a lateral brace, a floor beam, and a longitudinal girder. A dimensioned plan view of the bridge showing the lateral bracing system and the location of floor beams is shown on Figure 3.9. Note that the floor beam numbering system (1 to 39) is also presented on

the plan view. These numbers are used throughout this thesis to describe instrumentation locations.

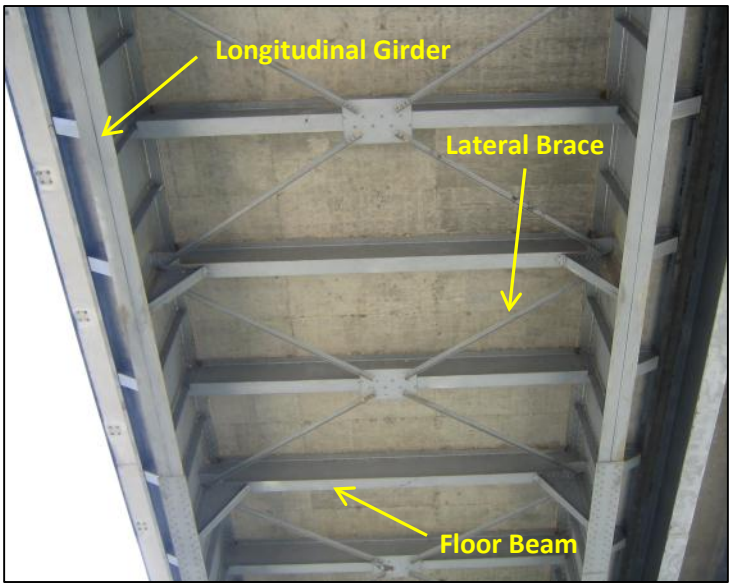

Figure 3.7 View of lateral bracing system at the Medina River Bridge from below.

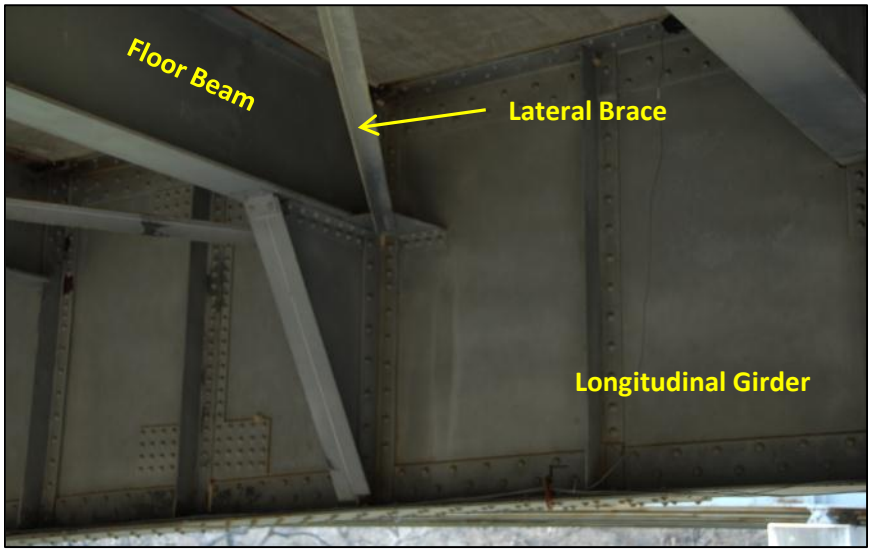

Figure 3.8 Close-up view of lateral brace and floor beam framing into a longitudinal girder at the Medina River Bridge.

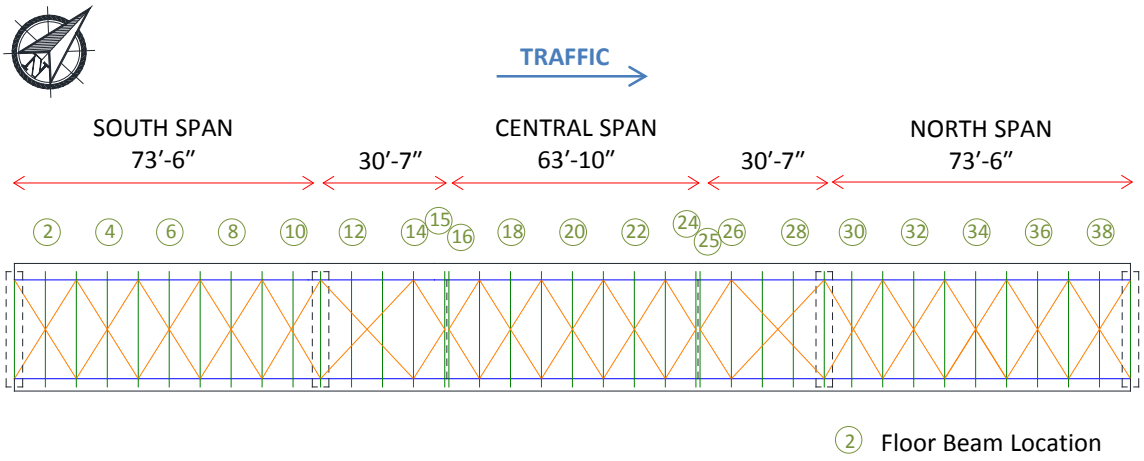

Figure 3.9 Dimensioned plan view of the Medina River Bridge showing the floor beam numbering system.

A cross-section view of the Medina River Bridge is presented in Figure 3.10. Note that this drawing is consistent with the current state of the bridge. The cantilever brackets that were welded to the existing floor beams in 1974 are shown. However, the independent plate-girder structure to the right of the east girder is not shown.

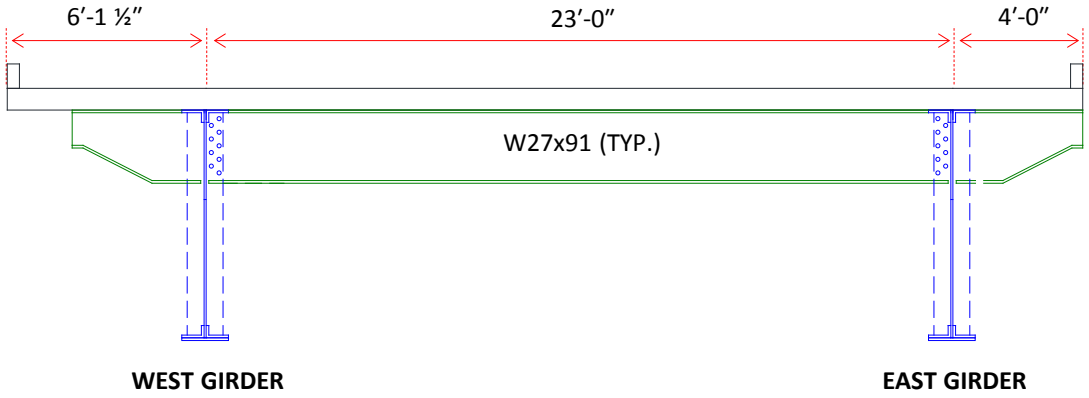

Figure 3.10 Typical cross-section at the Medina River Bridge.

Because it is nearing the end of its service life and it is fracture-critical, the Medina River Bridge is an ideal candidate for continuous monitoring to supplement visual inspections. As a result, a significant amount of acceleration data at many different

locations along the length was recorded to understand the response of the bridge. As is presented in Chapter 8, vibrational amplitudes were considerably higher than those measured at the other four bridges monitored as part of this investigation. This may be explained by the inherent flexibility of discontinuous flanges as well as deterioration of an aging bridge.

3.1.2 Instrumentation Plan of Medina River Bridge

Instrumentation of the Medina River Bridge was the most extensive of the five bridges studied. A dense array of sensors is necessary to quantify spatial effects of bridge vibrations (i.e. amplitude and frequency changes along the length of a bridge). The team used only six, ±2g accelerometers to measure the dynamic response of the bridge. Therefore, in order to achieve a high sensor density, several trips to the bridge were made to reposition accelerometers. The locations of the accelerometers were moved frequently throughout the investigation.

During the months of October 2010, March 2011, April 2011, July 2011, and December 2011, the team used accelerometers to measure the response of the Medina River Bridge. With data collected at different times of the year, temperature effects on the bridge stiffness can also be evaluated. In total, data were captured at 28 different locations along the length of the bridge. At each location, data was measured continuously for at least one week.

Every accelerometer was positioned either on the bottom flange of a girder at a location where the floor beam was attached or on a lateral brace. When sensors were attached to the lateral brace, a 13-lb steel plate was clamped underneath the accelerometer to investigate the influence of the additional mass of an energy harvester on the frequency content and amplitude. Figure 3.11 shows an example of typical configurations. Figure 3.12 provides an additional view of the accelerometer locations for a typical cross-section of the bridge.

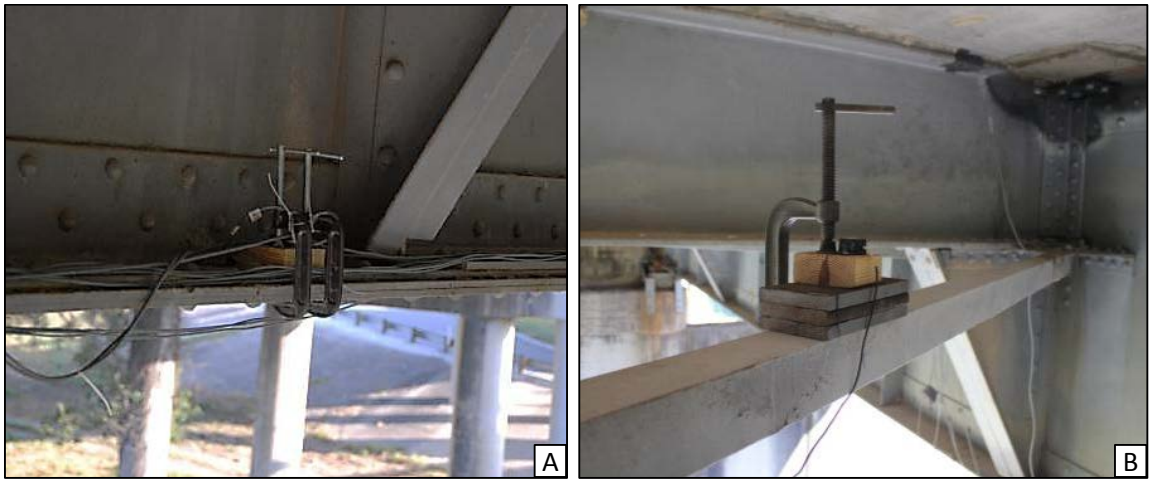

Figure 3.11 C-clamps were used to attached the accelerometers to the Medina River bridge at (a) the bottom flange of a longitudinal girder and (b) midspan of a lateral brace (13 lb of steel plates are also shown).

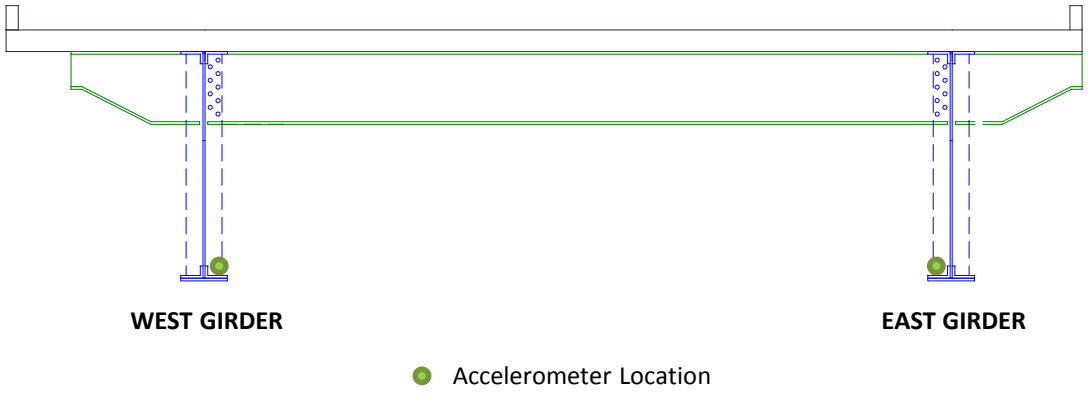

Figure 3.12 Cross-section view of the Medina River Bridge showing typical accelerometer locations on the bottom flanges of the longitudinal girders (brace sensors not shown).

Ground access to the bridge was preferred over a snooper truck so that traffic diversion was avoided. However, instrumentation was limited to the north span and north cantilever section of the central span due to manlift height restrictions. The suspended section was not instrumented due to limited access from the Medina River that the bridge

spans (Figure 3.4). As a result, every floor beam location on the north span and five more locations on the central cantilever-suspended span were instrumented with accelerometers. A detailed summary of this plan, including exact locations and dates, is described in Section 3.7.

3.2 TX-71E Bridge over US-183 in Austin, TX

The TX-71E Bridge over US-183N (Figure 3.13) is located in south Austin near Austin-Bergstrom International Airport (Figure 3.14). The bridge consists of six I-shaped girders and due to the significant redundancy is therefore not considered fracture critical. Despite the NIST research being focused on fracture-critical bridges, evaluation of many different types of steel bridges in the U.S. will aid in assessing the feasibility of a vibration energy harvester.

Figure 3.13 TX-71E Bridge over US-183N.

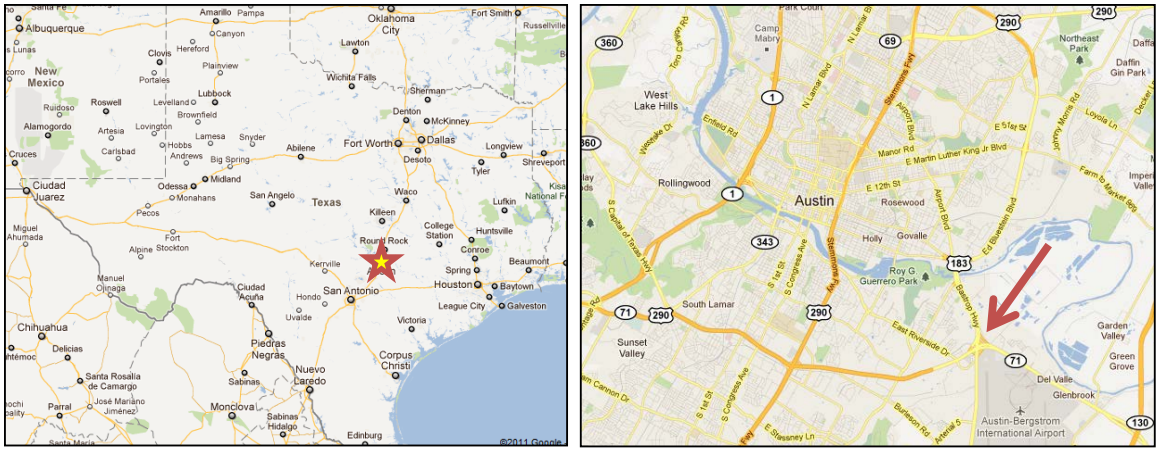

Figure 3.14 Location map of the TX-71E Bridge (Google Maps, 2011).

The TX-71E Bridge was constructed in 1959. It serves three lanes of eastbound traffic. The right lane also functions as an exit ramp at the end of the bridge. Based on observations by the research team, the daily truck traffic at this bridge is significantly less than the Medina River Bridge. Consequently, the degree of truck-induced vibration is less, as is presented in Chapter 8. An aerial view of the bridge is also presented in Figure 3.15.

Figure 3.15 Aerial view of TX-71E Bridge showing direction of traffic (Google Maps, 2011).

3.2.1 Geometry of TX-71E Bridge

The TX-71E Bridge has five continuous spans and is 210 ft long. The westernmost span of the bridge will be referred to as the first span, and the easternmost span as the fifth span. The two end spans and the middle span are 35 ft long. The second and fourth spans have traffic from US-183 underneath. Therefore, those spans are wider (47′-6″ and 57′-6″, respectively). Six identical, longitudinal girders sit on rocker supports over the four interior supports. The girders are rolled W27x102 sections. Cover plates (1/2″ thick) were used on the top and bottom flanges in the negative moment regions over the interior supports and at midspan of the 57′-6″ fourth span. The supports are skewed about 20 degrees from the orientation of the bridge. Figure 3.16 and Figure 3.17 show a dimensioned plan and cross-section view of the TX-71E Bridge.

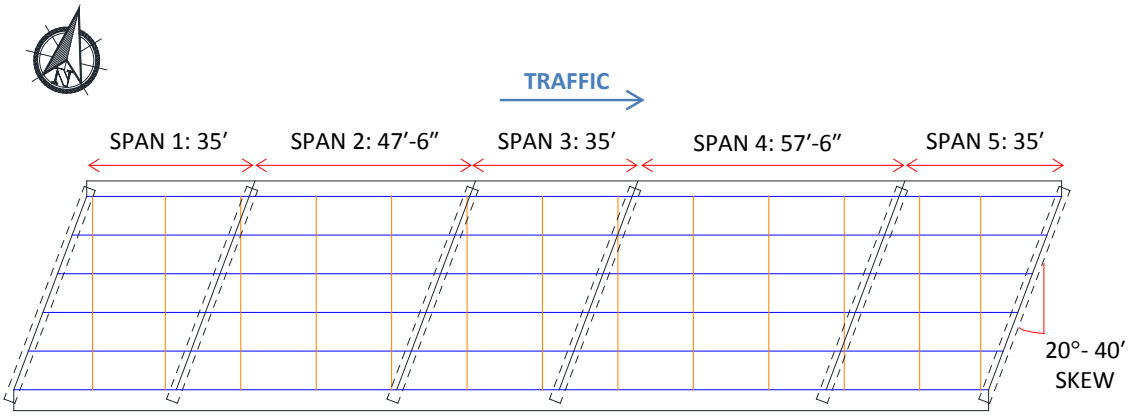

Figure 3.16 Dimensioned plan view of the TX-71E Bridge.

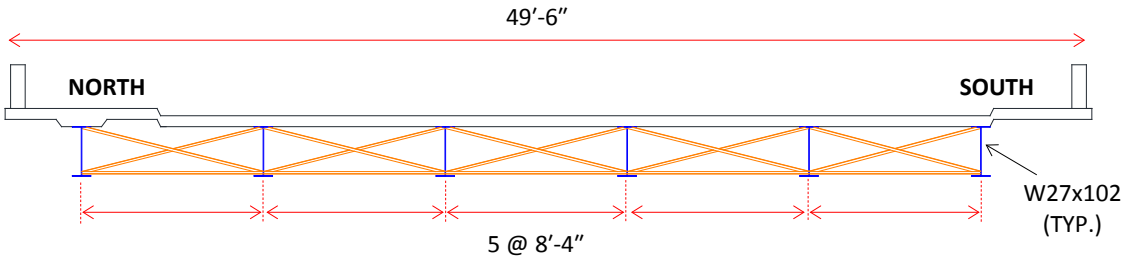

Figure 3.17 Dimensioned cross-section view of the TX-71E Bridge.

Due to the relatively short spans and redundancy of the multi-girder structure, the bridge owner would not likely implement a continuous monitoring system at this site. However, TX-71E is a very common type of highway bridge. Thus, vibrational analysis of this structure provides a lower-bound comparison for more flexible bridges like the Medina River Bridge.

3.2.2 Instrumentation Plan of TX-71E Bridge

Unlike the Medina River Bridge, sensor density was not a major priority for instrumentation of the TX-71E Bridge. Therefore, the scope of the instrumentation plan was much less. The team was mostly concerned with temperature effects and overall vibration amplitudes. As a result, only one span was instrumented. Due to the presence of traffic underneath the two longest spans, instrumentation was limited to the middle span (span 3). Figure 3.18 shows the location of the span designated as span 3. Two accelerometers were attached to the bridge, one at midspan and one near the interior support. The sensors were attached to the bottom flange of the third girder from the north in a similar fashion to the Medina River Bridge setup. Figure 3.19 provides an additional view of accelerometer locations for a typical cross-section of the bridge.

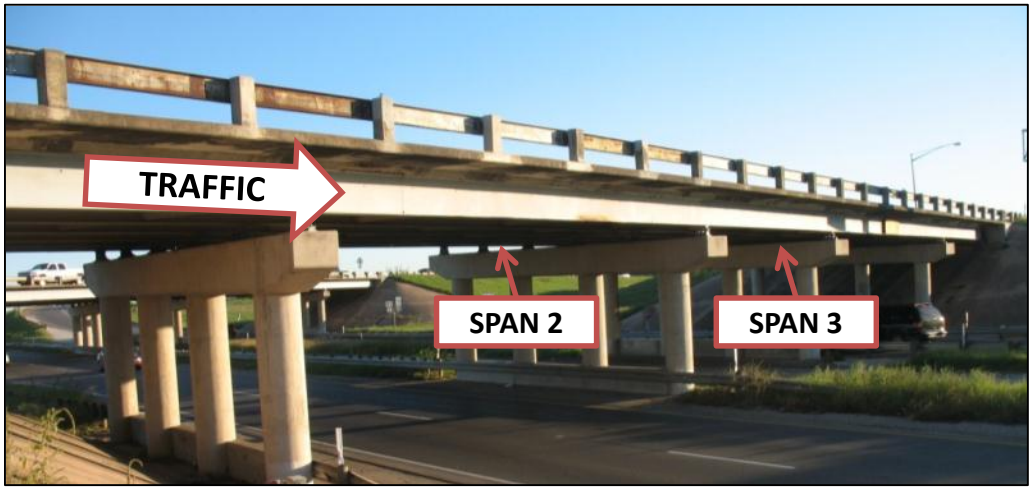

Figure 3.18 TX-71E Bridge showing instrumented spans 2 and 3.

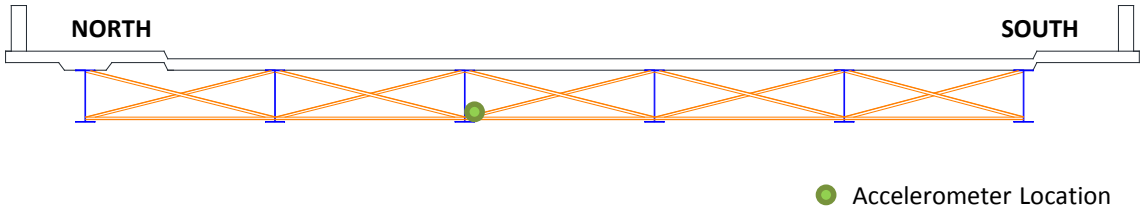

Figure 3.19 Cross-section view of the TX-71E Bridge showing typical accelerometer location on the bottom flange of an interior longitudinal girders.

Instrumentation was completed in March 2010. Nine days of acceleration data were acquired from each accelerometer. A detailed summary of this plan is discussed in Section 3.7.

3.3 I-35N TO US-290E DIRECT CONNECTOR IN AUSTIN, TX

The I-35N to US-290E Direct Connector Bridge (Figure 3.20) is located in Austin, Texas (Figure 3.21). It serves as a one-lane ramp for northbound I-35 traffic traveling onto eastbound US-290. The US-290 Direct Connector is a twin, trapezoidal box girder bridge. Because the bridge has only two girders, the bridge is classified as fracture-critical.

Figure 3.20 I-35N to US-290E Direct Connector Bridge.

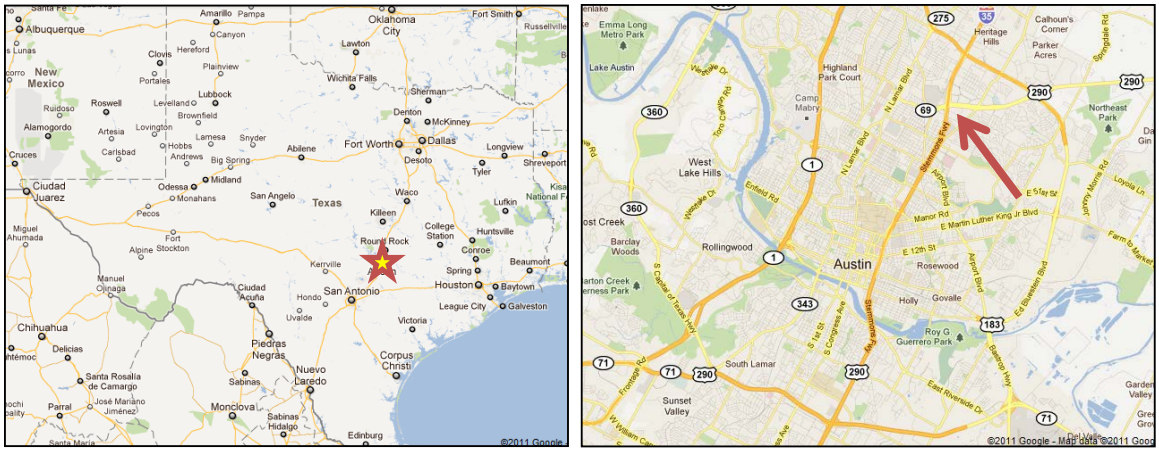

Figure 3.21 Location map of the I-35N to US-290E Direct Connector Bridge (Google Maps, 2011).

The bridge was constructed in 2002. Based on observance during site visits, drivers tend to reduce speed when approaching the connector bridge. Also, truck traffic is less frequent than observed at the Medina River Bridge. Due to the infrequency of large vehicles using the US-290E Connector Bridge, high vibrational amplitudes were not sustained. This behavior is explained in more detail in Chapter 8. An aerial view of the bridge is presented in Figure 3.22.

Figure 3.22 Aerial view of I-35N to US-290E Direct Connector Bridge showing direction of traffic (Google Maps, 2011).

3.3.1 Geometry of US-290 Bridge

The US-290E Connector Bridge has four continuous spans, and the overall length is 880 ft. Two end spans are 210 ft long, and two middle spans are 230 ft long. The bridge is straight for approximately the first 270′ at the south end while the remaining portion of the bridge has a horizontal radius of approximately 610′ (at the centerline of the bridge) and an angle change of roughly 90°.

The twin trapezoidal box girders are 6.5′ deep and are spaced roughly 15.5′ apart on center. The boxes are slightly offset in elevation so that road surface is inclined from horizontal. This provides for an easier turn radius for drivers. The inside of the box girder is open, except at each intermediate support, where steel plate diaphragms with a small access hole are used to provide torsional restraint. The hammerhead piers bear against the bottom flange of the box at these three locations (Figure 3.23). The girders are supported by elastomeric bearings at two outside supports at either end of the bridge and have a steel rocker bearing at the middle support. The rocker bearing is located on a steel box straddle cap. Figure 3.23 shows the first interior support at the south end of the bridge with the straddle cap in the background. The shimmed elastomeric bearings are relatively stiff in the vertical direction and the bearing type was believed to have no measureable effect on the vibrational behavior of the bridge. Figure 3.24 and Figure 3.25 show a dimensioned plan and cross-section view of the US-290 Bridge.

Figure 3.23 Bottom flanges of the longitudinal box girders at the US-290 Bridge bear on the piers.

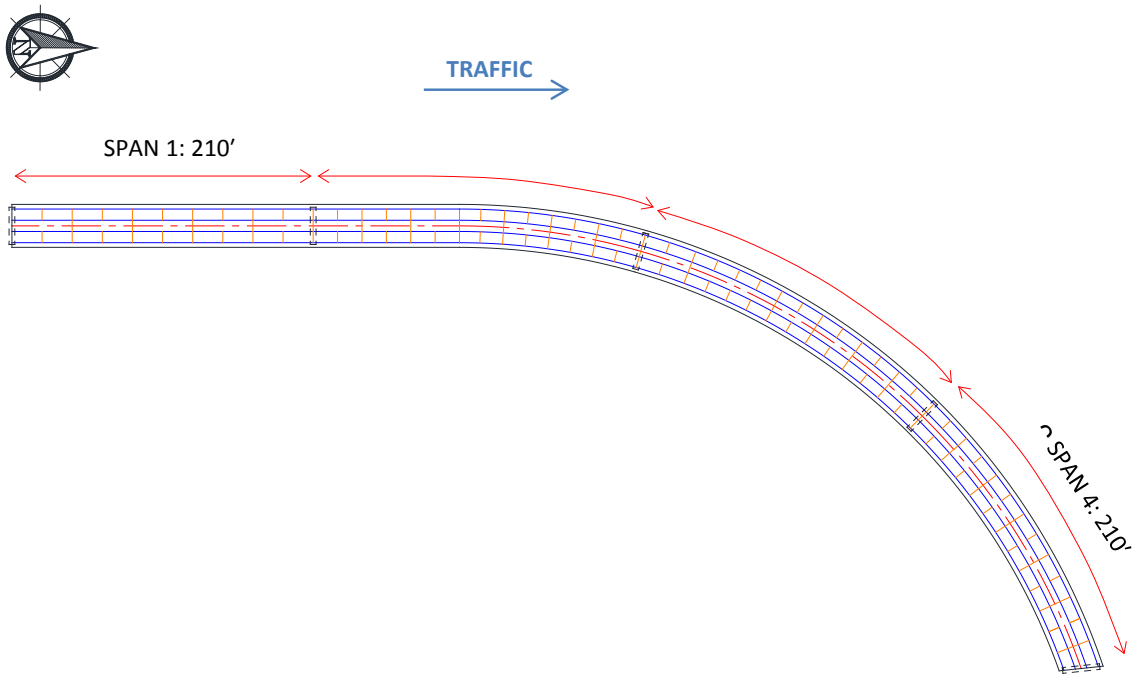

Figure 3.24 Dimensioned plan view of the US-290 Bridge.

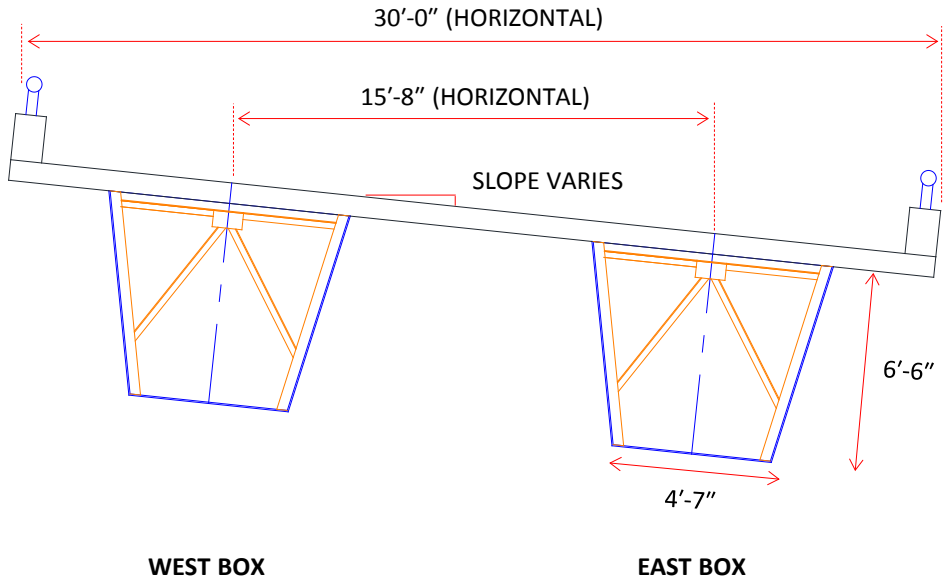

Figure 3.25 Dimensioned cross-section view of the US-290 Bridge.

3.3.2 Instrumentation Plan of US-290 Bridge

Instrumentation of the US-290E Direct Connector included ten different locations. The primary objective of the field tests was to determine the amplitude and frequency content of the acceleration records. Because access to the inside of the trapezoidal box was available, the research team was able to position the accelerometers at any location along the length of the bridge. Data were collected during July 2009 inside the east box, and seven days of continuous data were captured at ten different locations.

Accelerometers could not be clamped to the bottom flange of the box girder as with the Medina River Bridge setup (Figure 3.11a). Instead, the accelerometers were screwed into wood blocks, which were epoxied to the bottom flange. Figure 3.26 shows this instrumentation setup. Figure 3.27 provides an additional view of accelerometer locations for a typical cross-section of the bridge.

Figure 3.26 Typical accelerometer setup at the US-290E Direct Connector Bridge.

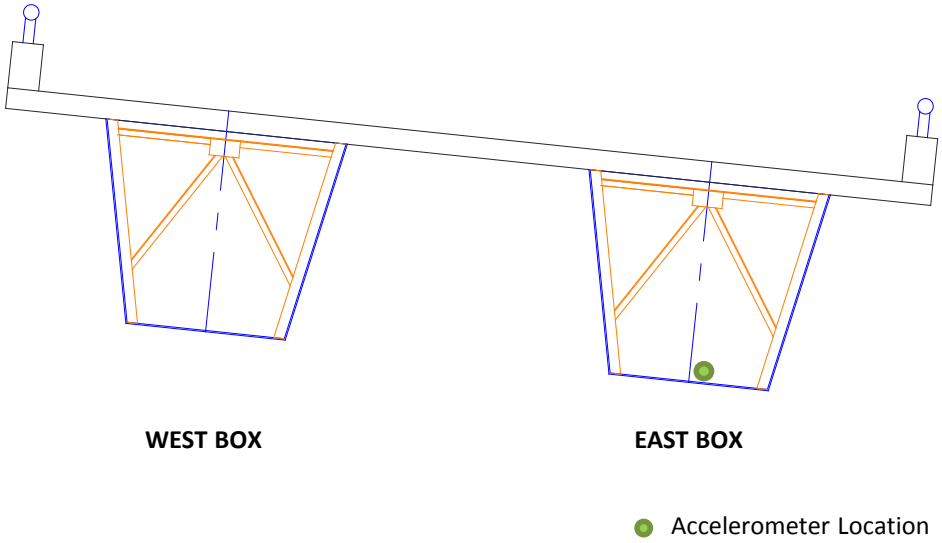

Figure 3.27 Cross-section view of the US-290 Bridge showing typical accelerometer location on the bottom flange of the east box girder.

The two south spans of the east box were instrumented at the quarter points. Two sensors were positioned near the intermediate supports and three at the quarter, half, and three-quarter locations of each span. Due to the symmetry of the bridge and the limited number of sensors, the third and fourth spans were not instrumented during the July 2009

visit. Note that the first span was instrumented in the same manner. A detailed summary of this plan, including exact locations and dates, is described in Section 3.7.

3.4 I-205W TO I-5S INTERCHANGE BRIDGE IN TUALATIN, OR

I-205W to I-5S Interchange (Figure 3.28) is a fracture-critical bridge located in Tualatin, Oregon, which is just south of Portland (Figure 3.29). The I-5/I-205 Interchange Bridge is also a twin, trapezoidal box girder bridge and is therefore similar in geometry to the US-290 Direct Connector Bridge. However, The Oregon box girder differs in age, boundary conditions, and traffic patterns. It serves as a two-lane ramp for westbound I-205 travelling unto I-5S.

Figure 3.28 I-205W to I-5S Interchange Bridge (Lindenberg, 2011).

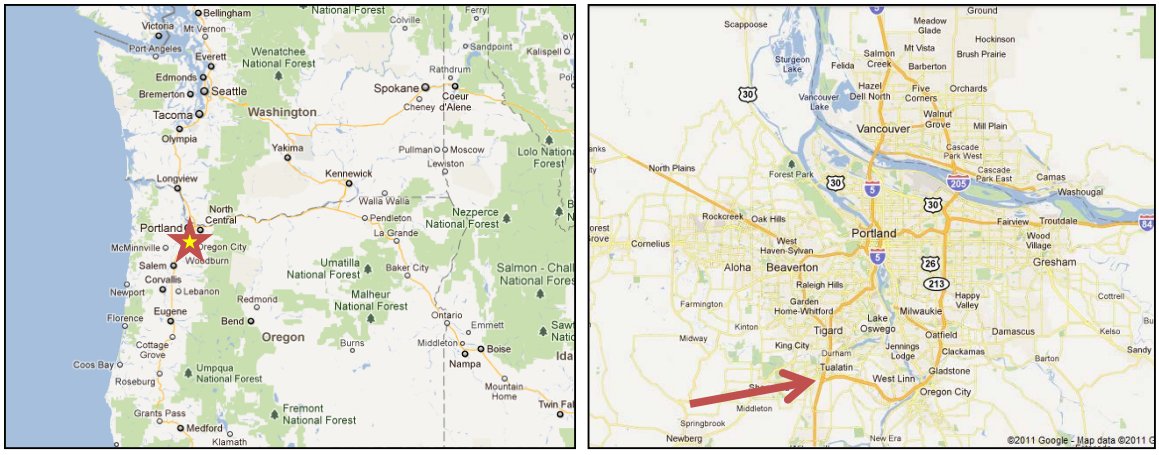

Figure 3.29 Location map of the I-205W to I-5S Interchange Bridge (Google Maps, 2011).

Construction of the bridge was finished in 1969, 33 years before the US-290 trapezoidal box bridge in Austin, Texas. As is presented in Chapter 8, the age of the bridge could explain the differences in vibrational amplitudes between the two similar bridges. An aerial view of the I-5 Interchange Bridge in Tualatin is presented in Figure 3.30.

Figure 3.30 Aerial view of I-205W to I-5S Interchange Bridge showing direction of traffic (Google Maps, 2011).

3.4.1 Geometry of I-205W to I-5S Bridge

The I-5/I-205 Interchange Bridge has four continuous spans, and the overall length is 527 ft. In this thesis, the northernmost span of the bridge is referred to as the first span, and the southernmost span as the fourth span. The first and fourth spans are 101-ft long, the second span is 152-ft long, and the third span is 172-ft long. I-5 traffic flows underneath the two interior spans of the bridge. The bridge is slightly curved over the entire length. There is a horizontal radius of approximately 1350 ft (at the centerline of the bridge) and an angle change of approximately 16°.

The trapezoidal boxes are roughly 4.5′ deep and are spaced 25′ on center. The boxes are slightly offset so that the road surface is tilted. Similar to the US-290 box bridge in Austin, a small 2-ft diameter access hole is provided in each steel plate diaphragm (located at the interior supports). However, I-5 Interchange Bridge utilizes a frame-through bent substructure. The cross beam connecting the two trapezoidal boxes, not the bottom flange of the boxes themselves, bears against the interior supports (Figure 3.31). This detail differs substantially from the support detail from the US-290 Bridge in Austin, where the longitudinal girders themselves bear on the piers. Figure 3.32 and Figure 3.33 show a dimensioned plan and cross-section view of the I-5 Interchange.

Figure 3.31 The cross beam at the I-5 Interchange Bridge bear on the piers.

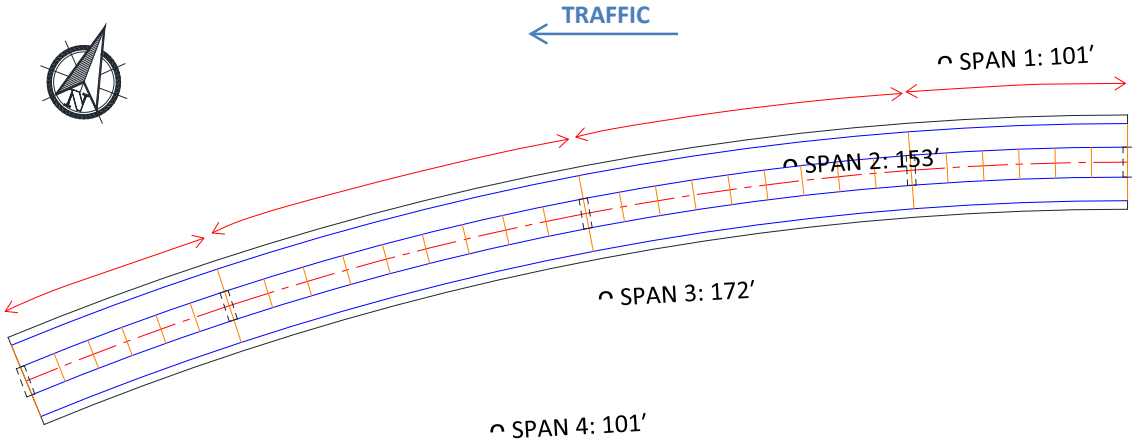

Figure 3.32 Dimensioned plan view of the I-5 Interchange Bridge.

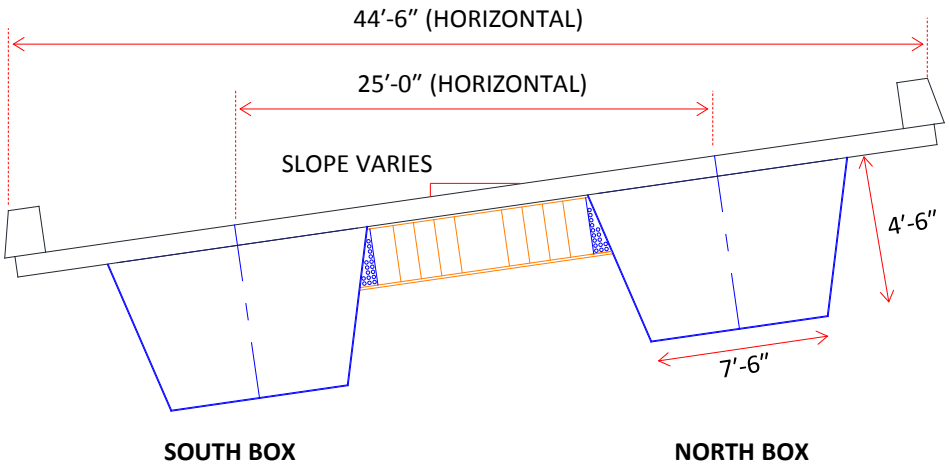

Figure 3.33 Dimensioned cross-section view of the I-5 Interchange Bridge.

3.4.2 Instrumentation Plan of I-205W to I-5S Bridge

Instrumentation of the I-5 Interchange Bridge in Tualatin, Oregon was completed in August 2011 by Rich Lindenberg and other members of Wiss, Janney, Elstner Associates (Northbrook, Illinois). Their team accessed the bridge from inside the box, so instrumentation could be done over the two middle spans (spans 2 and 3), which cross I-5S traffic lanes. To compare the vibrations near the supports and at midspan, three accelerometers were positioned inside the south box of the bridge. One was placed near

the interior support, and the other two were placed at center of the 153-ft and 172-ft middle spans. All three accelerometers were attached to the bottom flange of the box girder (Figure 3.34). Approximately three hours of raw data was captured at these locations during the field test. A detailed summary of this plan, including exact locations and dates, is described in Section 3.7.

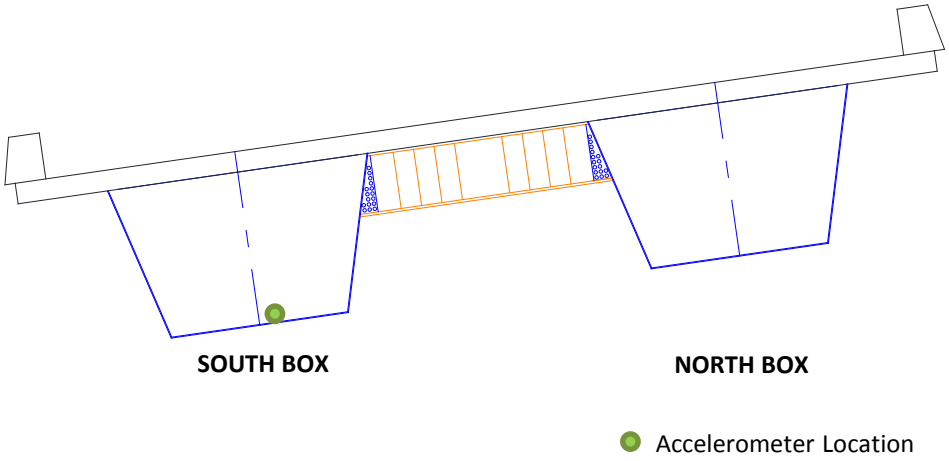

Figure 3.34 Cross-section view of the I-5 Interchange Bridge showing typical accelerometer location on the bottom flange of the south box girder.

3.5 I-5 BRIDGE OVER COLUMBIA RIVER IN PORTLAND, OR

The I-5 Bridge over the Columbia River (Figure 3.35) connects Portland, Oregon and Vancouver, Washington (Figure 3.36). It is a twin, steel through-truss bridge. The original bridge, which now carries northbound traffic, was built in 1916 and opened in 1917. This single bridge carried two-way traffic until 1958 when a second, identical truss bridge was built adjacent to it. Traffic was changed in 1958 so that each bridge carried one direction of traffic. Today each bridge serves three lanes traffic. A unique feature of this bridge is that the fifth span from the north is a vertical-lift span. An additional aerial view of the bridge is presented in Figure 3.37.

Figure 3.35 I-5 Portland-Vancouver Bridge over Columbia River from north end (Wikipedia, 2011).

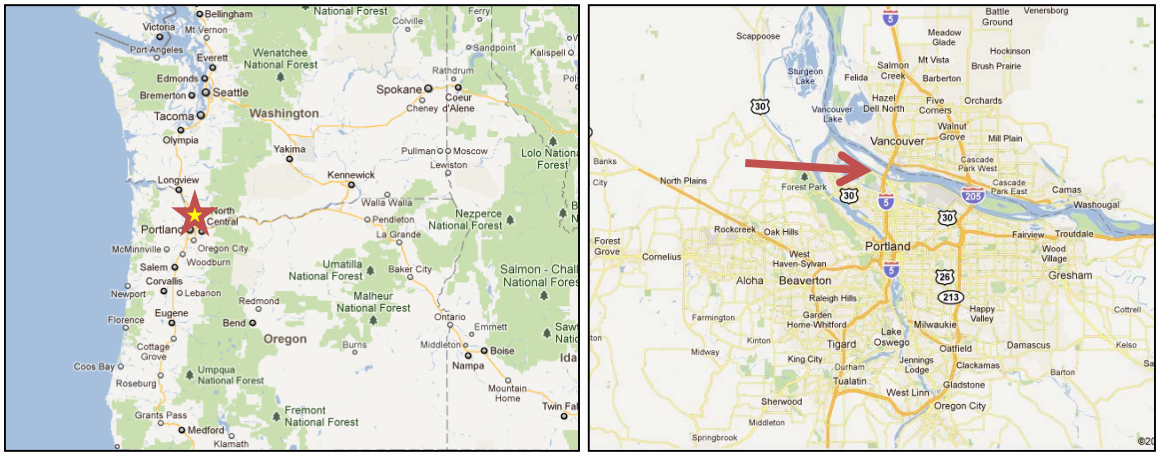

Figure 3.36 Location map of I-5 Portland-Vancouver Bridge over Columbia River (Google Maps, 2011).

Figure 3.37 Aerial view of I-5 Portland-Vancouver Bridge over Columbia River (Google Maps, 2011).

3.5.1 Geometry of Columbia River Bridge

The Columbia River Bridge has fourteen, simply-supported spans ranging from 256′-8″ and 278′-9″ in length. In this thesis, the northernmost spans of the bridges are referred to as the first spans, and the southernmost spans as the fourteenth spans. In total, the bridge is 3,531-ft long. Nine of the spans traverse water while the other four can be directly accessed from the ground below the bridge. Geometry of each truss is nearly identical with a height of 44.5 ft and a center-to-center spacing of 45′-5″. A dimensioned elevation view of the fourteenth span of the northbound bridge is shown in Figure 3.38. Note that the rest of the spans are nearly identical to this.

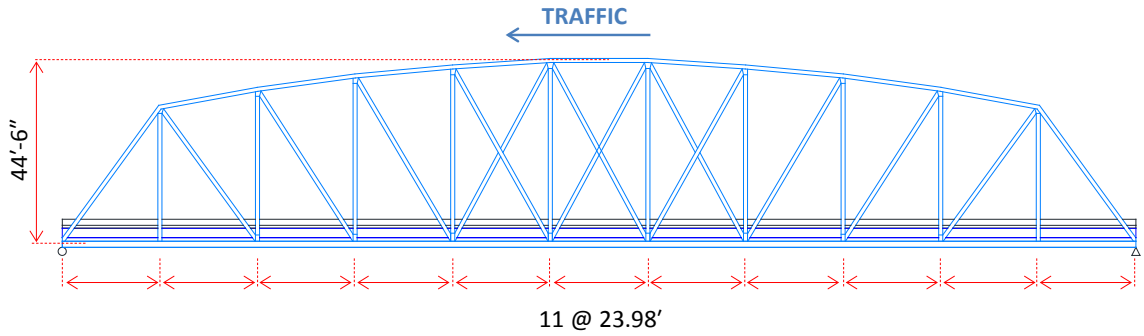

Figure 3.38 Dimensioned elevation view of the fourteenth span of the northbound I-5 Columbia River Bridge.

The deck is supported by six longitudinal stringers that frame into a deep girder, which is a plate girder system in the older northbound bridge and a built-up truss in the newer southbound bridge. These contrasting details are presented in Figure 3.39 and Figure 3.40.

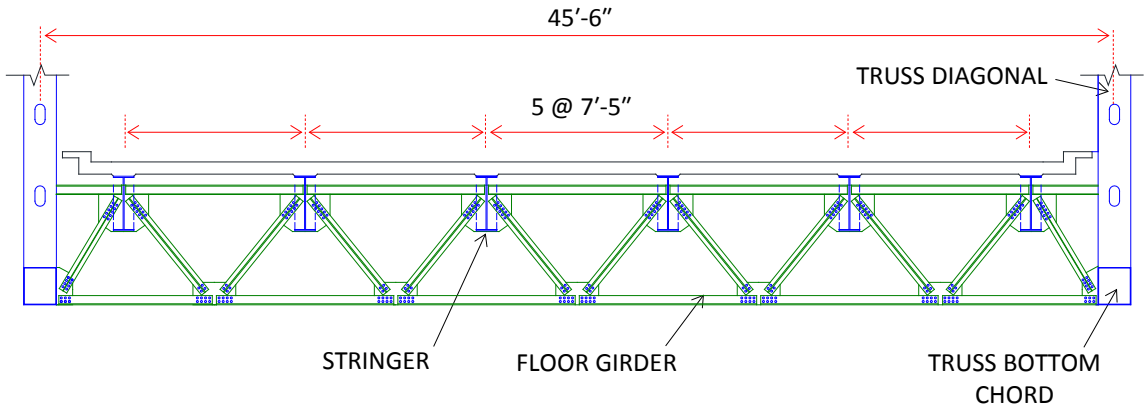

Figure 3.39 Dimensioned cross-section view of the southbound I-5 Columbia River Bridge constructed in 1958.

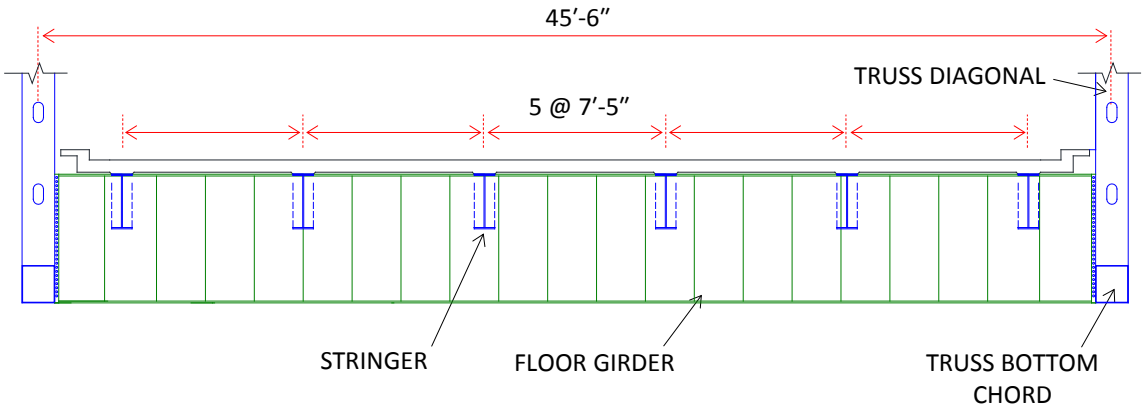

Figure 3.40 Dimensioned cross-section view of the northbound I-5 Columbia River Bridge constructed in 1916.

Long, slender WT 4x12 sections (roughly 26 feet long) brace the bottom chords of the truss. Figure 3.41 shows the floor and bracing systems from underneath the deck. A dimensioned plan view of the fourteenth span of the northbound bridge showing the lateral braces, stringers, and floor girders is shown on Figure 3.42.

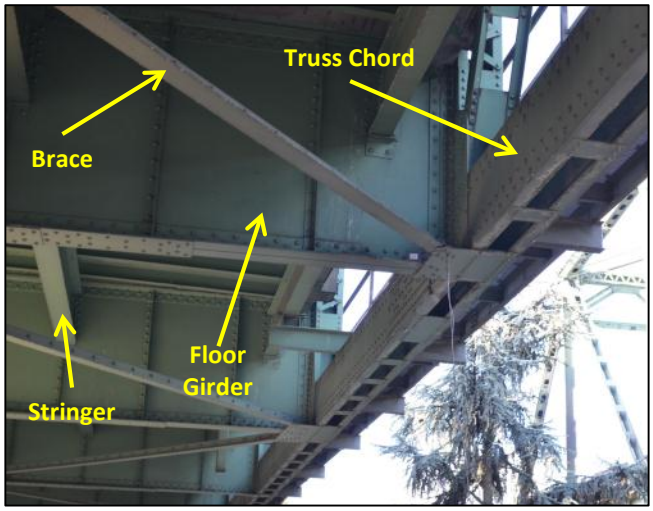

Figure 3.41 Floor and bracing system of northbound I-5 Columbia River Bridge from below (Lindenberg, 2011).

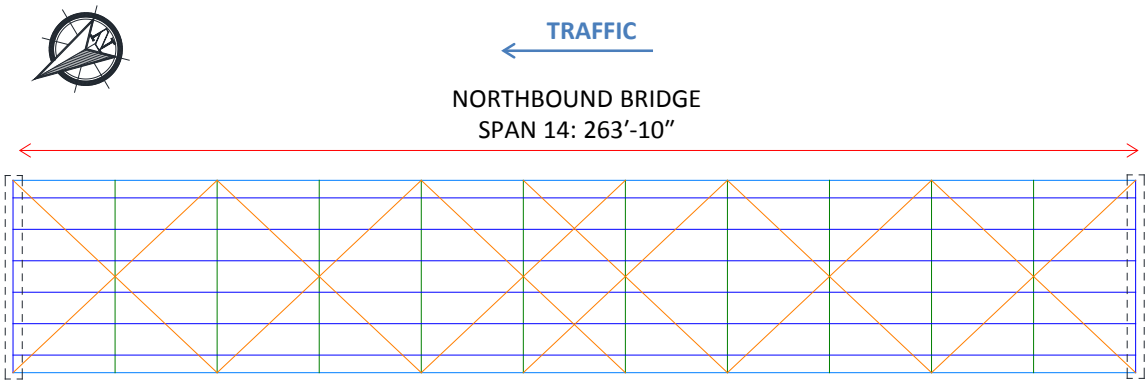

Figure 3.42 Dimensioned plan view of the fourteenth span of the northbound I-5 Bridge showing the lateral bracing system.

3.5.2 Instrumentation Plan of Columbia River Bridge

Instrumentation of the I-5 Columbia River Bridge was completed August 2011 by Rich Lindenberg and other members of Wiss, Janney, Elstner Associates. Only the southernmost span (span 14) of each bridge was instrumented due to limited ground access. The fourteenth span is 263′-10″ long for both bridges. Three accelerometers were used in the field test. Two of the three sensors were clamped to the connection plate at the girder-bottom chord intersection of the northbound bridge (Figure 3.43). One was near the support, and the other was at midspan of the truss. The third sensor was placed on a long, slender brace at midspan (Figure 3.44). This procedure was then repeated for the southbound bridge. About three hours of intermittent girder and brace vibration data were collected for both the northbound and southbound bridges. A detailed summary of this plan, including exact locations and dates, is described in Section 3.7.

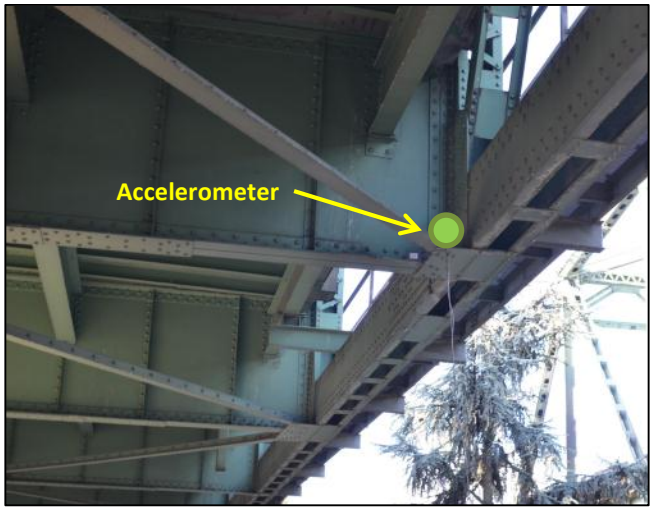

Figure 3.43 Typical accelerometer setup on a floor girder at the northbound I-5 Columbia River Bridge (Lindenberg, 2011).

Figure 3.44 Accelerometer clamped to bottom chord brace on southbound I-5 Columbia River Bridge

3.6 SELECTION OF SENSORS AND DATA ACQUISITION

The research team at FSEL instrumented the three bridges in Texas, and the WJE staff instrumented the two bridges in Portland. Different data acquisition systems and sensors were used by the two teams. As a result, different techniques were used to

process the measured data in order to achieve a consistent format. This section provides a discussion of the different acquisition systems, sensor selections, and post-processing methods for both instrumentations.

3.6.1 Data Acquisition System used by the FSEL Team

The research team at FSEL instrumented the three bridges in Texas, the Medina River Bridge in San Antonio, the TX-71E Bridge in Austin, and the US-290 Direct Connector in Austin. The same data acquisition system was used for all three bridges. An NI CompactRIO served as the data acquisition system, and two different modules were incorporated in the cRIO chassis to power the system and sample the data. A Digital Input Module (NI 9414) supplied 5 V to power the data acquisition system, and a 24-Bit Universal Analog Input (NI 9219) sampled the data. The NI 9219 has a four channel capacity. In many cases, more than four sensors were used at the site. Therefore, two NI 9219 modules were typically used in the cRIO. Figure 3.46 shows how the data acquisition system was configured in the field.

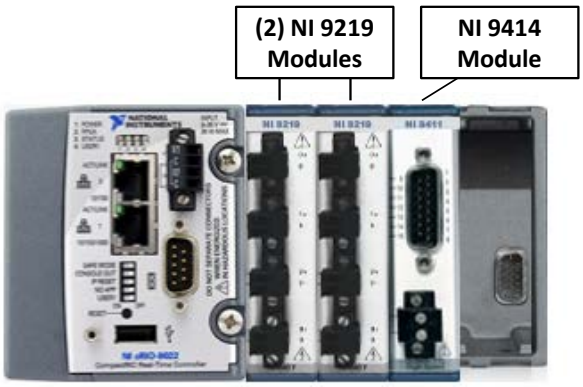

Figure 3.45 NI CompactRIO data acquisition system used by the FSEL team.

The acceleration data were sampled at 50 Hz continuously. In observing the frequency domain of the data, only half of the sample rate can be evaluated. This is because the Nyquist frequency is half of the sampling rate. Therefore, a frequency range of 0-25 Hz can be evaluated in the frequency domain for a 50-Hz sampling rate. Based on the literature and previous experiences, bridge vibrations are typically in this range. Thus,

a 50-Hz (0.02-second time step) sampling rate is appropriate for this application. Frequency domain analyses are presented in more detail in Section 4.2.

3.6.2 Sensor Selection by the FSEL Team

Two different sensors were considered in the instrumentation of the Texas bridges, Crossbow CXL02LF1Z and Crossbow CXL04GP1Z. The CXL02LF1Z series is a single axis, ±2g (1 g = 32.2 ft/s^2) accelerometer with 1000 mV/g sensitivity. There is a 0.5-mg root mean square (RMS) noise level. The CXL04GP1Z series is a single axis, ±4g accelerometer with 500 mV/g sensitivity and a 10-mg RMS noise level (Crossbow Technology, 2011). Although the two types of accelerometers were obtained from the same manufacturer, the biggest difference between the accelerometers is the sensitivity and the noise thresholds. Due to the low-frequency, low-amplitude nature of bridge vibrations, the typical vehicular-induced amplitudes must exceed the noise level of the accelerometer by a substantial amount. Otherwise, distinguishing between noise and real bridge vibrations is difficult. The ±4g sensors have twice the range, but half the sensitivity and 20 times the noise threshold. Because sensitivity is much more important than range for this application, the ±2g accelerometer was selected for all instrumentations.

3.6.3 Post-Processing Techniques used by the FSEL Team

The acquired data was converted to engineering units (g) using the sensitivity factor provided by the manufacturer for each accelerometer. Then, the data were further post-processed using a bandpass Butterworth filter.

Selecting the appropriate filter limits depends on typical frequency ranges and noise levels of bridge vibrations. Frequencies below the lower threshold and frequencies above the upper threshold are rejected. For this application, a lower threshold of 0.5 Hz and an upper threshold of 24 Hz were selected. Therefore, frequencies between 0 and 0.5 Hz and between 24 and 25 Hz were removed in the filtering process. Noise is typically

registered in extreme low- and high-frequency ranges, which explains the chosen 0.5-Hz and 24-Hz threshold values.

3.6.4 Data Acquisition System used by WJE

Instrumentation of the two Oregon bridges, the I-5/I-205 Interchange and the I-5 over the Columbia River, was conducted by Rich Lindenberg and WJE. Acquisition of data was the same for both Oregon bridges. An NI CompactDAQ served as the data acquisition system. Only one module, an accelerometer measurement module (NI 9234), was needed in this system to capture the data. Similarly to the NI 9219, the acceleration module has a four-channel capacity. Figure 3.47 shows how the system was configured.

Figure 3.46 NI CompactDAQ data acquisition system used by WJE Associates.

WJE sampled the data continuously at 2048 Hz (0.00049-second time step). Therefore, a frequency range of 0-1024 Hz can be evaluated in the frequency domain. WJE typically samples acceleration at high rates to capture the presence of high-frequency, transient shock. Because ambient vibration energy harvesters are usually designed for low-frequency ranges (0-25 Hz), the high-frequency activity of the bridge response is not important for this application.

3.6.5 Sensor Selection by WJE

PCB Piezotronics Single-Axis Accelerometers (PCB337A26) were used to

instrument the I-5/I-205 Interchange and the I-5 Columbia River Bridge. PCB337A26 sensors have 100 mV/g sensitivity (PCB Piezotronics, 2011), which is ten times smaller than the ±2g Crossbow accelerometers used by the FSEL team. As a result, noise was more prominent in this data.

3.6.6 Post-Processing Techniques used by WJE

Post-processing of the raw data included conversion to engineering units and filtering, similar to the UT method. However, an extra step of downsampling was required to keep all data in a consistent format.

In order to successfully convert 2048-Hz data to 50-Hz dynamic data without compromising its integrity and affecting the frequency content, a filter directly followed by a downsampling routine must be applied. Therefore, the 2048-Hz data was sent through the same bandpass filter (0.5-Hz lower threshold and 24-Hz upper threshold), so that frequencies between 0 and 0.5 Hz and between 24 and 25 Hz were removed. At this point, the data still has a 0.00049-second time step, which is disadvantageous when long-term analysis of data is required. Downsampling from 2048 to 50 Hz can then be done to increase the time step without losing any important time-domain or frequency-domain characteristics of the data. Through this procedure, the Oregon bridge data was formatted in the same way as the Texas bridge data. Frequency analysis on all the data can be done with confidence knowing the signal is clean, consistent, and reliable.

3.7 SUMMARY OF INSTRUMENTATION PLANS

In this section, the comparison of bridge geometries (Table 3.1) and the respective instrumentation plans (Table 3.2), which include dates and sensor locations, are summarized. As previously discussed, the bridges represent a variety of highway bridges in the United States. Although the feasibility of a vibration energy harvester at only five bridges in Texas and Oregon will be discussed, the results can potentially be extrapolated to many other bridges if conditions are similar. The rest of this section summarizes the important aspects of the individual instrumentations.

Table 3.1 Summary of type and geometry of five instrumented bridges.

Bridge	Location	Year Constructed	Traffic	Bridge Type	No. of Spans	Lengths (Min/Max)
I-35N Medina River Bridge	San Antonio, TX	1935*	Two lanes, northbound	Statically-determinate, riveted plate girders	3	73′-6″ / 94′-5″
SH-71E Bridge	Austin, TX	1959	Three lanes, eastbound	Continuous, six rolled girders	5	35′ / 57′-6″
I-35N to US-290E Direct Connector	Austin, TX	2002	One lane, exit ramp	Continuous, twin trapezoidal box girder	4	210′ / 230′
I-205W to I-5S Interchange	Tualatin, OR	1969	Two lane, exit ramp	Continuous, twin trapezoidal box girder	4	153′ / 172′
I-5 Columbia River Bridge	Portland, OR	1916 (N), 1958 (S)	Three lanes, north & south	Simply-supported, twin trusses	14	256′-8″ / 278′-9″

* Bridge was widened in 1974

Table 3.2 Summary of instrumentation plans for five instrumented bridges.

Bridge	Location	Dates	Year	No. of Sensor Locations	Span	Position
I-35N Medina River Bridge	San Antonio, TX	Oct. 27 - Oct. 31	2010	6	North Span	Girder (at floor beams 31, 33, 35)
		Mar. 29 - Apr. 25	2011	26	North & Central Span	Girder (at floor beams 24-28, 31-38)
		Jul. 17 - Jul. 31	2011	5	North & Central Span	Girder (at floor beams 25, 33, 35)
		Nov. 29 - Dec. 5	2011	3	North Span	Girder (at floor beam 33), Midspan Braces
		Total Data = 55 days		***Total Locations = 28***		
SH-71E Bridge	Austin, TX	Mar. 25 - Apr. 3	2010	2	Span 3	Interior Girder (midspan & support)
		Total Data = 9 days		***Total Locations = 2***		
I-35N to US-290E Direct Connector	Austin, TX	Jul. 7 - Jul. 10	2009	5	Span 1	Girder (quarter points)
		Jul. 10 - Jul. 13	2009	5	Span 2	Girder (quarter points)
		Total Data = 7 days		***Total Locations = 10***		
I-205W to I-5S Interchange	Tualatin, OR	Aug. 17	2011	3	Spans 2 & 3	Girder (midspan & support)
		Total Data = 3 hours		***Total Locations = 3***		
I-5 Columbia River Bridge	Portland, OR	Aug. 18	2011	3	Northbound Bridge - Span 14	Girder (midspan & support), Brace
				3	Southbound Bridge - Span 14	Girder (midspan & support), Brace
		Total Data = 5 hours		***Total Locations = 6***		

The I-35N Medina River Bridge was instrumented on five different occasions in 2010 and 2011. In October 2010, sensors were positioned on the bottom flange of both east and west girders at three floor beam locations (31, 33, and 35). In total, data from six accelerometer locations were acquired. In March and April 2011, the same six accelerometers were used. However, the position of those sensors was changed weekly. By the end of April, 13 different floor beam locations for both girders (26 total locations) had been instrumented for at least a week. Both the north anchor span and the central cantilever/suspended span were included. Five more locations were instrumented in July 2011. In December 2011, a week of vibrational data from two north span lateral braces was collected. At first, data from the brace only were taken. A 13-lb weight was then added to the brace to simulate the energy harvester and its effect on the frequency signature and amplitudes of the member (Figure 3.11).

Note that there was overlap between these five instrumentations. For example, the girders at floor beams 33 and 35 were instrumented four separate times. As a result, the total number of sensor locations for the Medina River Bridge is not equal to the sum of the four individual instrumentations, as shown in Table 3.2. In total, 55 days of data were collected at the site at various locations on the north and central spans. With such a dense array of sensors and a large amount of data, spatial effects of the vibrations can be quantified. Figure 3.48 and Figure 3.49 provide a summary of accelerometer locations for a plan view and elevation view of the bridge, respectively.

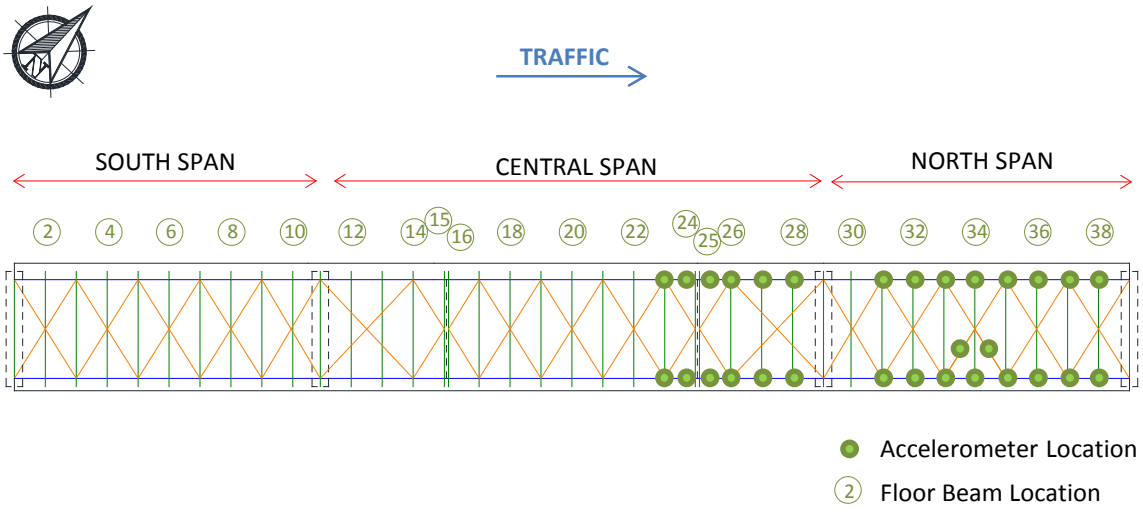

Figure 3.47 Plan view of the Medina River Bridge showing accelerometer locations.

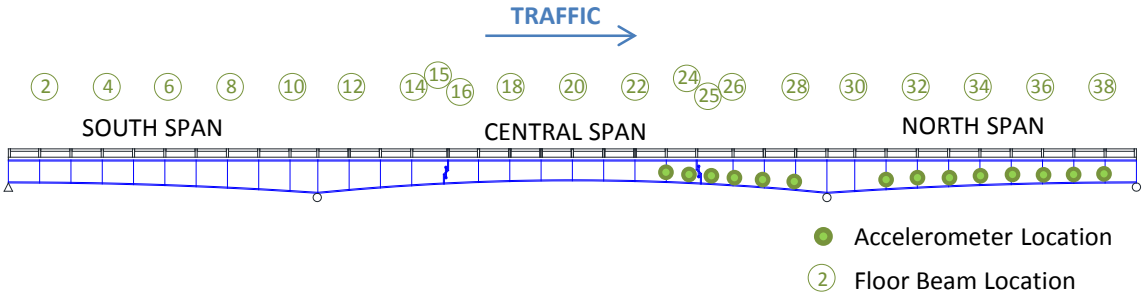

Figure 3.48 Elevation view of the west longitudinal girder at the Medina River Bridge from the inside showing accelerometer locations (brace sensors not shown).

The scale of the instrumentation plans of the other four bridges was much simpler and less substantial. Only two locations on the TX-71E Bridge in Austin were considered. Accelerometers were positioned on an interior girder of the middle, third span. One was near the interior support, and the other at midspan. Nine days of continuous data were acquired during March and April 2010. Figure 3.50 provides a summary of accelerometer locations for a plan view of the TX-71E Bridge.

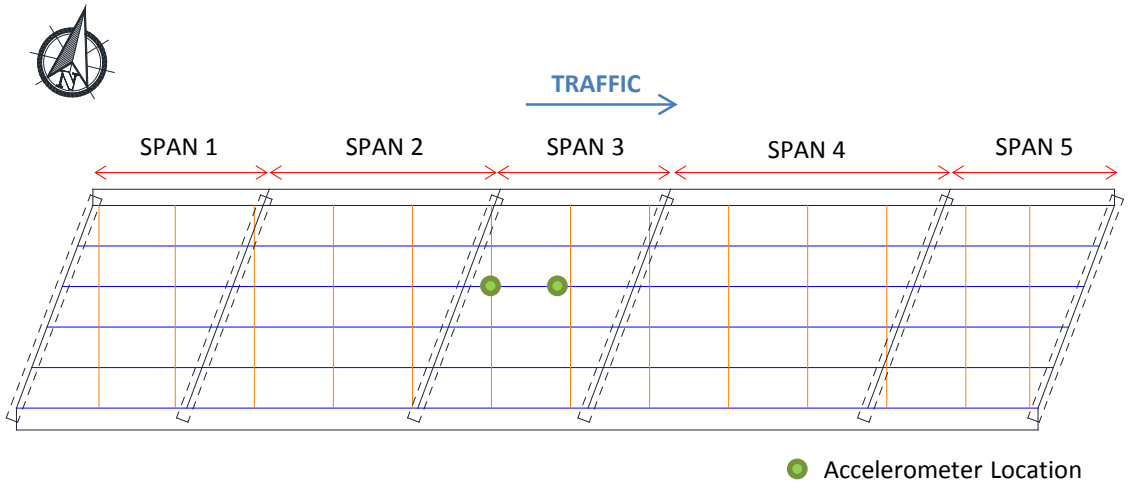

Figure 3.49 Plan view of the TX-71E Bridge showing accelerometer locations.

The right girder (east box) of the US-290 Direct Connector was instrumented in two stages during July 2009. Five accelerometers were placed at the quarter points of the first span from July 7 through July 10. On July 10, the second span was instrumented in similar fashion. Three days of continuous acceleration data was collected for the first and second spans at five different locations. Figure 3.51 provides a summary of accelerometer locations for a plan view of the US-290 Bridge.

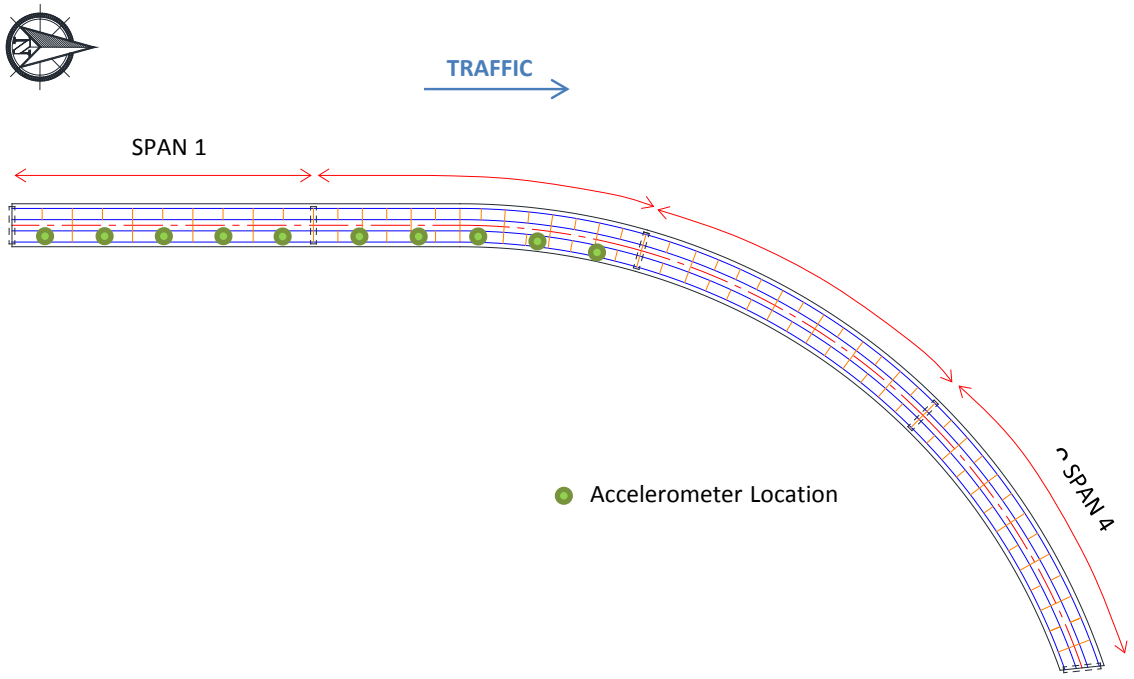

Figure 3.50 Plan view of the US-290 Bridge showing accelerometer locations.

Only three hours of intermittent data were captured at the I-5/I-205 Interchange in Tualatin, Oregon. The two middle spans of the left lane (south) box girder were instrumented with sensors, specifically midspan of span 2, midspan of span 3, and just above the support connecting spans 2 and 3. Figure 3.51 provides a summary of accelerometer locations for a plan view of the I-5/I-205 Interchange Bridge.

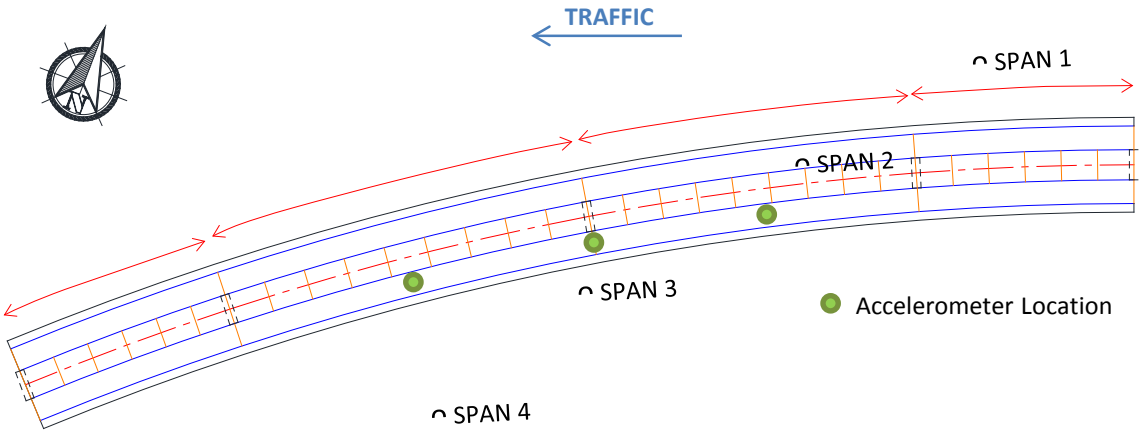

Figure 3.51 Plan view of the I-5/I-205 Interchange Bridge showing accelerometer locations.

Instrumentation of the I-5 Columbia River Bridge was divided into two phases. The fourteenth span of the northbound bridge was first instrumented, followed by the fourteenth span of the southbound bridge. Approximately three hours of data were acquired from the northbound truss and two hours from the southbound truss. In both cases, an accelerometer was placed near the interior support, at midspan of span 14, and on a long, slender brace near midspan. Figure 3.52 and Figure 3.53 provide a summary of accelerometer locations for a plan view and elevation view of the northbound bridge, respectively. Note that the southbound instrumentation was the same.

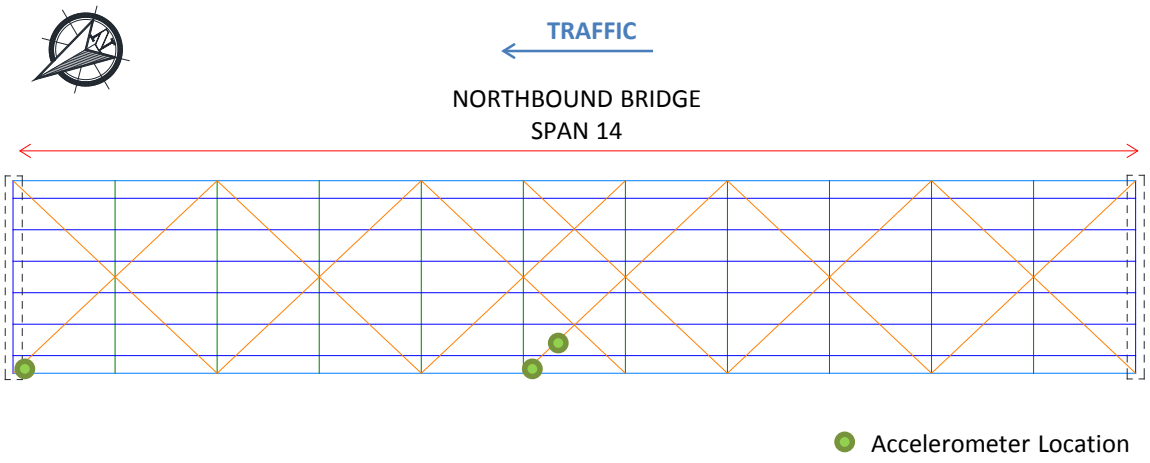

Figure 3.52 Plan view of the northbound I-5 Columbia River Bridge showing accelerometer locations.

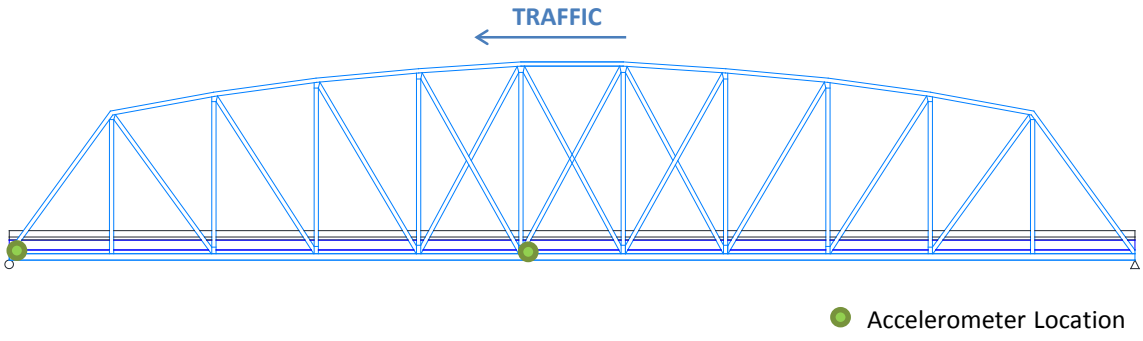

Figure 3.53 Elevation view of the northbound I-5 Columbia River Bridge showing accelerometers locations (brace sensor not shown).

3.8 CHAPTER SUMMARY

This chapter presented a summary of the five bridges instrumented and analyzed for its vehicular-induced dynamic behavior. Basic information such as age, construction type, and geometry of the structure was discussed. An understanding of these factors is important in interpreting the comparisons of vibrational responses of the bridges in subsequent chapters. Also, the instrumentation, namely the sensor locations and dates, for each bridge was described. With data at different locations on a bridge, at different days of the week, and at different times of the year, variability in the acceleration data can be fully understood.

Chapter 3 described acquisition and preparation of reliable, filtered data. Chapter 4 begins the discussion of data analysis to determine relevant information regarding vibration energy. Frequency domain analysis is the first step in this process, as will be explained in the next chapter.

CHAPTER 4
Spectral Analysis

Spectral analysis is a useful tool in characterizing the dynamic behavior of a bridge. It can be classified as either time-domain or frequency-domain analysis. As stated in Chapter 1, measured acceleration data provide information about the amplitude and frequency content of the vibrations. This chapter summarizes approaches used to analyze the acceleration data in the time domain and the frequency domain. Specifically, root mean square (RMS), Fourier transforms, power spectral density, Parseval's theorem, and spectrograms are introduced. This information is coupled with examples from the data acquired at the instrumented bridges (Chapter 3). The significance and limitations of spectral analysis with respect to this research will also be discussed.

4.1 TIME-DOMAIN ANALYSIS

The time domain refers to a signal presented as a function of time. Raw acceleration data acquired during a field test would be classified as a time domain series. Prior to analyzing the frequency content of a signal, important information can be gathered from the response history. In particular, acceleration amplitudes can be assessed in the time domain. Typical time-domain analysis approaches are averaging, minimum/maximum, and root mean square (RMS). RMS was selected as the primary time-domain tool in this research because it provides a good indication of overall amplitudes and truck traffic volumes. Higher RMS values generally mean that peak acceleration amplitudes and the volume of trucks crossing the bridge are high. Therefore, a short-span bridge that serves mostly small vehicular traffic will likely have small RMS values, and a long-span bridge with heavy truck traffic will likely have high values.

RMS is just as the name suggests. This singular value is the "root of the squared mean." To compute the RMS of a given response history, each reading in the acceleration array is squared to make all the values positive. Next, the average of this squared array is

taken. The RMS of the sample is then the square root of that average value. The units of the calculation are the same as the raw data, which is typically a percent of gravity (g's). Equation 4.1 shows the mathematical expression for root mean square. An example of this procedure is presented in Figure 4.1.

$$RMS = \sqrt{\frac{1}{N}\sum_{i=1}^{N}[y(i)]^2} \qquad \textbf{Equation 4.1}$$

where: N = number of data points in processing interal
y(i) = acceleration response history array

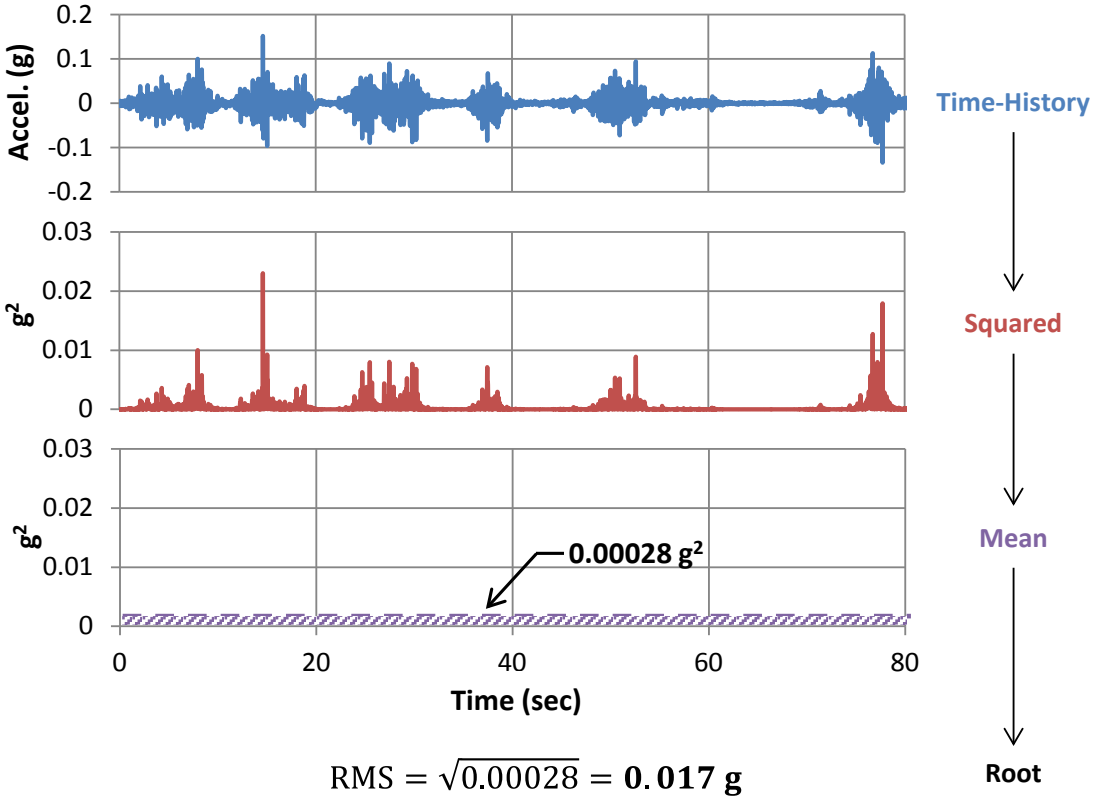

$$\text{RMS} = \sqrt{0.00028} = \mathbf{0.017\ g}$$

Figure 4.1 Sample RMS calculation for a representative acceleration history from the Medina River Bridge.

Note that RMS values for structures like bridges with variable traffic patterns will vary over time. RMS values are expected to be higher during rush hour traffic than during

early morning hours and higher on weekdays than on weekends because of increased traffic volume. RMS values are also indirectly related to the power potential of a vibration energy harvester, as will be discussed in Chapter 6.

4.2 FREQUENCY-DOMAIN ANALYSIS

The frequency domain refers to a signal presented with respect to frequency. Rather than having time as the x-axis, frequency is typically graphed on the x-axis in frequency-domain plots. The frequency content of a signal can be evaluated in the frequency domain. There are many different types of analysis techniques in the frequency domain, but only power spectral density (PSD) and spectrograms were used in this research. In order to understand these analytical tools, a brief review of Fourier transforms and Parseval's theorem will also be presented in this section.

4.2.1 Fourier Transform Basics

A Fourier transform is a mathematical operation that transforms a signal from the time domain to the frequency domain. A signal generally consists of a wide range of frequencies with varying magnitudes. The Fourier transform decomposes an acceleration response history in the time domain into its individual frequency components. There are many variations of the Fourier transform used in mathematics, but the most common for signal processing are the discrete Fourier transform (DFT) and the fast Fourier transform (FFT). A DFT is a finite-duration algorithm that utilizes discrete time-steps. The FFT algorithm yields the same results as the DFT, except the computing time is much faster because it utilizes symmetry (Hrovat, 2004).

A FFT requires that the number of data points in a processing interval be a power of two. The results from the FFT algorithm are expressed over a range of frequencies. The maximum output frequency, the Nyquist frequency, is half the input sampling rate. In other words, if the acceleration response history was sampled at 50 Hz, a range of 0-25 Hz can be evaluated in the frequency domain. The frequency content from 25-50 Hz is returned as the mirror image of the 0-25 Hz content.

The Fourier transform provides complex numbers for each frequency interval, which is commonly referred to as the complex amplitude. The frequency intervals, or the frequency resolution, of a FFT plot is directly related to the sampling rate and the number of data points in the sample. This is presented in Equation 4.2. Based on this equation, it can be seen that increasing the processing window will produce a FFT plot with higher frequency resolution. Equation 4.3 shows the DFT formulation, which is applicable for FFTs. This mathematical operation serves as the basis for power spectral density calculations.

$$\Delta f = \frac{f_s}{N} \qquad \textbf{Equation 4.2}$$

where: Δf = frequency resolution
f_s = sampling rate
N = number of data points in processing intervals

$$X(k) = \sum_{n=0}^{N-1} x(n) e^{i2\pi \frac{k}{N} n} \qquad \textbf{Equation 4.3}$$

where: $X(k)$ = complex amplitude for given frequency interval
x(n) = acceleration response history array
k = 0,1,2, … , (N − 1) in frequency domain
n = 0, 1, 2, … , (N − 1) in time domain

4.2.2 Power Spectral Density

Similarly to the fast Fourier transform plot, a power spectral density (PSD) plot relates a magnitude to a frequency interval. PSD is a function that quantifies the relative contribution or "power" from any given frequency interval to the entire signal. The distribution of frequencies can then be determined in an absolute sense with this calculation. The results of the power spectral density are expressed in terms of real numbers. Units for spectral power are g^2/Hz, meaning real amplitudes and real frequencies are included. Spectral power density is important because it indicates which frequencies are dominant relative to others.

The Fourier transform is the core of PSD calculations. This is demonstrated in Equation 4.4. A window function must also be selected, which describes how the frequencies are filtered through the transform. In all cases, a Hanning window was chosen. Note that the first and last frequency intervals considered are not multiplied by two because those are unique solutions. Remember that the FFT utilizes symmetry between frequencies above and below the Nyquist frequency.

$$P(k) = \begin{cases} \frac{2|X(k)|^2}{NUf_s} \text{ for } k = 1,2,\dots,\left(\frac{N}{2}\right) - 1 \\ \frac{|X(k)|^2}{NUf_s} \text{ for } k = 0, \frac{N}{2} \end{cases}$$ **Equation 4.4**

where: $X(k) =$ FFT for given frequency interval
$U =$ window function compensating factor

An example of this transformation procedure is shown in Figure 4.2. A response-history sample from midspan of the US-290 Bridge was transformed into the frequency domain as a PSD plot. Note that the frequency range is 0-25 Hz because the response history was sampled at 50 Hz and that the two dominant modes are 2.0 and 4.1 Hz. These frequency intervals contribute the most to the total 80-second signal and, as a result, their spectral power values are substantially higher than any other frequencies in the range.

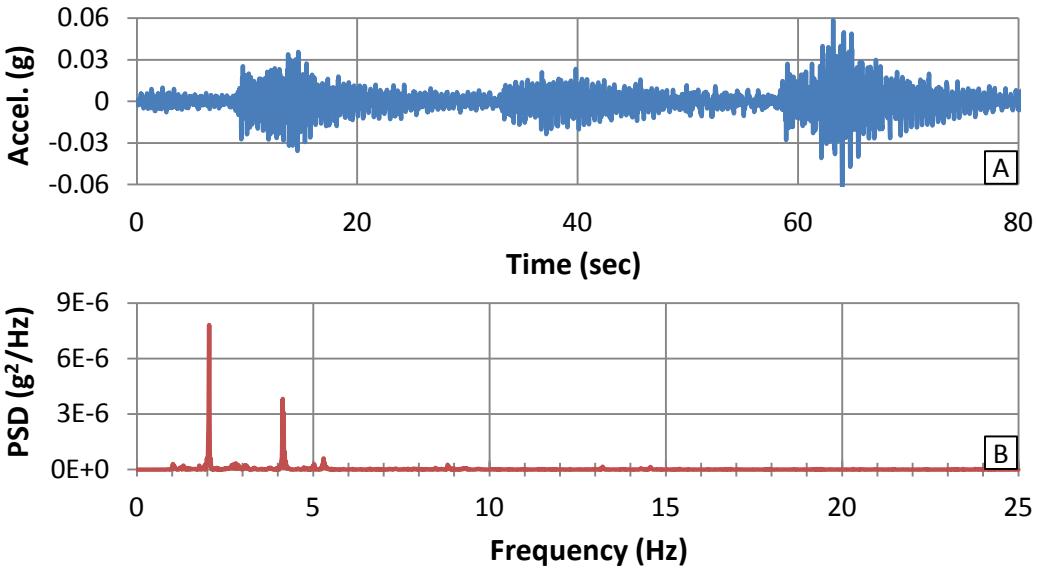

Figure 4.2 (a) Sample response history at the US-290 Bridge; (b) Corresponding PSD plot.

4.2.3 Parseval's Theorem

Parseval's theorem relates the information gathered in the time-domain analysis and the frequency-domain analysis. In general terms, it states that the area underneath a response-history sample and its corresponding PSD curves are directly related. The RMS of the response history is equivalent to the square root of the area underneath the PSD frequency distribution. The relationship is stated in Equation 4.5.

$$\sqrt{\frac{1}{N}\sum_{i=1}^{N}[y(i)]^2} = \sqrt{\sum_{k=1}^{N/2}P(k)\Delta f} \qquad \textbf{Equation 4.5}$$

$$RMS_t = Area_f$$

Parseval's theorem is essentially a conservation of energy principle. The total energy of the response history must be conserved when transforming it to the frequency domain. The vibration is distributed fully over a wide range of frequencies, but the sum is still the same such that all the components of the signal are considered. A narrowband

signal is one where the vibration energy is distributed over a small window of frequencies, and a wideband signal is distributed over a wide range. Excitation bandwidth has important implications in energy harvesting, as is discussed in Chapters 6 and 7. Figure 4.3 shows a PSD plot for an 80-second sample of midspan data at the Medina River, US-290, and TX-71E bridges. It should be noted that the Medina River signal is extremely wideband, whereas the US-290 Bridge is narrowband. Although the peak spectral power for US-290 is greater, there is more total area underneath the Medina River Bridge PSD plot. The amplitudes of the TX-71E data, on the other hand, are negligible when compared with the amplitudes of the other two bridges. As a result, it is expected that the amplitudes of the Medina River Bridge response-history signal are the highest due to Parseval's theorem. These types of relationships are critical when determining the feasibility of a vibration energy harvester at a given bridge.

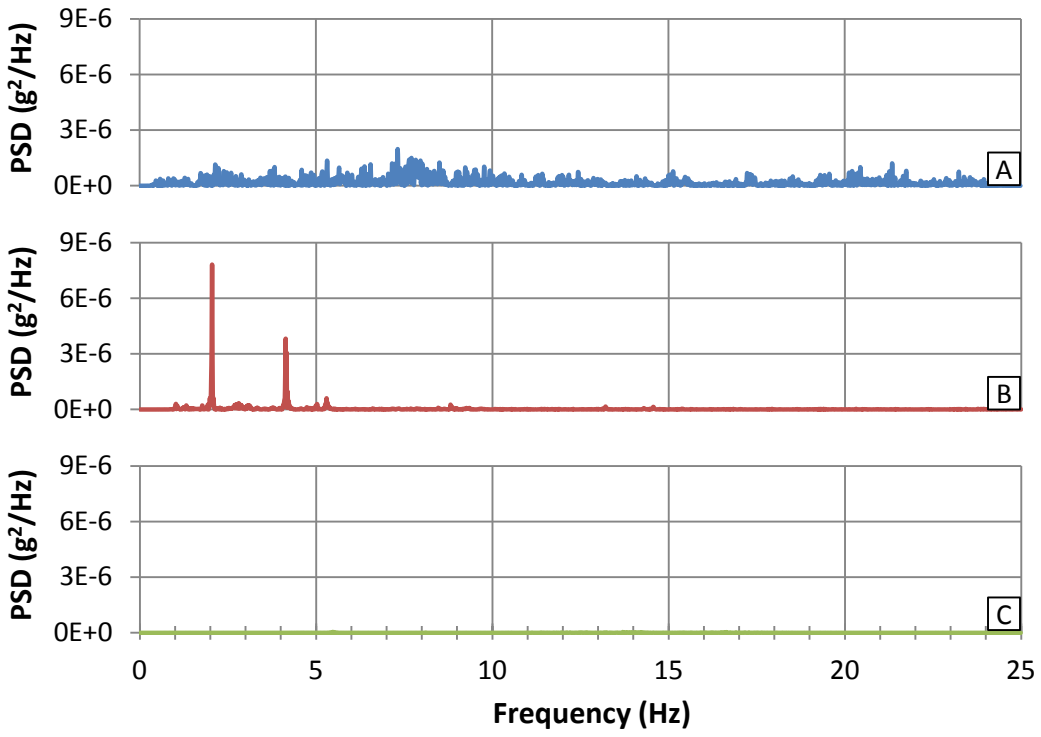

Figure 4.3 Comparison of sample PSD plots for (a) Medina River Bridge, (b) US-290 Bridge, and (c) TX-71E Bridge.

4.2.4 Spectrogram Analysis

Spectrograms combine the time- and frequency-domain results, usually in the form of three-dimensional color intensity plots, where time, frequency, and spectral power are the variables. Spectrograms piece together small time interval FFT plots over an entire processing sample. Like PSD plots, spectrograms utilize Fourier transform operations. But because small time intervals are preferred, short-time Fourier transforms (STFTs) are used instead of typical FFTs. STFT algorithms are the same as standard Fourier transform algorithms, except that both a frequency resolution and a temporal resolution must be specified.

Temporal resolution of a spectrogram is related to the windowing function selected. Again, a Hanning window was applied to the transformation. In many cases, there can be an overlap between a STFT and the subsequent one. This is typically done to smooth out the plot. Spectrograms are useful graphical tools because the distribution of the frequency content can be identified as a function of time. If a spectrogram is developed for a long period of time, the stability of dominant frequencies can be assessed. But most importantly, the intensity of a frequency can be examined before, during, and after a truck event. The energy associated with a forced vibration scenario (truck crossing) and a free vibration scenario (bridge dampening out) can be compared.

Spectrograms are commonly used in data processing to determine damping characteristics of civil structures. Each mode of vibration has a different damping ratio, and spectrograms are capable of displaying this information in a visual sense. For example, Brownjohn et al. (2006) used spectrogram analysis to determine modal damping of suspension cables in the Tamar Suspension Bridge in Plymouth, U.K. Ghanaat et al. (2000) conducted similar research, but for an arch dam. And Luscher et al. (2001) utilized spectrogram plots to evaluate the differences between a controlled hammer test and ambient acceleration data of the Z24 Bridge in Switzerland.

From an energy harvesting perspective, it was determined through spectrogram analysis that forced vibration yielded significantly more vibrational energy than free

vibration. Figure 4.4 shows a sample spectrogram for acceleration data at midspan of the Medina River Bridge. There are two major points to note from this plot. First, the color is most intense while trucks are crossing the bridge, and the intensity is low between trucks in the decay period. This is also demonstrated by the acceleration peaks in the response history above the spectrogram. Second, the vibrational energy is dissipated over a wide range of frequencies, which agrees with the results of Figure 4.3a. The frequencies excited during forced vibration and free vibration, though, are not necessarily the same. But it is more advantageous to design a vibration energy harvester for the forced frequencies because the total energy available is substantially higher in these situations.

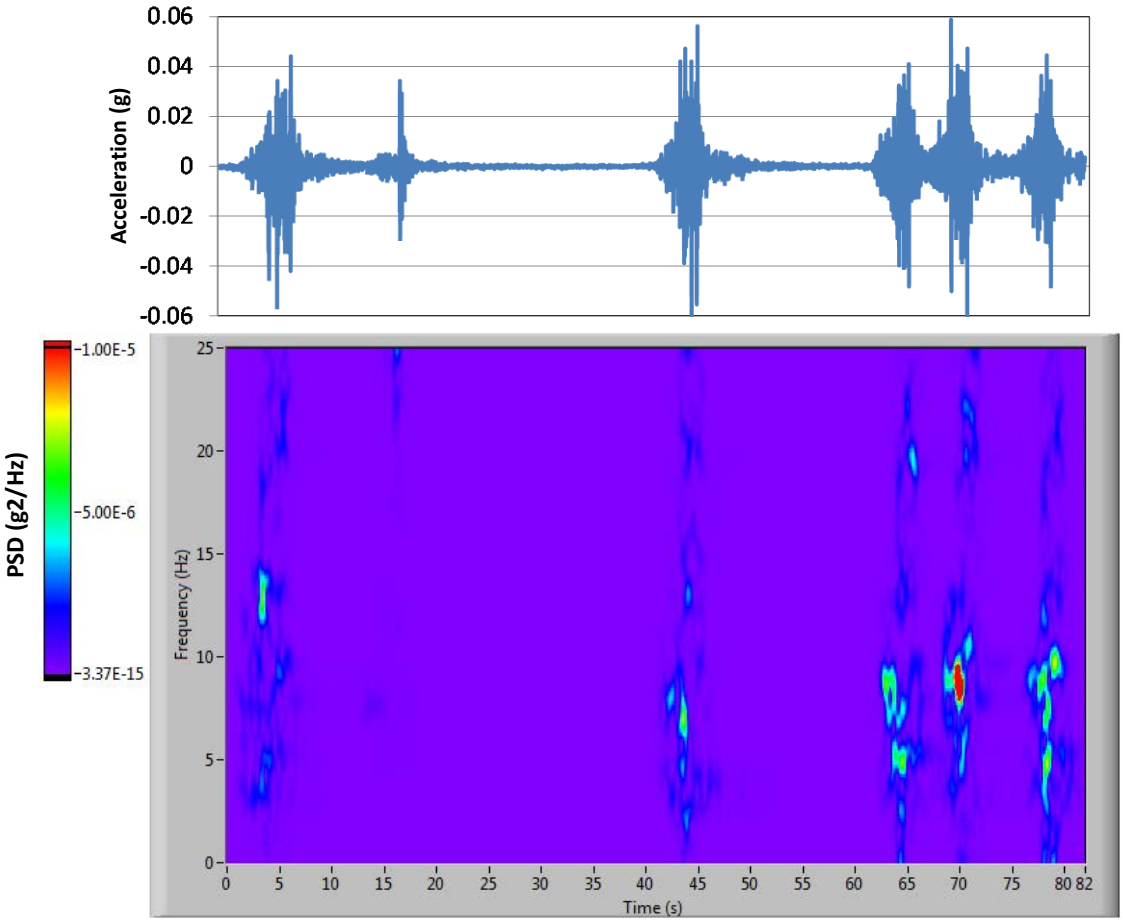

Figure 4.4 Spectrogram for sample representative acceleration data at midspan of the Medina River Bridge.

Although spectrograms are good visual aids, they do not provide a quantitative analysis of bridge dynamics. The color intensities are only relative, and should not be taken as absolute amplitudes (Hrovat, 2004). As a result, spectrograms along with PSD plots have limitations when analyzing vibrations for energy harvesting applications.

4.3 Significance and Limitations of Spectral Content

As previously stated, the main goal of this research is to determine dominant frequencies and amplitudes of bridge vibrations. Spectral analysis does provide both to a certain extent. The amplitudes of spectral analysis, namely FFTs and spectrograms, are generally relative values, and have no physical meaning. Even spectral power, which is an absolute magnitude, does not provide any useful information about real, mechanical power. In order to assess the feasibility of a vibration energy harvester in a quantitative sense, a physical model must be developed to estimate power potential in terms of familiar units like Watts.

It must be emphasized that spectral analysis is still extremely important for energy harvesting applications. Tuning frequencies of a harvester can be determined based purely on spectral content. But power output cannot be determined based on amplitudes alone. In other words, spectral analysis cannot be a standalone method. It must be coupled with some reasonable estimation of peak power and bandwidth, as is discussed in Chapter 5.

4.4 Chapter Summary

Chapter 4 outlined the basic spectral analysis techniques used throughout this thesis. Fourier transform principles and how they relate to power spectral density and spectrogram plots were described. A few examples were provided from the Medina River, US-290, and TX-71E bridges to demonstrate the difference between time-domain and frequency-domain analysis. The relationship between these was identified using Parseval's theorem, and signal bandwidth was introduced. These relationships are useful

for understanding the estimates of power potential of a vibration energy harvester that is presented in the subsequent chapters.

Spectral analysis provides important information about the frequency content of the bridge vibrations, but it lacks the capability to quantify mechanical energy. To do so, an analytical model must be established to supplement spectral analysis. Chapter 5 describes the development of the analytical model for power prediction.

CHAPTER 5
Analytical Model for Power Prediction

As suggested in Chapter 4, spectral analysis does show dominant frequencies of a vibration signal, but does not provide quantitative results for power. To estimate power potential of a vibration energy harvester based on accelerometer field data, an analytical model was developed. Using approaches from earthquake engineering, a simple model was made to quantify the energy associated with traffic-induced bridge vibrations. This chapter outlines the development of the model and explains how to reach power estimations from measured acceleration data. More specifically, discussions of the model, the numerical integration techniques utilized, power calculation methods, and the concept of response spectra are presented.

5.1 SDOF Damped Mass Oscillation

The electromagnetic vibration energy harvester, as described in Chapter 2, can be modeled as a damped, single degree-of-freedom (SDOF) oscillator. This allows the calculation of physical power from bridge vibrations. Figure 5.1 shows the SDOF oscillator schematically. The motion of the mass is governed by the well-known, second-order differential equation shown in Equation 5.1. Equation 5.2 is the equivalent expression, which has been normalized by the mass of the harvester.

The differential equation is a statement of equilibrium. The sum of the internal forces is equal to the external force applied by the source vibration (the bridge). The internal forces include the inertial force of the moving mass, the damping force, and the spring force. Note that the internal forces are all related to the motion of the harvester mass relative to the bridge, not its absolute motion. The external force is applied by the vibrating bridge component to which the energy harvester is attached. Therefore, only a small fraction of the total bridge vibrational energy excites the harvester (Section 1.2.4).

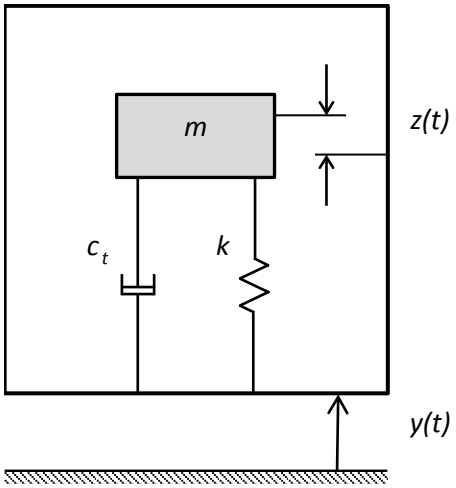

Figure 5.1 SDOF damped mass oscillator model for electromagnetic energy harvester.

$$m\ddot{z}(t) + c_t\dot{z}(t) + kz(t) = -m\ddot{y}(t) \qquad \textbf{Equation 5.1}$$

where: m = mass of magnet
c_t = total damping coefficient
k = spring stiffness
$\ddot{z}, \dot{z}, z$ = relative acceleration, velocity, and displacement of mass
$\ddot{y}$ = source (bridge) acceleration

$$\ddot{z}(t) + 2(\zeta_m + \zeta_e)\omega_h\dot{z}(t) + {\omega_h}^2 z(t) = -\ddot{y}(t) \qquad \textbf{Equation 5.2}$$

where: ζ_m = mechanical damping
ζ_e = electrical damping
$\omega_h = \frac{f_h}{2\pi}$ = harvester angular frequency

In order to solve the governing differential equation, the acceleration response of the bridge ($\ddot{y}(t)$) must be known. This term is the measured response from accelerometers. Once $\ddot{y}(t)$ is known, the relative motion (displacement, velocity, and acceleration) of the mass can be solved numerically, which is discussed in the next section. These solved variables will aid in determining the power potential of the vibrations.

Williams et al. (1997) originally developed this model for a similar application. The researchers were assessing the feasibility of an electromagnetic generator, very similar to the one designed by the UT Austin team. The model is a good mechanical-to-electrical representation of the harvester as long as the moving mass is negligible compared with the mass of the vibrating source. If the vibration of the harvester disrupts the vibration of the bridge, the model will be inaccurate.

5.2 NEWMARK-BETA INTEGRATION FOR LINEAR SDOF OSCILLATOR

The relative motion of the damped mass must be determined to estimate the mechanical energy driving the energy harvester. The governing differential equation (Equation 5.2) is typically solved by numerical integration. A common method used in earthquake engineering is the Newmark-Beta method, which is also applicable to this case.

The Newmark-Beta integration method is a time-step approach, meaning the motion of the damped mass is described at discrete intervals in time. A change in displacement, velocity, and acceleration are calculated at each time step, and are added to the values from the previous step. The change in the relative displacement of the mass is defined in Equation 5.3. The remaining calculations (Equation 5.4 and Equation 5.5) are derived based on that equation. Equation 5.6, Equation 5.7, and Equation 5.8 demonstrate that the change in motion is added to the value from the previous time step. These calculations are repeated at every point in time in the sample until the displacement, velocity, and acceleration of the translating mass relative to the bridge can be plotted as a function of time.

$$\Delta z = \frac{-\Delta\ddot{y} + \left(\frac{6}{\Delta t}\dot{z}_i + 3\ddot{z}_i\right) + 2\zeta_t\omega_h\left(3\dot{z}_i + \left(\frac{\Delta t\ddot{z}_i}{2}\right)\right)}{\frac{6}{(\Delta t)^2} + \frac{12\zeta_t\omega_h}{\Delta t} + {\omega_h}^2} \qquad \textbf{Equation 5.3}$$

$$\Delta\dot{z} = \frac{3}{\Delta t}\Delta z - 3\ddot{z}_i - \frac{\Delta t \ddot{z}_i}{2} \quad \textbf{Equation 5.4}$$

$$\Delta\ddot{z} = \frac{6}{(\Delta t)^2}\Delta z - \frac{6}{\Delta t}\Delta\dot{z} - 3\ddot{z}_i \quad \textbf{Equation 5.5}$$

$$z_{i+1} = z_i + \Delta z \quad \textbf{Equation 5.6}$$

$$\dot{z}_{i+1} = \dot{z}_i + \Delta\dot{z} \quad \textbf{Equation 5.7}$$

$$\ddot{z}_{i+1} = \ddot{z}_i + \Delta\ddot{z} \quad \textbf{Equation 5.8}$$

The damped mass is typically assumed to be at rest at the beginning of the integration. Also, a damping coefficient (ζ), a time step (Δt), integration coefficients (β, γ), and a spring stiffness (k_o) must be assigned. The damping coefficient used was 9.86% which is the same value estimated for the UT electromagnetic harvester (Section 2.4.3). The time step should be sufficiently small as to satisfy convergence criteria. Because the field data were captured at a 50-Hz sampling rate, the time step for integration was chosen as 0.02 seconds. This satisfies the convergence requirement, and, therefore, the solution does not diverge as time increases. The integration coefficients also affect the convergence and accuracy of the numerical solution. For the most accurate results, β is typically chosen as 1/6, and γ as 1/2.

The spring stiffness can either be a constant or a function of the relative displacement of the mass. For this section, only a constant stiffness is considered. In the subsequent section, nonlinear spring stiffness is discussed. For the linear case, the spring force is linearly related to the displacement of the translating mass, meaning the slope (the stiffness) of the function is constant. In other words, the spring stiffness is independent of displacement; it is always a value of k_o. By assigning a value of the spring stiffness, the natural frequency of the harvester is also assigned due to relationship between frequency, mass, and stiffness (Equation 2.1).

Note that displacement limitations could also be imposed in cases where the motion of the mass is restricted by the harvester housing. But because the analysis was conducted with consideration to the UT harvester, which is approximately 12″ in height, no limitations were needed. It is unlikely that the excited mass would displace that much.

5.3 NEWMARK-BETA INTEGRATION FOR NONLINEAR SDOF OSCILLATOR

The Newmark-Beta method can also be modified to account for spring nonlinearity. Nonlinear springs are often used in energy harvesting applications to increase bandwidth (Chapter 7), so a reliable analytical method must be developed to account for it. Numerical integration for nonlinear cases is the same as for linear cases except that an iterative subroutine must be completed at each time step to determine the current spring stiffness and harvester frequency. For linear springs, this is unnecessary because the spring stiffness and harvester frequency are constants. The spring force for nonlinear springs, however, is not linearly related to displacement.

Duffing-type nonlinearities are typically used to describe the spring force-displacement relationship (Equation 5.9). It consists of a linear term described by a linear stiffness term, k_o, and a third-order, nonlinear term described by a nonlinear stiffness coefficient, k_1. The nonlinear coefficient can be either positive or negative. If it is positive, the spring is described as a hardening spring because the stiffness increases with increasing displacements. If it is negative, the spring is a softening spring because stiffness decreases with increasing displacements. This is presented graphically in Figure 5.2. Note that the linear stiffness term is the same as the one discussed in the previous section. Also, hysteretic behavior of the spring was neglected. In other words, the spring is assumed to load and unload along the same path. Therefore, no permanent deformations occur when the energy harvester vibrates.

$$F_s = k_o z + k_1 z^3 \qquad \textbf{Equation 5.9}$$

where: k_o = initial spring stiffness
k_1 = nonlinear spring stiffness coefficient

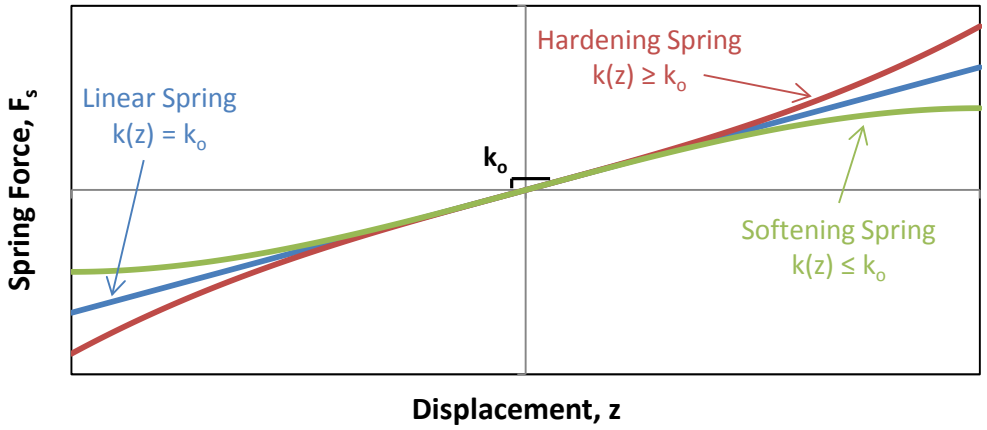

Figure 5.2 Spring force-displacement relationship comparing linear and nonlinear cases.

Equation 5.10 is the derivative of Equation 5.9, and defines the spring stiffness at any given displacement of the mass. Equation 5.11 shows that the natural frequency of the harvester also varies as displacements become large. Note that when displacement is zero, the natural frequency of the harvester is the initial, linear value.

$$k_i = k_o + 3k_1 z^2 \qquad \textbf{Equation 5.10}$$

where: k_i = spring stiffness at given time step, i

$$f_{h,i} = \frac{1}{2\pi}\sqrt{\frac{(k_o + 3k_1 z^2)}{m}} \qquad \textbf{Equation 5.11}$$

where: $f_{h,i}$ = harvester frequency at given time step, i

By adding a third-order nonlinear term to the spring force-displacement equation, the governing differential equation for the relative motion of the mass is altered, as shown in Equation 5.12. Newmark-Beta numerical integration still applies to this new differental equation as long as an iterative subroutine is incorporated to calculate the current spring stiffness. This can be done by utilizing Newton-Raphson iteration at each time step. The stiffness is adjusted within each time step until a convergence criterion is satisfied. If no iterative routine is used, the solution will likely diverge as the spring force continues to increase over time.

$$m\ddot{z}(t) + c_t\dot{z}(t) + k_0 z(t) + k_1 z(t)^3 = -m\ddot{y}(t) \qquad \textbf{Equation 5.12}$$

In any case, Newmark-Beta integration can be utilized to estimate the relative motion of a SDOF damped mass excited by a massive source. This is beneficial in determining the energy content of bridge vibrations.

5.4 CALCULATION OF POWER

Once the motion of the bridge and the harvester are known, calculating the energy imparted on a harvester by traffic-induced bridge vibrations is based on fundamental principles of physics. However, there a several stages of energy transfer during the process, so understanding what stage is being calculated is vital. Energy must be conserved starting from the moving truck and ending with electrical energy passed through a wireless node.

The kinetic energy of a crossing truck causes a bridge to vibrate. Although the energy associated with the vibration of the entire bridge is massive, only a small fraction of it is transferred to the harvester. The "input energy" is then further distributed in the harvester. Some of it is lost in the form of damping losses. The remainder of it is converted into electrical energy and delivered to the sensor node. As established in Chapter 1, the "input energy" is the major focus of this research. The efficiency of the harvester itself, the ratio of input energy and output energy, has been described in detail by Dierks of the UT mechanical engineering team (2011).

Basic principles of physics can be applied to calculate instantaneous power. Power is the product of a force and the resultant velocity. For this case, power can be computed from multiplying the inertial force of the translating mass and its velocity. The product of these time-dependent variables is instantaneous power, which is the power at a given instance in time. The total energy of that traffic-induced vibration is simply the sum of those instantaneous bursts of power. Energy can also be calculated by taking the average power over a given processing period, and multiplying by time.

In reviewing the relevant literature, there does not appear to be consensus regarding how to calculate instantaneous power. Williams et al. (1995) derived Equation 5.13 for instantaneous power of a mass moving relative to the harvester housing. Note that Equation 5.13 requires an additional integration of the measured bridge acceleration data to determine the velocity of the bridge ($\dot{y}(t)$). The form of the equation was then changed in a later paper (Williams et al., 1997). This change is presented in Equation 5.14. The difference is in the form of the velocity term. Absolute velocity is used in Equation 5.13, while relative velocity is used in Equation 5.14.

$$P(t) = m\ddot{y}(t)[\dot{y}(t) + \dot{z}(t)] \qquad \textbf{Equation 5.13}$$

$$P(t) = m\ddot{y}(t)[\dot{z}(t)] \qquad \textbf{Equation 5.14}$$

Although there appears to be a discrepancy in the literature regarding total "input power," there is no dispute over the total power delivered to the electrical load. Li et al. (2008), Roundy (2003), and Sazanov et al. (2010) all derived the same basic equation for instantaneous power to the load (Equation 5.15). The differences between the two equations above and Equation 5.15 is in the force term. The result of Equation 5.15 would be smaller than what is calculated in Equation 5.13 and Equation 5.14 because the electrical damping force ($c_e\dot{z}$) is only a fraction of the total inertial input force ($m\ddot{y}$).

$$P_{load}(t) = (c_e\dot{z})\dot{z} = c_e\dot{z}^2 \qquad \textbf{Equation 5.15}$$

Because the "input energy" prior to electrical conversion is the focus, the derivation of the power equation requires a slight adjustment to that which is presented in the literature. In combining the theories expressed above, Equation 5.16 was developed as the power calculation used throughout this thesis, and offers an expression of instantaneous power as a function of time. This formulation represents the case in which all internal forces were converted into electrical energy, not just the electrical damping force.

$$P(t) = \left[m\left(\ddot{y}(t) + \ddot{z}(t)\right)\right]\dot{z}(t) \qquad \textbf{Equation 5.16}$$

Again, frictional losses are neglected, so this equation yields upper-bound values. The efficiency of a harvester can be evaluated by comparing actual output and this maximum, theoretical value.

It must be noted that Equation 5.13, Equation 5.14, and Equation 5.16 yield nearly identical results, despite the slight discrepancies. This is demonstrated in the example provided in Figure 5.3. The procedure outlined in this chapter was used to determine the "input power" of a vibration energy harvester tuned to 4 Hz under a 0.1g, 4-Hz sinusoidal excitation. The results of Equation 5.13, Equation 5.14, and Equation 5.16 were then compared.

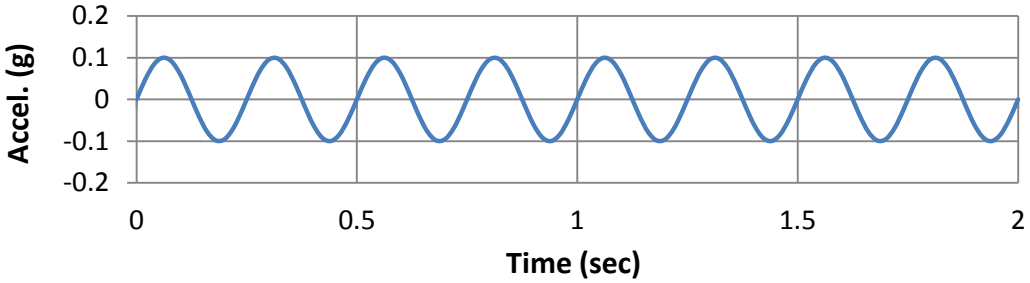

Equation	Estimated Power for 4-Hz Harvester (mW/kg)
5.13	128.44
5.14	128.436
5.16	128.439

Figure 5.3 Comparison of the different power calculations derived for a 4-Hz harvester under a 0.1g, 4-Hz sinusoidal excitation.

It can be seen that negligible differences exist between the different power equations. It is theorized that the small amount of damping within the system leads to nearly identical results between the contrasting approaches. Ultimately, Equation 5.16 was chosen over Equation 5.13 and Equation 5.14 because of its computational ease.

5.5 POWER RESPONSE SPECTRUM

The field of earthquake engineering commonly uses response spectra in design to predict the response of a structure to specific ground motions. The response is predicted at various natural frequencies of the structure. If the natural frequency of the building is the same as the frequency of the base shaking, amplitudes will be high. The stiffness (and frequency) of the structure can be designed accordingly so that the resulting amplitudes are small and resonance is avoided. The same principles can be applied to the vibration energy harvester except that high amplitudes and resonance are desired.

As mentioned in Section 5.2, the natural frequency of the energy harvester is an input to the Newmark-Beta routine. Similar to ground motion and buildings, if the natural frequency of the harvester and the bridge vibrations are the same, amplitudes are expected to be high. Higher amplitudes of the translating mass result in higher power potential of the harvester. If the power calculation routine outlined in this chapter and demonstrated in Figure 5.3 was iterated for varying natural frequencies of the harvester, a response spectrum would be developed similar to those used in earthquake engineering. The spectrum would not only show what the power potential of a given response history would be, but it would also show to which ideal frequency the harvester should be tuned. These plots provide useful information about dominant frequencies and power potential of the harvester, unlike spectral analysis which only reveals frequency content of the bridge. Based on the theory of resonance, it is expected that peaks in a bridge data FFT would match with power peaks in a response spectrum plot. The tuning frequency of the harvester should be the same or very close to the dominant modes of vibration of the bridge (Williams et al., 1997).

Besides the harvester frequency, the mass and damping properties of the harvester are the other inputs to the Newmark-Beta integration algorithm. Mass is taken as a unit value for all calculations because its value does not affect the imparted motion of the translating magnet (Equation 5.3). Also, the power formulation (Equation 5.16) can be easily scaled by the actual mass. The damping of the system, however, does have a

significant impact on the peak power output and bandwidth. Figure 5.4 is a Bode plot for a sinusoidal signal that shows power output of a system for various frequencies and damping properties.

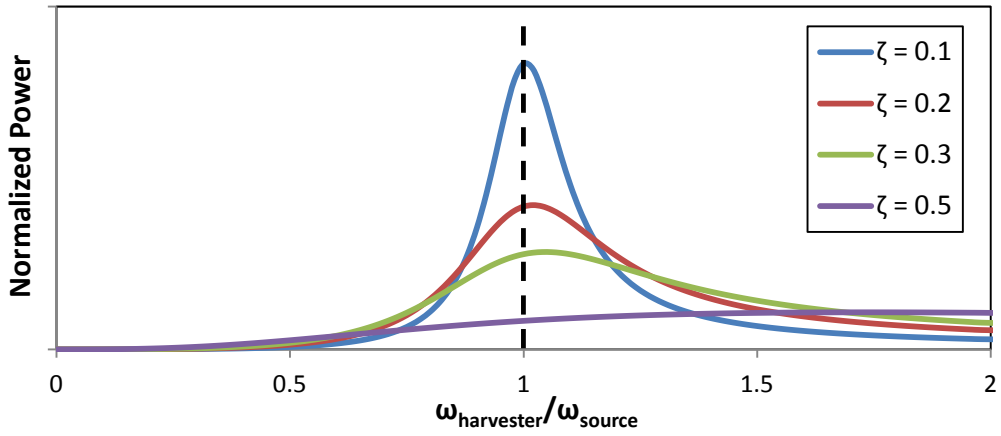

Figure 5.4 Bode plot showing power output versus harvester frequency with various damping coefficients.

For low damping, the natural frequency of the harvester and the source (the bridge) should be the same as to maximize power. At higher damping, the peak power is not only lower, but the optimal harvester-to-source frequency ratio is no longer unity. For general purposes though, it can be concluded that tuning the harvester frequency close to or slightly higher than the source vibration frequency maximizes power output whether it is a sinusoidal signal or ambient bridge data. This is also demonstrated in Figure 5.5. A response spectrum is overlaid by a FFT of the same midspan response-history sample at the US-290 Bridge. The dominant frequencies (2.0, 4.1 Hz) match for both the spectral and the analytical model analyses. Peak power output occurs at these two dominant tuning frequencies.

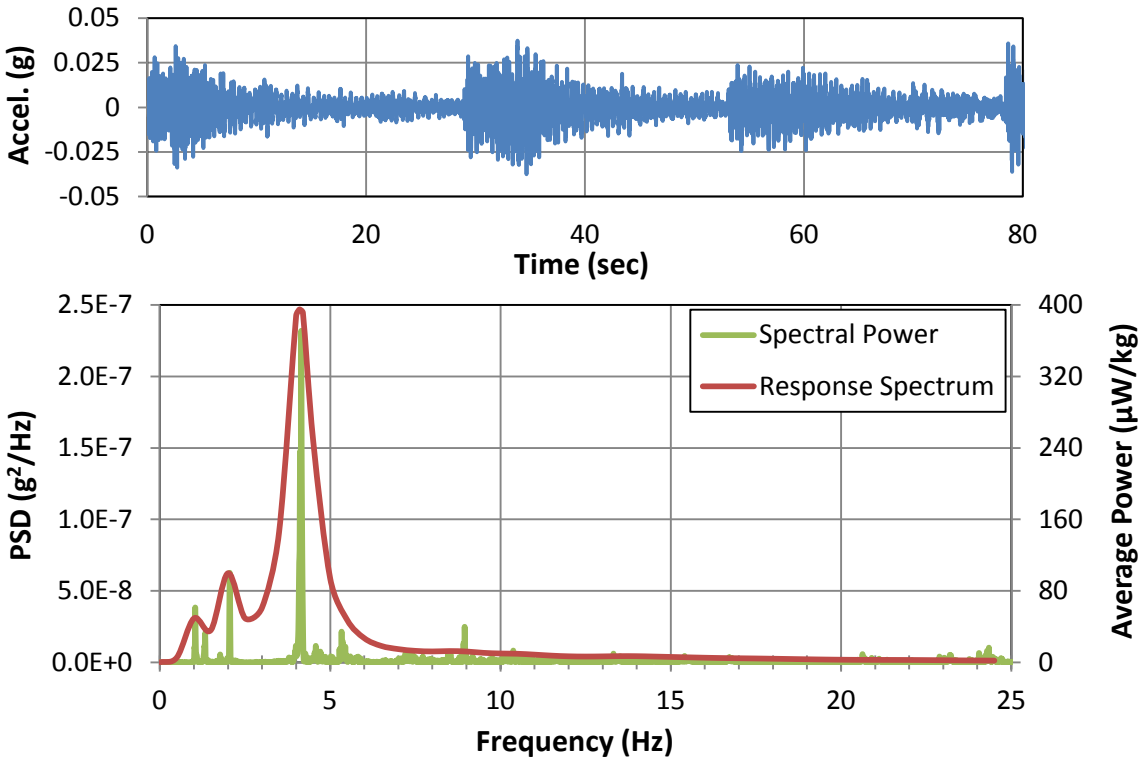

Figure 5.5 PSD curve and response spectrum of sample midspan response-history at US-290 Bridge.

Figure 5.6 shows an example of the entire process outlined in this chapter. First, raw acceleration data from midspan (floor beam 35) at the Medina River Bridge are filtered and processed, as discussed in Section 3.6.3 and 3.6.6. The acceleration response history is entered into a Newmark-Beta integration routine assuming 9.86% damping (Table 2.1), a unit 1-kg mass, and a 1-Hz harvester. The motion of the mass is estimated, and instantaneous power is computed based on Equation 5.16. The average power is then calculated as the mean of the individual instances of power throughout the response-history sample. From this, one point on the response spectrum is plotted. This process is then repeated for various natural frequencies of the harvester to develop a full spectrum. This spectrum can be modified for different damping values as well as nonlinear spring properties, but these effects are discussed in Chapter 7.

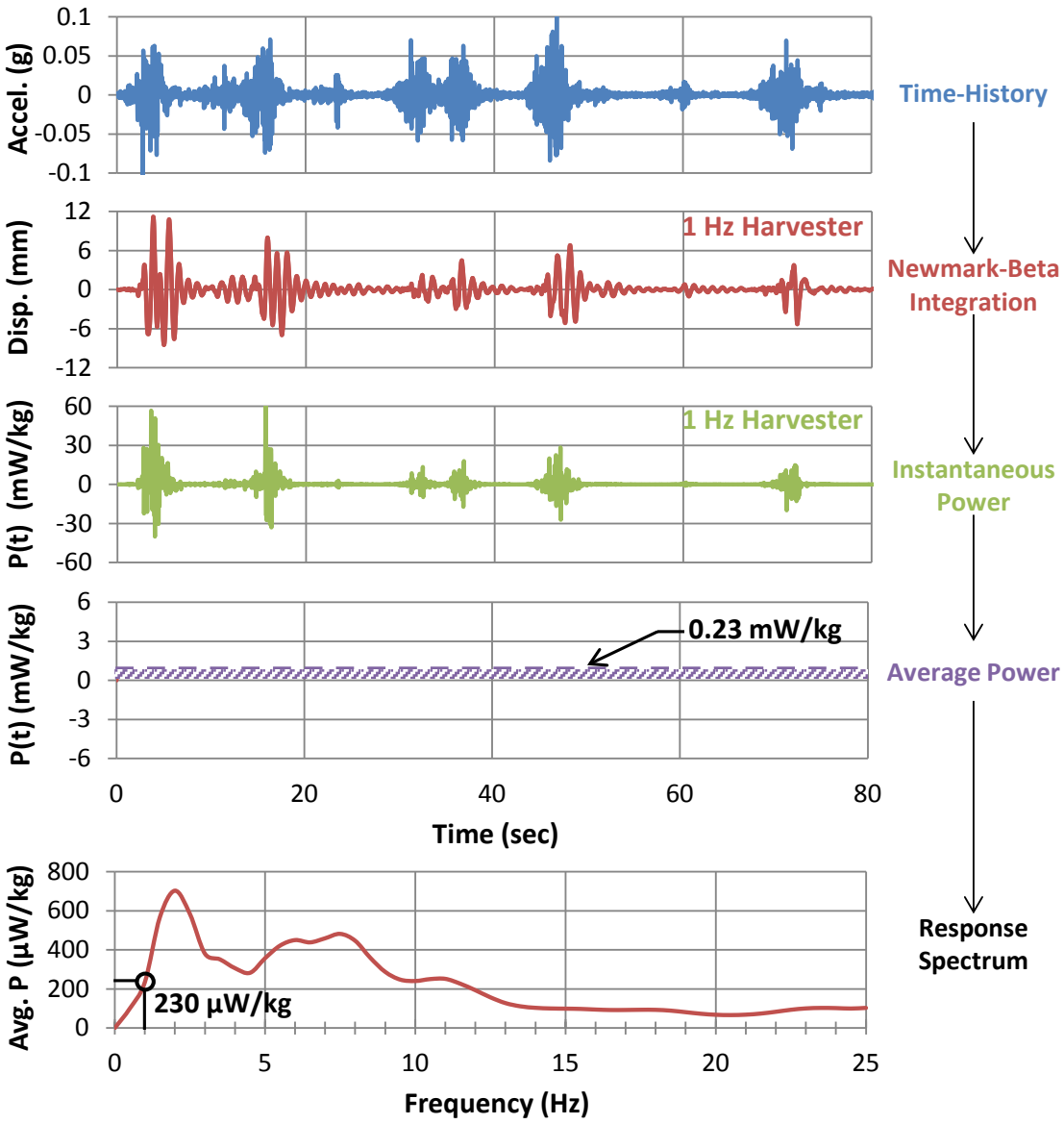

Figure 5.6 Sample procedure showing transformation of raw acceleration data into a response spectrum (for 1-Hz harvester).

5.6 CHAPTER SUMMARY

In this chapter, the development of a response spectrum was outlined and detailed. An explanation of the SDOF oscillator model and the integration techniques for linear and nonlinear springs was made. A formulation for instantaneous power was also

derived. And finally, the entire process was pieced together, and an example calculation was provided.

The response spectrum supplies useful information not only on frequency content, but also harvester power potential. Spectral analysis, on the other hand, is only capable of identifying the dominant modes of vibration of the bridge. Response spectra are very powerful tools for vibration energy harvesting applications. Chapters 6, 7, and 8 utilize these plots in developing trends and comparisons between bridges. Chapter 6, in particular, addresses variability in bridge dynamics and harvester performance due to temperature, truck traffic volume, bridge configuration and stiffness, and spatial effects. Response spectrum analyses are the basis of this investigation.

CHAPTER 6
Quantifying Variability in Data

Response spectrum analysis is a useful tool in the design of an electromagnetic vibration energy harvester. However, the frequency content and amplitudes of bridge vibrations are time-dependent, temperature-dependent, and location-specific. Power potential can be greatly affected by these factors. Because a standalone wireless sensor network with ten years of service life is envisioned, the powering system should also operate for ten years without any on-site readjustments. As a result, considerations for variability must be made when designing the harvester. This chapter describes and quantifies these effects so that the harvester parameters, namely tuning frequency and damping, can be optimized for maximum efficiency.

The chapter introduces the four main sources of variability in bridge vibration: bridge configuration and stiffness, temperature, truck traffic volume, and spatial effects. Note that bridge stiffness and temperature primarily affect the frequency content of the signal, whereas truck traffic volume affects amplitudes. Spatial effects, on the other hand, impact both frequency content and amplitudes. Because a dense array of sensors was used to monitor the response of the I-35 Medina River Bridge, much of the work presented is based on this bridge; however, the data from the TX-71E and US-290 bridges are also analyzed throughout the chapter.

6.1 Bridge Configuration and Stiffness Effects

Bridge configuration and stiffness, which are a function of the age and boundary conditions, can affect the frequency content of a bridge over time. As mentioned in Chapter 4, the tuning frequency of the harvester and the natural frequency of the bridge should be as close as possible to maximize the power generated by the energy harvester. Therefore, changes in the bridge frequency will also shift the optimal tuning frequency of

the harvester. If such adjustments are not considered, significant loss in efficiency and power can occur.

The age of a bridge is often related to the current level of damage and distress due to load cycles. As a bridge becomes more damaged, the frequency content of the structure can vary. With accumulated damage, the stiffness can change, which in turn changes the frequency characteristics. Significant work has been done in the area of damaged-induced changes to the frequency content of steel bridges.

As referenced in Chapter 2, Alampalli et al. (1995), Doebling et al. (1997), Lauzon et al. (2006), Mazurek et al. (1990), and Zhao et al. (2002) have studied the effects of damage on the frequency content of steel bridges. The researchers, in particular, have developed damage detection algorithms to monitor and track changes in natural frequencies of the structure. Much of the findings show that vibration frequencies of a bridge can change slightly as structural damage is incurred. Although substantial shifts in frequencies are unlikely, effects of age and damage accumulation are still observed in acceleration data.

In comparing the dynamic behavior of the bridges instrumented in Texas, it was observed that the Medina River Bridge possesses an extremely broadband frequency content. The other bridges have distinct modes of vibration, as revealed by an FFT of the acceleration data. Note that the Medina River Bridge, which already had a flexible structural system from design, is beyond its intended service life and is much older than the TX-71E and US-290 bridges. It is theorized that the accumulated damage and flexibility of the Medina River Bridge has widened the bandwidth of the dynamic response, as was demonstrated by Figure 4.3, and has made it more susceptible to time-dependent variables.

Changing boundary conditions, like age, can affect the natural frequencies of a steel bridge. The end restraints of a bridge can have a significant impact on the dominant vibrating frequencies that are excited. If the end restraints stiffen over time, the stiffness of the vibrating beam increases, and thus the natural frequency also increases. The natural

frequencies of a bridge are very sensitive to the boundary conditions, as was revealed by Mazurek et al. (1990). Changes in the natural frequencies of up to 30% were recorded when the support conditions of the test bridge changed. Different modes of vibration were also discovered when altering the boundary conditions. Because the bridges in Texas and Oregon on this research study were instrumented over relatively short periods of time, boundary condition effects were not detected in any of the data. Also note that boundary conditions are temperature-dependent, which are discussed in the subsequent section.

Lastly, truck mass and speed has been shown to affect the frequency characteristics of a bridge as well. In theory, a passing truck adds mass to the vibrating structure, which in turn lowers its resonant frequency. Changes in the frequency, however, are only expected if the mass of the vehicles crossing the bridge is significant compared with the mass of the bridge. A small car would not likely change the total vibrating mass enough to change the frequency appreciably. Much research on this topic has been documented in the literature.

Farrar et al. (1997) reported little change in the fundamental frequency of a bridge due to truck mass effects. It was also determined through controlled hammer and ambient tests that the source of excitation slightly affects the frequency content. Therefore, a bridge can respond differently depending on the speed and size of a passing truck. Halling et al. (2004) performed similar tests, but concluded that the differences between the frequencies during a controlled hammer test and ambient traffic were minimal. Mazurek et al. (1990) and Williams et al. (1997) investigated standard highway bridges and revealed that the frequencies of vibration are independent of truck mass and speed, but the relative intensity of a particular mode is dependent on them. Williams, in particular, showed that heavy trucks had a tendency to excite the lower modes of vibration, whereas, lighter vehicles excited higher modes.

Li et al. (2003) and Ren et al. (2010) both studied the dynamic behavior of railway bridges under railcar excitations. Li determined that the natural frequency of the

bridge decreased periodically as the train crossed, but then returned to its initial state once the train left the bridge. The decreases were found to be as high as 9% from the initial value. Ren analyzed a steel truss bridge, and found only 3% periodic changes in a few of the vibration modes. From the literature review, there appears to be no consensus on the effects of truck mass and speed on the frequency content of a bridge. Some researchers found significant changes in frequency, whereas others found that only the relative intensity of a particular mode changed.

Based on the data acquired from the five instrumented bridges, only the Medina River Bridge appears to be affected by the weight and speed of passing trucks. The near randomness of the acceleration signal alludes to these effects. To compare the measured data during ambient truck traffic with a more controlled test, a live load test was conducted in July 2011. A three-axle snooper truck, which weighed 64.9 kips in total, was driven across the bridge at known speeds. Regular I-35 traffic was delayed such that only the snooper truck excited the bridge during the test (Figure 6.1). Figure 6.2 compares the resulting PSD plots for an ambient acceleration history and a controlled acceleration history, for which the snooper truck was traveling 63 mph in the right lane. Note that a midspan accelerometer (floor beam 34) was used for both cases and that the y-axes of the plots have been normalized to unity.

Figure 6.1 Snooper truck live load test (63 mph) conducted in July 2011.

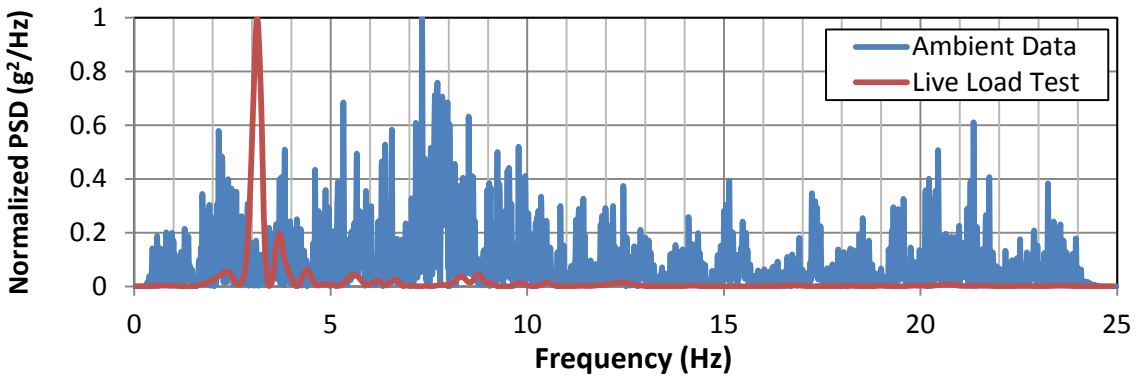

Figure 6.2 Comparison of PSD plots for an ambient acceleration history and the controlled live test (63 mph).

During the controlled live load test, one specific frequency (3.1 Hz) was excited under forced vibration. However, a wide range of frequencies were excited during the ambient tests, which include both forced and free vibration. It is theorized that the presence of several vehicles and trucks on the bridge simultaneously changes the response of the bridge because of its configuration and relative flexibility. In particular, the additional truck weight widened the bandwidth of the response.

Because of the wideband nature of its excitations, vibration energy harvesters at the Medina River Bridge also yield a wideband response. With age, boundary conditions, and truck mass effects considered, Figure 6.3 shows the differences between sample daily response spectra for midspan accelerometers at the Medina River, US-290, and TX-71E bridges assuming 10% damping. The response spectra shown are averages of data collected on Thursdays.

Note that the area underneath the spectrum and the peak value are highest at the Medina River Bridge. In other words, the total vibrational energy is greatest at Medina River, so the total energy supplied to the energy harvester is also greatest there. That energy is dissipated over a wide range of frequencies, unlike the US-290 Bridge which is mostly dissipated by just two modes of vibration (2.0 and 4.1 Hz). The wide frequency bandwidth and peak power of the harvester at Medina River is likely due to the increased

flexibility and age of the bridge. As is discussed in the next section, wide bandwidth is beneficial from an energy harvester perspective.

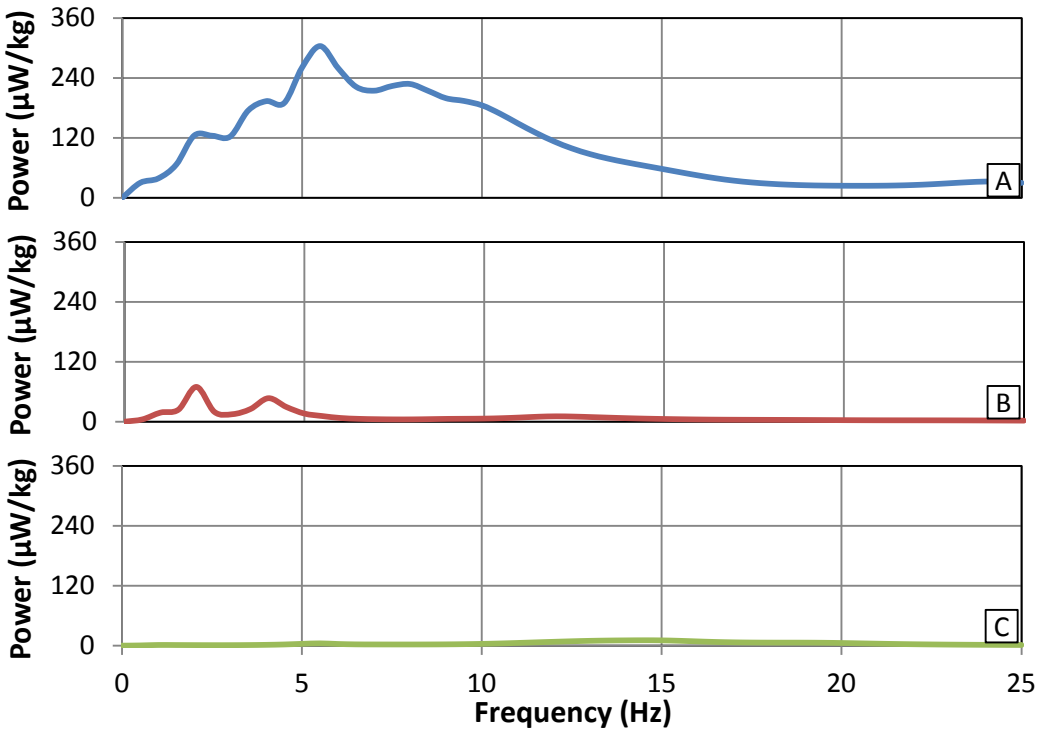

Figure 6.3 Comparison of sample response spectra for the (A) Medina River Bridge, (B) US-290 Connector Bridge, and (C) TX-71E Bridge.

6.2 TEMPERATURE EFFECTS

Similarly to changing bridge conditions, ambient temperature can shift the natural frequencies of a bridge. In theory, a decrease in temperature stiffens the structure, which results in an increase in frequency. Likewise, an increase in temperature should lower the natural frequencies. A bridge that is exposed to a wide range of temperatures can ultimately experience substantial shifts in frequencies. If these effects are not considered in the harvester design, a slight deviation between harvester frequency and bridge frequency could result in significant power loss.

Several researchers have investigated the effects of temperature on modal frequencies. Cornwell et al. (1999) and Farrar et al. (1997) found that temperature swings changed some natural frequencies of a steel bridge up to 6% over a 24-hour period. Much of this variation was attributed to differential temperature across the bridge due to its north-south orientation. Lloyd et al. (2003) tracked the first four modes of vibration of a prestressed concrete bridge for seven months. With a temperature range of 5 to 91°F, a roughly linear relationship between bridge temperature and natural frequency was discovered for three of the four modes. A 3-5% variation in frequencies was recorded. Wahab et al. (1997) also examined a prestressed concrete bridge. With a temperature range of 32 to 59°F, a 4-5% variation for each of the first eight modes was reported.

Similarly to Lloyd, Peeters et al. (2000) studied the dynamic behavior of the Z-24 steel bridge in Switzerland for one year. Frequency changes up to 18% were noted for the first four modes of vibration. However, a nonlinear relationship between frequency and temperature was discovered at very low temperatures, which was attributed to changing boundary conditions. Lastly, Zhao et al. (2002) studied a steel girder bridge and found 9-15% changes in frequency for the three lowest modes over a 4 to 55°F temperature range. A noticeable, irregular change in the trend was observed at 30°F for all modes, which was also attributed to a change in end bearings.

Similar studies were performed on the Medina River, US-290, and TX-71E bridge data. A few modes of vibration and the ambient temperature were tracked for one week at each bridge. For the TX-71E Bridge, the data were taken from the midspan accelerometer during the months of March and April 2010 when the temperature range was 45 to 85°F. The first and second modes of vibration were tracked. Figure 6.4 shows ambient temperature versus time overlaid by the second frequency versus time for the TX-71E data. Figure 6.5 compares how the first and second vibration frequencies for the TX-71E Bridge vary with ambient temperature.

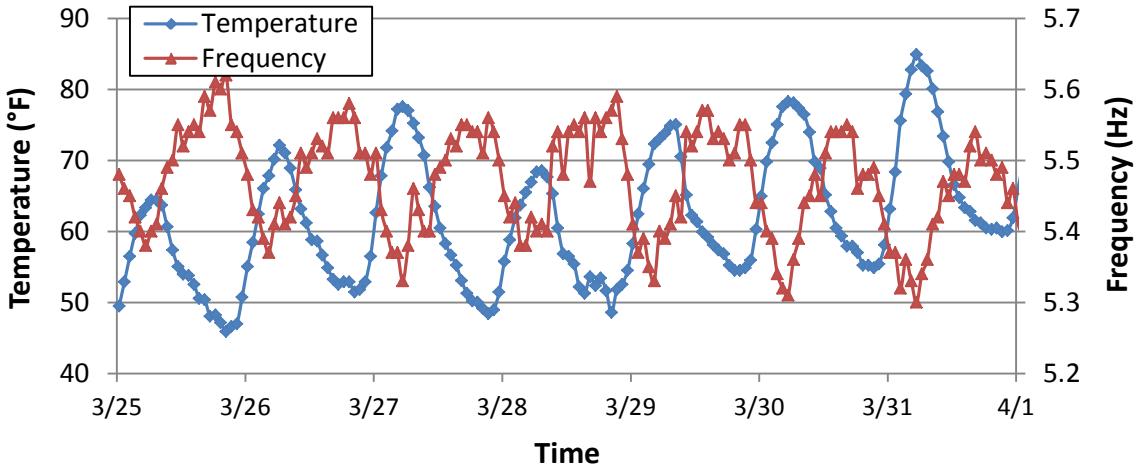

Figure 6.4 Temperature and second modal frequency tracked as a function of time for TX-71E Bridge.

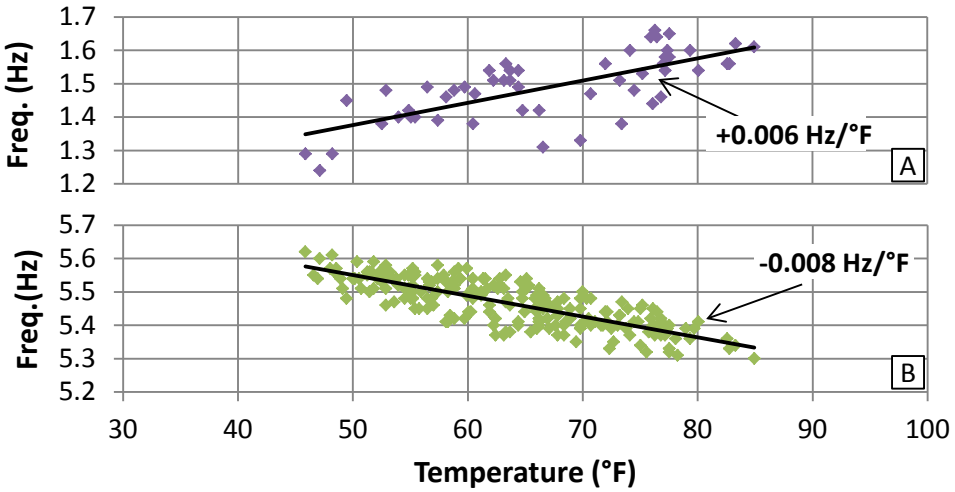

Figure 6.5 Frequency versus ambient temperature for (A) the first mode of vibration and (B) the second mode of vibration for the TX-71E Bridge.

For the Medina River Bridge, brace vibration data was used during December 2011 when the temperature range was 35 to 72°F. In this case, only the fundamental mode was tracked. Midspan girder vibration data at the US-290 Bridge was studied during July 2009 when the temperatures were between 72 and 105°F. Again, only the first mode was tracked. Figure 6.6 shows the relationship between ambient temperature

and frequency for the Medina River brace, the US-290 girder, and the TX-71E Bridge (second vibration mode).

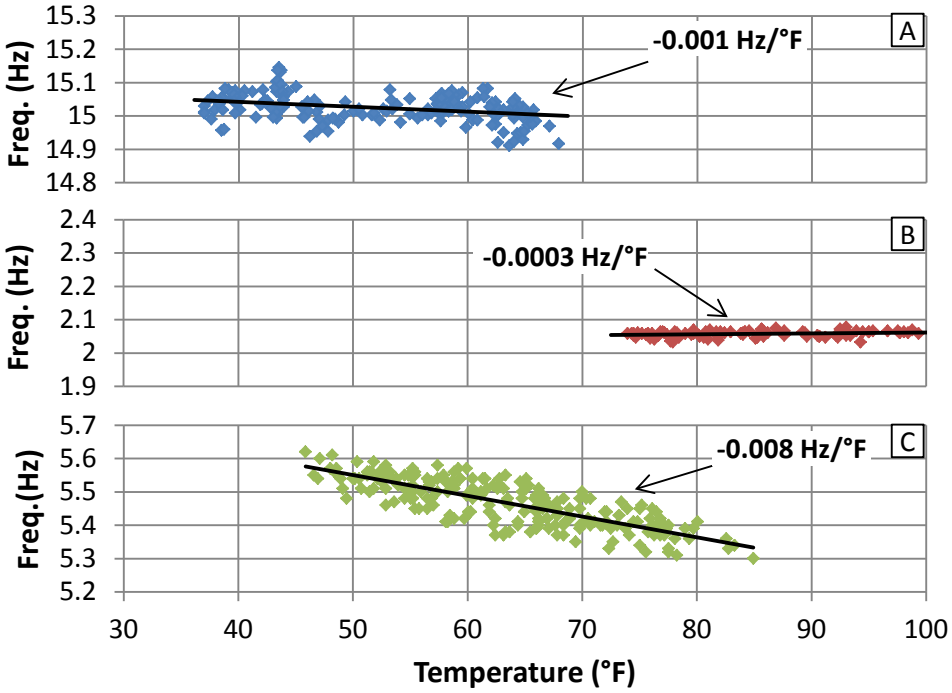

Figure 6.6 Modal frequency versus ambient temperature for (A) Medina River brace, (B) US-290 box girder, and (C) TX-71E girder (second mode).

It should be noted that the frequency curve (second vibration mode at TX-71E) is nearly the mirror image of the temperature curve in Figure 6.4. As the temperature increases during the afternoon hours, the frequency decreases, as expected. During the early morning hours, the temperatures drop and the frequency increases. However, contradictory trends are observed for the first vibration mode at the same bridge.

Figure 6.5 and Figure 6.6 take out the time variable so that a trend between frequency and temperature can be developed. For the TX-71E data, a roughly linear trend exists despite some scatter for both modes. The second frequency shifted in a negative, linear fashion and ±4% from the mean value at 65°F. However, the first frequency shifted in a positive, linear fashion and ±3% from the mean value, which is opposite of what is

expected. This demonstrates the complexity of vibration modes under different thermal conditions. Moreover, data from the Medina River brace exhibits even more scatter than the TX-71E data, and the variation with temperature is less obvious. Only a ±0.1% shift from the mean was detected over a 37-degree range. This can be considered a negligible change. The US-290 data, on the other, shows almost no correlation between the fundamental frequency and ambient temperature.

Note that frequency shifts due to temperature fluctuations are not the same across all modes. Some frequencies are influenced more than others (Figure 6.5), and some bridges experience more changes than others (Figure 6.6). Although temperature effects are not necessarily a major concern for all bridges, they should still be considered in the design of an energy harvester.

Because the harvester frequency and bridge frequency should be very close as to maximize power production, any fluctuations in the bridge frequency can negatively affect the efficiency of the harvester system. As previously stated, it is not feasible to manually alter the natural frequency of the harvester on-site during every seasonal change. Rather, the harvester should be able to account for these effects itself without losing efficiency. Ideally, the harvester should be tuned to the average frequency, and the bandwidth of the system should compensate for any temperature effects. As a result, temperature changes affect narrowband excitations more than wideband excitations as demonstrated by Figure 6.7. This plot represents a worse-case scenario with 8% variation in the frequency. In most cases, the frequency shift would be less.

From Figure 6.7, a typical Medina River response spectrum would not lose substantial power potential (5% reduction) if the harvester tuning frequency was off by ±4% from the actual, temperature-affected bridge frequency. This is because the Medina River Bridge excitations are wideband, and, as a result, the harvester response is also wideband. The US-290 Bridge response spectrum, on the other hand, shows a 35% loss in power potential due to an 8% change in the bridge frequency. Again, the US-290 Connector Bridge vibrates in a narrow band of frequencies, so the harvester responds in a

small window of frequencies too. The TX-71E, in contrast, would lose roughly 11% of power. But note that the power production at Medina River is still orders of magnitude greater than the other two because acceleration amplitudes are relatively large in comparison at that site.

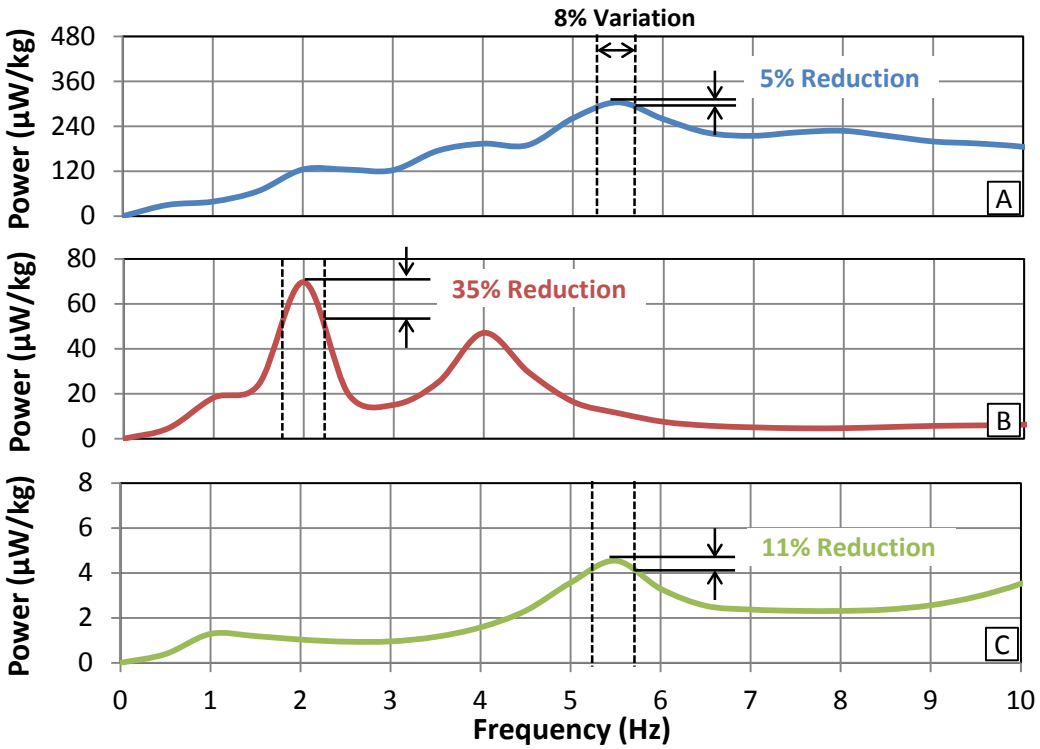

Figure 6.7 Effect of temperature-dependent frequency shifts on power production of an energy harvester.

The response spectra in Figure 6.7 were developed assuming 10% harvester damping (Table 2.1). The bandwidth of the harvester response can be widened or narrowed depending on this value. Therefore, the response of a harvester to a narrowband signal such as the US-290 Bridge can be widened by changing the parameters of the system. In that case, the effects of temperature swings would be less severe. Adjusting harvester parameters to maximize efficiency are discussed in depth in the subsequent chapter.

6.3 TRUCK TRAFFIC VOLUME EFFECTS

Unlike bridge stiffness and temperature effects which affect the frequency content, truck traffic volume affects the amplitude of an acceleration signal and, consequently, the power potential of a vibration energy harvester. As seen with spectrogram analysis in Section 4.2.4, forced vibration energy is orders of magnitude greater than free vibration energy. So quantifying the frequency of large trucks crossing a bridge is very important to assessing the feasibility of vibration energy harvesting. Even if a bridge is extremely flexible and acceleration amplitudes resulting from a single truck event are high, total power production will be low if truck traffic volume is low.

Because the root mean square (RMS) of a response history is directly related to acceleration amplitude, it is also tied to vibration power potential. As expected, harvester power is greatest when high amplitudes occur over long periods of time. Thus, the RMS of a response history and power potential are both maximum at high acceleration and low damping locations. As is demonstrated subsequently, this direct relationship between RMS and power production is useful when analyzing accelerometer data.

RMS is a good indication of truck traffic volume, as discussed in Chapter 4. This singular value can be computed for different times of the day and different days of the week to show trends in truck traffic volume over time. For example, the RMS of a sample response history during daylight hours on a weekday would likely be considerably higher than the RMS during early morning hours on a weekend. In applying the direct relationship between RMS and harvester power potential, power potential in daylight hours on a weekday is also expected to far exceed the potential during early morning hours on a weekend.

Several researchers have investigated the temporal effects of power generation for their respective energy harvesters. Li et al. (2008) tested a linear generator, similar to the UT electromagnetic harvester, on ambient bridge vibrations and compared its average power output over a 24-hour period. It was determined that average power output during the early morning hours was about 18 times less than during heavy traffic periods.

Similarly, Williams et al. (1997) found that their linear, vibration generator produced roughly 1300 times more power from a single double decker bus event than a small car event. Power generation is related to the square of the acceleration amplitudes, which explains the enormous disparity between these events. Lastly, Sazonov et al. (2010) tested a self-powered sensor on a steel bridge, and determined that Wednesday was the most active day on average, and 10 AM during morning after rush hour was the most active hour of the day.

Acceleration data from the Medina River Bridge were evaluated in the time domain to demonstrate the time-dependent nature of truck traffic volume. Figure 6.8 shows RMS acceleration values as a function of time for a midspan accelerometer (floor beam 34) at the Medina River Bridge. The RMS of the acceleration readings for an entire hour was computed for all seven days of the week. Monday through Friday data was averaged together, and Saturday and Sunday was averaged together. It can be seen that the weekdays on average see higher volumes of large trucks than the weekend days. Moreover, evening rush hour traffic (4-6 PM) produced the most truck activity, which is slightly different than the results of Sazonov. In general though, a bridge will experience highest accelerations during rush hour due to peak traffic volume, except in cases where rush hour traffic is moving at a relatively slow speed. But because the Medina River Bridge is an open I-35 corridor in a rural San Antonio area, this is not a concern.

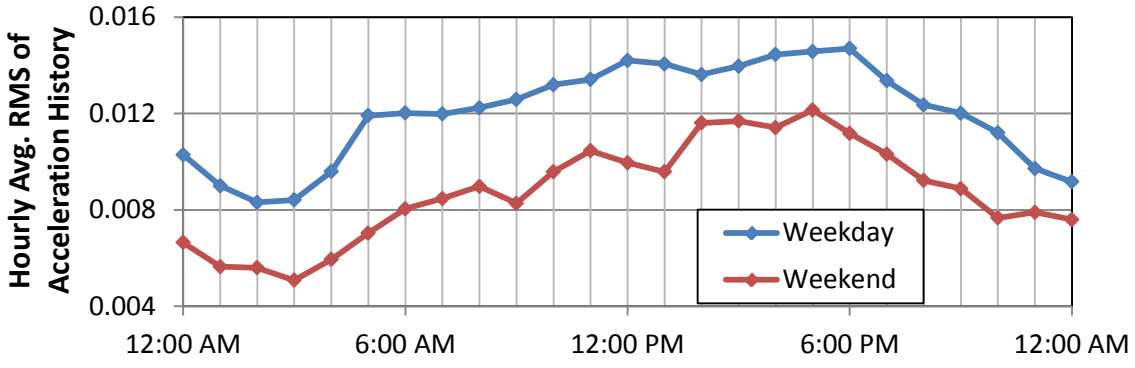

Figure 6.8 RMS vs. time for midspan accelerometer at Medina River Bridge.

Based on the trends observed in Figure 6.8, power production of a harvester during evening rush hour traffic would be expected to exceed production during the early morning. The hourly average power production was computed for an entire week at the same location (floor beam 34) at the Medina River Bridge. The weekdays and weekends were averaged separately to highlight the differences. Peak power was taken assuming the harvester was turned to 5.5 Hz because that frequency was the most stable and dominant. The results of this study are shown in Figure 6.9.

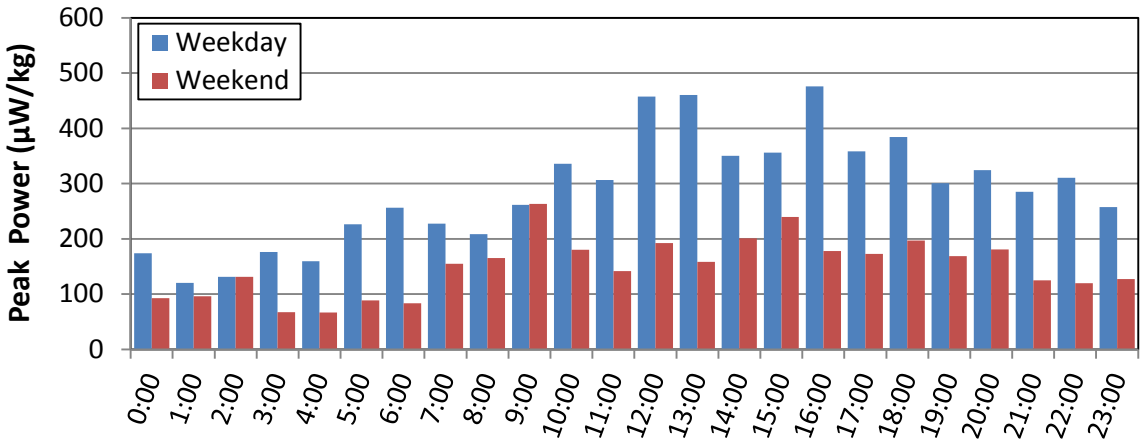

Figure 6.9 Average hourly peak production for a 5.5-Hz harvester located at midspan of the east girder (floor beam 34) at the Medina River Bridge (10% damping assumed).

Similar to the trends in the RMS acceleration data (Figure 6.8), peak activity occurs during evening rush hour during the weekdays, and low activity occurs in the early hours of the weekend. And in general, weekend production is less than weekday production for all 24 hours of the day because the traffic volume is less. In fact, the peak power production at 4 PM on a weekday is over seven times greater than peak production at 4 AM on a weekend.

To further evaluate the effects of truck traffic, full response spectra, not just peak values at one specific frequency, were computed for different times of the week. Figure 6.10 compares an average response spectrum for a weekday between 4-6 PM, representing a maximum power potential situation, and a weekend between 3-5 AM,

representing a minimum situation. Note that data from the same accelerometer (floor beam 34) at Medina River were used as in Figure 6.8 and Figure 6.9, and 10% damping was again assumed.

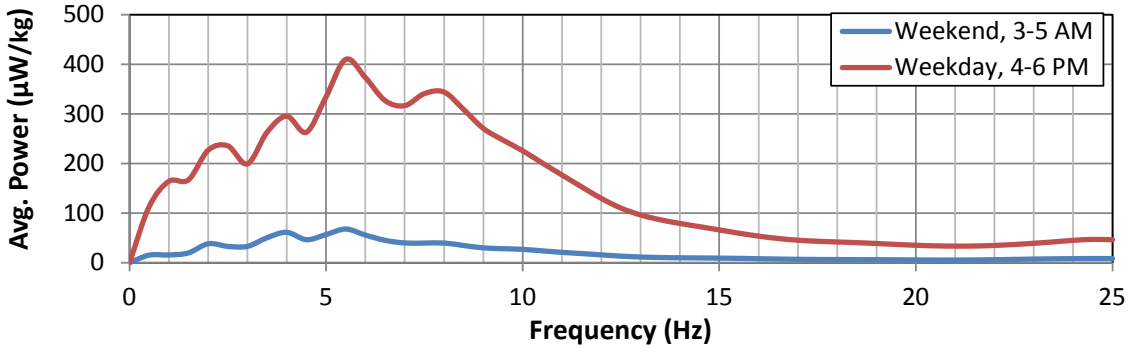

Figure 6.10 Sample average response spectra demonstrating minimum and maximum scenarios.

Figure 6.10 yields the same results as the previous two. The peak power generation at 5.5 Hz during maximum traffic conditions is nearly seven times greater than the peak power during minimum traffic conditions, as before. Also, the total area underneath the curve (total power at all frequencies) is substantially greater on weekday afternoons. This highlights the fact that power potential can fluctuate substantially depending on the time of day and the day of week. As a result, consideration for these low-traffic times must be made when assessing the feasibility of a vibration energy harvester. Energy storage during the early morning hours also becomes a priority when input into the harvester is minimal. When assessing the long-term performance of a harvester, an average weekly response spectrum is a good way to account for these low traffic times (Chapter 8).

6.4 SPATIAL EFFECTS

Another consideration to energy harvester design is that the frequency content and amplitudes of bridge vibrations vary with location along the bridge. Although natural frequencies are constant within a given span, the amplitude of vibration in each mode

varies with location. In other words, if multiple vibration harvesters are to be used on a bridge, the tuning frequencies and power production of each will not likely be the same. This behavior can be demonstrated by basic vibration theory of a simply-supported beam (Figure 6.11).

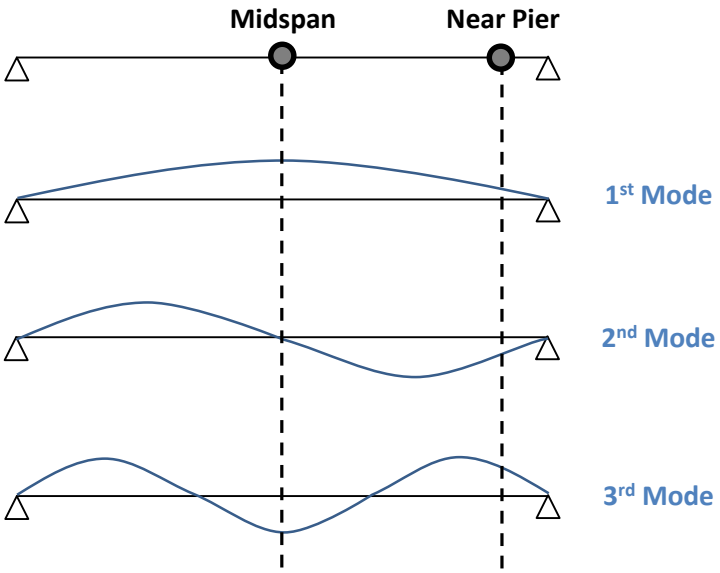

Figure 6.11 Schematic showing vibration theory of a simply-supported beam.

The first mode of vibration of a simple beam is a half-sine curve, the second mode is a full sine, and so on. At midspan, displacements for the first mode and third modes are greatest, and, as a result, the acceleration signal of this beam would be dominated by these two frequencies. Near the support, however, all three modes will be present in the signal. But the amplitudes would be smaller than at midspan. This simple example demonstrates that accelerations and vibrational energy will likely be maximum near midspan where displacements are greatest and that the frequencies contributing to the bridge vibration response vary along the length of a beam. Generally, lower modes of vibration dominate near midspan and higher modes are more prominent near the support. Galchev et al. (2011) confirmed this observation by testing a vibration energy harvester on a suspension bridge in California. They discovered that areas of maximum displacement yielded the highest power outputs. For a complex bridge, these same trends

can be seen through instrumentation and data analysis. Also note that torsional modes of vibration exist in real bridge structures.

Understanding the spatial effects of bridge dynamics through instrumentation can only be done with a dense array of sensors. In this investigation, only the Medina River Bridge was analyzed for these effects. By applying response spectrum analysis at various locations along the length of the bridge, a spatial energy plot can be developed (Figure 6.12). Average weekly response spectra at different locations (described by floor beam numbers) along both east and west girders were graphed in a 3-D color intensity plot assuming 10% damping. These are similar to spectrograms, except that time is replaced by location as the third variable. The plots shown in Figure 6.12 demonstrate the areas of highest vibration energy and the frequencies at which that energy is dissipated.

There are a few things that can be taken from this figure. First, the east girder possesses slightly more vibrational energy on average than the west girder. Heavy truck traffic typically uses the right lane, which is directly underneath the east girder. And as suggested before, higher truck traffic volume means more harvester power. Second, the vibration energy in the north anchor span is concentrated near midspan (near floor beam 35). This confirms the simple beam example presented in Figure 6.11. But the highest concentration of energy in the bridge exists just south of the hanger on the suspended span (near floor beam 25-S). This is likely due to the impact caused by a truck axle crossing the horizontal joint over the hanger (Figure 3.5b). A poor road deck surface can also increase the vibrational energy delivered to the bridge. In all cases, note that the energy is dissipated over a wide range of frequencies. The intense colors are spread over a range from 3-10 Hz. These are the same results as seen in Figure 6.3a.

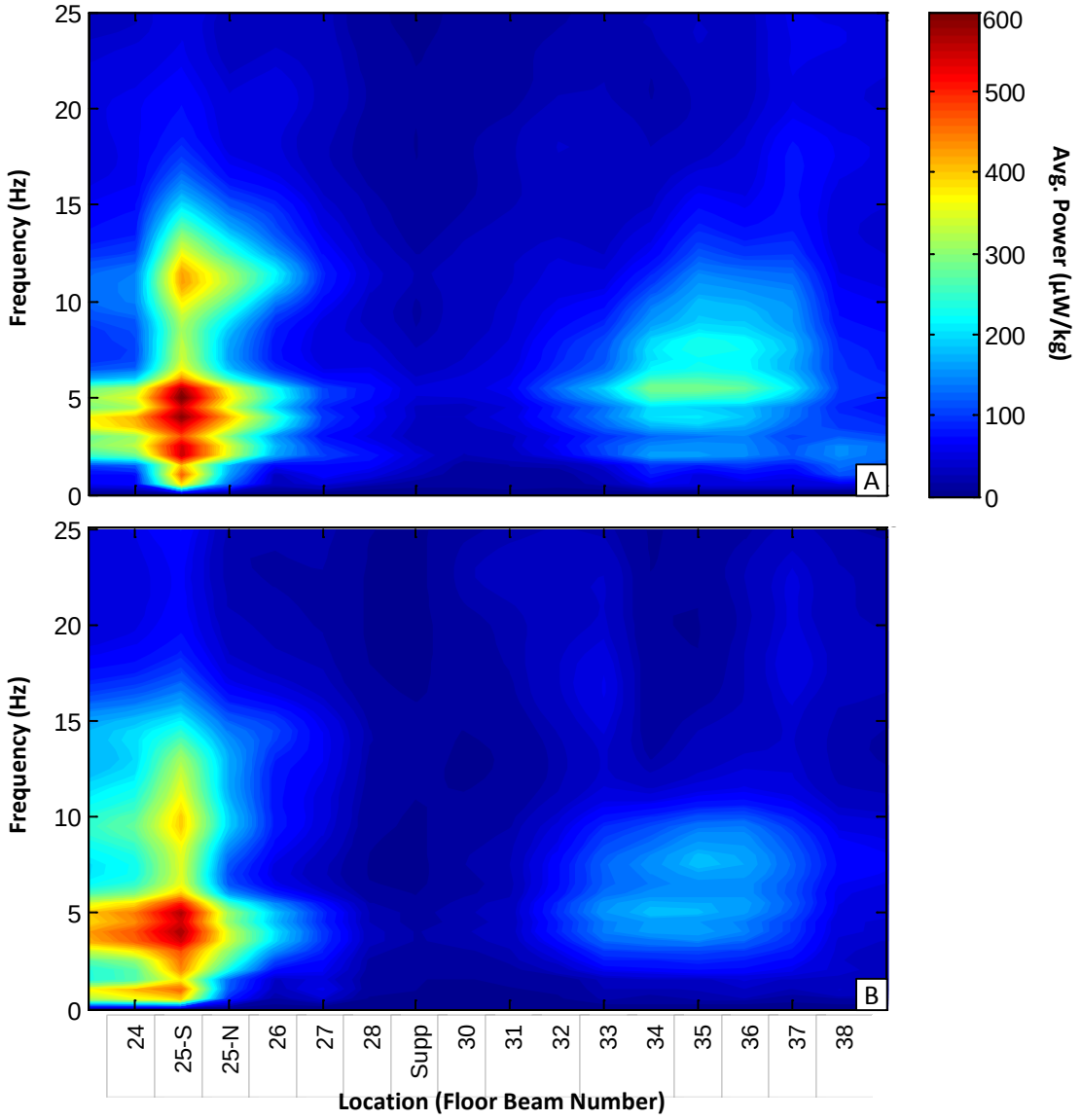

Figure 6.12 Spatial response spectrum plots for (A) east girder and (B) west girder of the Medina River Bridge.

The brace data are not shown on the spatial energy plot. Figure 6.13 compares the average response spectra for the east girder at floor beam 25-S, the highest in Figure 6.12, and for a brace in the north span. It can be seen that brace vibration has much higher energy content than girder vibration. Peak power is nearly eight times greater under brace

vibration. The dominant frequency is also much higher than girder frequency. Long, slender braces typically experience high amplitudes over a long period of time because they are extremely flexible and light in comparison to a deep girder.

As noted earlier in Chapter 3, the brace data used to develop the response spectrum in Figure 6.13 included a 13-lb weight at midspan of the member (Figure 3.11b). The added mass represents the weight of the harvester. The mass was rigidly connected to the brace in this experiment. Had the mass been vibrating, the average power would be expected to be less because the vibration of the mass would act as an active damper to the vibrating brace.

In all previous girder vibration cases, the harvester mass was considered negligible. But for a brace, this assumption is no longer valid. Figure 6.14 shows the differences in brace response if the harvester mass was not considered. With the added harvester mass, not only does the natural frequency decrease by 21% with increased mass, but the power input is also reduced by a factor of eight. The power production of a vibration energy harvester can be severely overestimated if the negligible harvester mass assumption is violated and/or is not considered. In both Figure 6.13 and Figure 6.14, 10% damping was assumed.

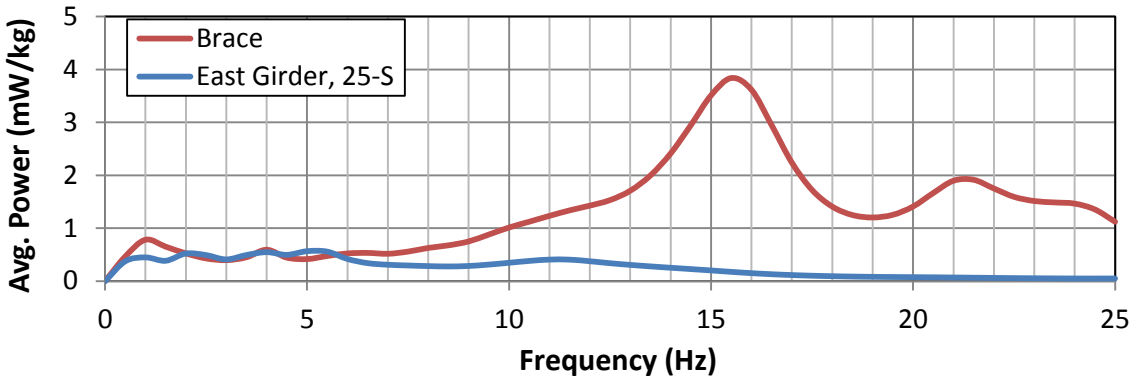

Figure 6.13 Comparison of response spectrum for east girder near floor beam 25-S and a brace in north span at the Medina River Bridge.

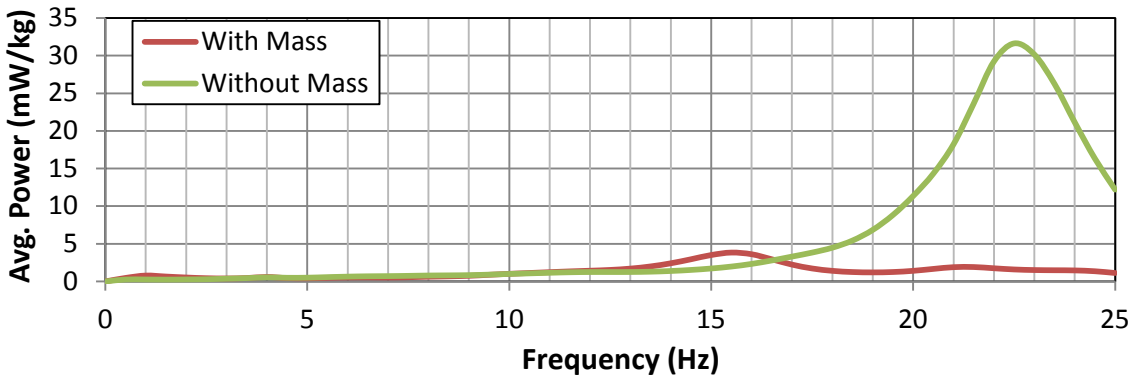

Figure 6.14 Comparison of response spectrum for brace in north span at Medina River bridge with and without 13-lb harvester mass.

In summary, spatial effects of bridge vibrations must be considered when tuning a vibration energy harvester. Although a particular frequency is dominant at one location on the bridge, it does not mean it will be dominant at another. In most cases, though, positioning a harvester on a long, slender brace will likely yield the highest energy content. The major issue is that these types of braces are not present in all highway bridges. So if such braces do not exist on a bridge, the next best location would be near a joint where impact is greatest. And if no joints are present on the deck, midspan of a longitudinal girder is likely the optimal location.

6.5 CHAPTER SUMMARY

The dynamic response, both the frequency content and amplitudes, of a steel bridge can vary over time. This chapter introduced the sources of variability and discussed how each affects the design of an energy harvester. Bridge configuration and stiffness, which are related to age and boundary conditions, and ambient temperature can affect the modal frequencies of a bridge. Truck traffic volume patterns affect the excitation amplitudes over time. And it was shown that amplitude and frequency content is not constant across the length of a bridge. Each of these has the potential to affect the power generated by a vibration energy harvester. If not considered in the design or

installation, these variables can reduce the efficiency of the system and energy can be lost.

Ideally, the harvester should maximize peak power potential, but still maintain wide bandwidth as to compensate for ambient temperature fluctuations and changing bridge conditions. Chapter 6 discussed the source of vibrational energy (the bridge) and how it can affect of the performance of a harvester. Metrics such as peak power and bandwidth were introduced. Chapter 7 focuses on the parameters of the harvester itself. Strategies on how to achieve sufficient bandwidth even with narrowband excitations will be discussed as well as the impacts of nonlinear springs.

CHAPTER 7

Quantifying Variability in Harvester Parameters

Because there is variability in the vibration source (the bridge), adjustments at the harvester level must be made to maximize power output. The influences of damping and nonlinear springs are discussed in this chapter. Both affect the bandwidth of the vibration energy harvester. As was discussed in Chapter 6, increased bandwidth widens the frequency range of the harvester response, which therefore, compensates for frequency shifts in bridge vibrations. This chapter addresses how damping and spring nonlinearity affect harvester response to bridge shaking. More importantly, the performance of the harvester as measured by peak power and bandwidth, is evaluated under different parameters.

7.1 HARVESTER DAMPING EFFECTS ON POWER POTENTIAL

The first of two adjustments that can be made to the harvester is damping. As discussed in Chapter 2, there are two forms of harvester damping: electrical and mechanical. Minimizing mechanical damping, which is a product of frictional losses within the harvester housing, is critical. These frictional losses do not contribute to the output of the system. It is beneficial to minimize these losses with friction-reducing techniques, so that the shaft can freely vibrate inside the coils. Electrical damping, on the other hand, directly relates to the power output of the system (Equation 5.15). As a result, it is desirable to maximize this value. Clearly, there is a trade-off between maximizing electrical damping and minimizing mechanical damping as both sum to total damping of the harvester. Several researchers have examined this issue, and the consistent conclusion is that matching electrical and mechanical damping is optimal (Roundy, 2003).

All of the response spectrum analysis performed thus far has been done assuming 10% total harvester damping based on the results of parametric study performed by Dierks (Table 2.1). However, the major uncertainty that is considered in this section is

the impact of different damping parameters on the performance of the idealized harvester. Figure 7.1 shows a sample response spectrum resulting from data taken from a midspan accelerometer (floor beam 35) at the Medina River Bridge. Four different harvester damping values were evaluated in this study. Unlike previous response spectrum plots, this one represents only one truck event (5-second sample).

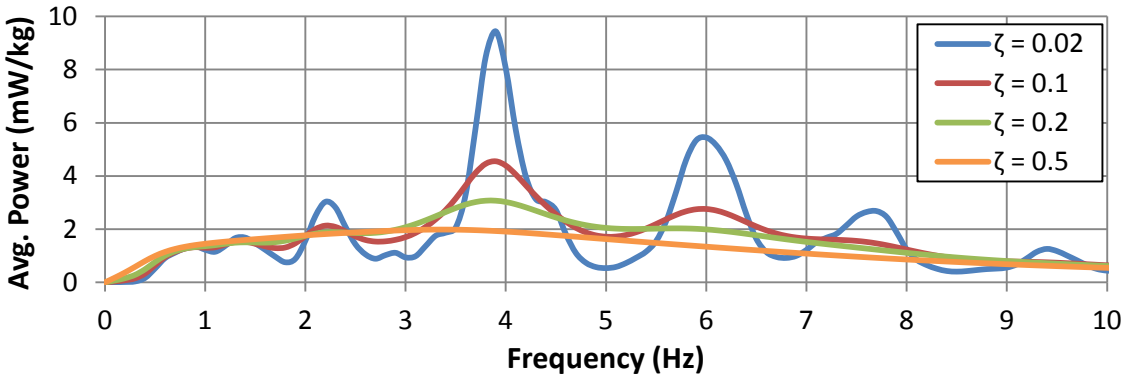

Figure 7.1 Sample response spectrum for midspan acceleration data at the Medina River Bridge showing variable harvester damping parameters.

The 2%-damping response spectrum clearly produces the highest peak power (at 3.9 Hz), as expected. However, the bandwidth around the peak frequency is relatively narrow. There are steep peaks and valleys with low damping systems. As damping increases, the peaks lower and the curves flatten, such that the bandwidth widens. From an energy harvester perspective, it is best to balance peak power and bandwidth. In ideal circumstances, the 2%-damping harvester would produce significantly more power than the 10% system. However, if the 3.9-Hz vibration mode shifted due to temperature changes, a substantial amount of energy would be lost in the 2% harvester. The 10% harvester could outperform the 2% harvester in such a scenario. Also note that the trends in this figure relate well with the Bode plot shown in Figure 5.4.

Another view of the results is obtained by examining total power input. By taking the area underneath the curves, the total power generated by the harvester is computed. As discussed earlier, the response spectrum is merely the distribution of total power over

a range of frequencies. Figure 7.2 plots the total area underneath the response spectrum curves in Figure 7.1 for all of the damping ratios that were considered. Note that total power represents the input power to the harvester, not the output. The low-damping harvester produces the most total power, as would be expected. In theory, a frictionless system should produce the most total power. But if output power was instead plotted, the results would likely be different. As previously mentioned, the electrical output power of the harvester is directly related to the electrical damping ratio. So the 2%-damping harvester that has very small electrical damping, would likely be outperformed by the other systems in this respect.

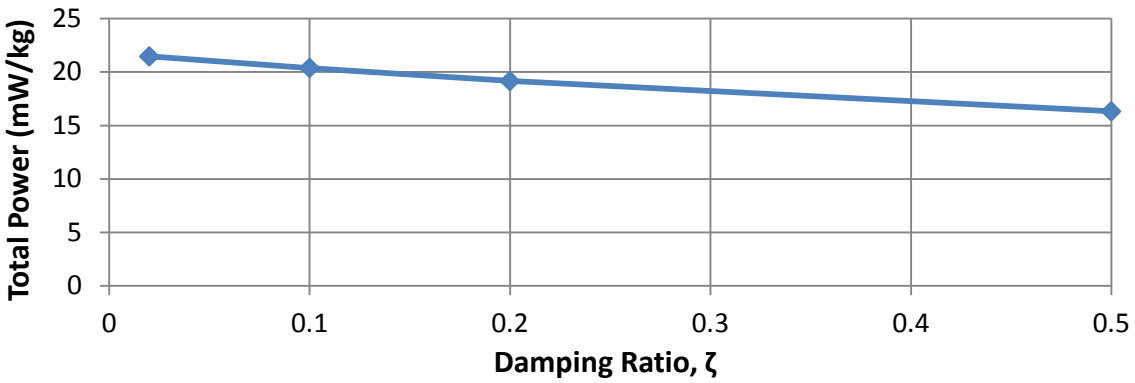

Figure 7.2 Comparison of total input power generated by harvester with different damping parameters.

Figure 7.3 and Figure 7.4 show similar trends for the effects of damping on harvester performance at the US-290 and TX-71E bridges, respectively. Increased damping reduces the peak power, but widens the bandwidth response in both cases. These trends are especially noticeable with the US-290 Bridge spectrum because the vibration source is extremely narrowband. The 2%-damping harvester at the US-290 Bridge produces a peak input power 180% greater than the 10% system. But if the bridge is very responsive to temperature- and/or time-dependent frequency shifts, those narrowband peaks would likely be an issue.

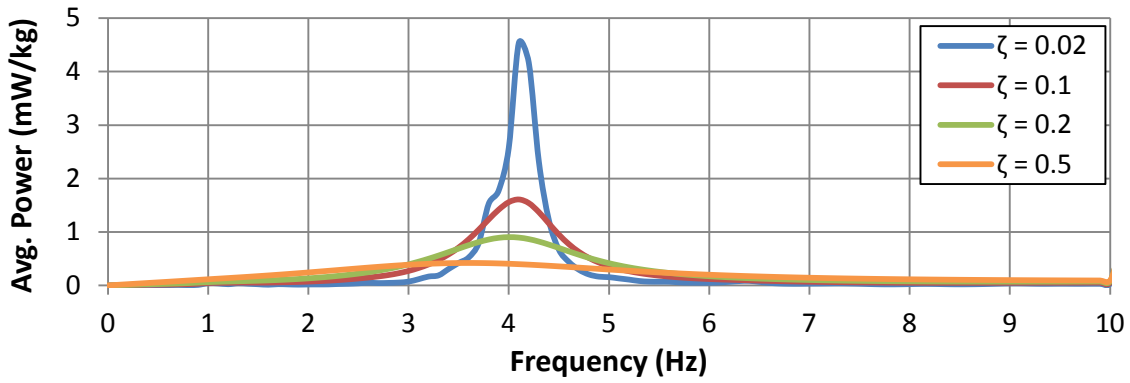

Figure 7.3 Sample response spectrum for midspan acceleration history (span 2) at the US-290 Bridge showing variable harvester damping parameters.

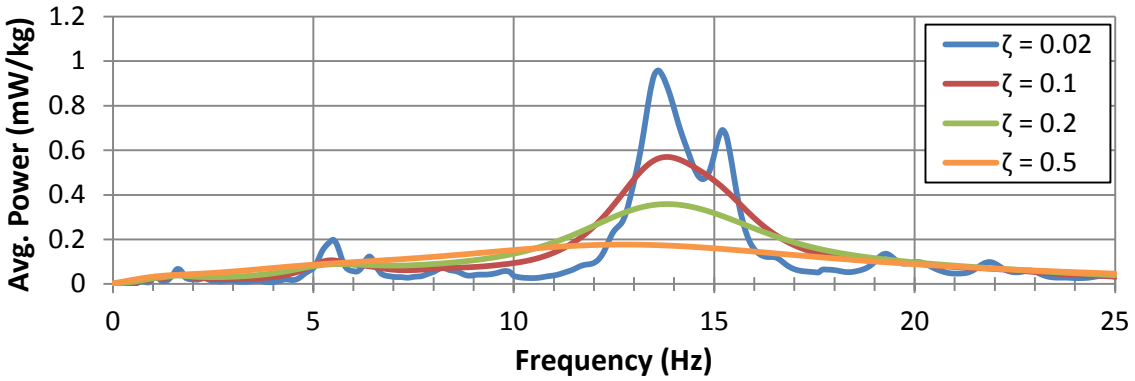

Figure 7.4 Sample response spectrum for midspan acceleration history (span 3) at the TX-71E Bridge showing variable harvester damping parameters.

Based on the results of Figure 7.1, Figure 7.3, and Figure 7.4, around 10% harvester damping appears to balance peak power and bandwidth well. The response peaks are sufficiently high and wide, such that the tuning frequency of the harvester does not need to be precisely at a single frequency. In other words, there is some room for reasonable variations or shifts in bridge or harvester behavior. These studies confirm that the 10%-damping value used throughout the thesis is valid.

Ideally, the damping of the harvester can be tailored for a specific bridge. For the Medina River Bridge, where the excitations are broadband, a lower damping value could be used without affecting the bandwidth of the harvester response too much. For the US-

290 Bridge, where the vibrations often occur at 2.0 and 4.1 Hz specifically, an increased damping ratio could be used to widen the harvester response around those specific frequencies. On average though, around 10% total damping is ideal for the peak power/bandwidth compromise, which is why this value was carried out through all response spectrum analysis in this thesis.

7.2 NONLINEAR SPRING EFFECTS ON POWER POTENTIAL

A second adjustment that can be made to a harvester is in the spring characteristics. As briefly discussed in Chapter 5, nonlinearities introduced to the spring stiffness affect the motion of the damped mass within the harvester. This nonlinearity has been theorized to widen bandwidth of a system without reducing peak power.

A significant amount of work has been done investigating the effects of nonlinear springs on energy harvester performance; however there are no well-established conclusions on the effects. Some work in the literature support the beneficial qualities of nonlinear springs, while others reject it. For instance, Cottone (2007), Marzencki et al. (2009), and Nguyen et al. (2010) all reported some benefits to using nonlinear springs in their vibration energy harvesters. Cottone applied Duffing-type nonlinear springs to a piezoelectric vibration harvester, and discovered that peak power of the nonlinear system was six times that of the linear case for white noise excitation. He found that the harvester did not need to be tuned to a specific frequency because bandwidth was significantly improved. Marzencki et al. (2009) developed a passive frequency adaptation device for a high-amplitude energy vibration harvester. Nonlinear springs proved to be more robust because frequency adaptation controlled displacements even under large acceleration amplitudes. Also, improvements in bandwidth were reported. Lastly, Nguyen et al. (2010) conducted numerical studies on both softening and stiffening nonlinear springs and found that the highest peak power and widest bandwidth occurred with nonlinear softening springs.

On the contrary, several researchers have rejected the premise that nonlinear springs improve the performance of a vibration energy harvester. Barton et al. (2010) conducted experiments with a nonlinear vibration energy harvester on a shaker table. Bandwidth was successfully widened for consistent vibration sources (sources with nearly constant amplitude and constant frequencies). However, such improvements have not been found for ambient sources of vibration such as bridges. Daqaq (2010) concluded that the performance of a harvester was unaffected by Duffing-type spring nonlinearities under constant vibration sources, and was worse in random vibration environments. Dierks (2011) performed similar shaker table tests as Barton, and found that a linear harvester outperformed a nonlinear harvester by a factor of three in peak power output. Lee et al. (2010) also showed that nonlinear springs are more useful for sinusoidal signals than for ambient bridge vibrations.

A discrepancy in the literature exists regarding the benefits of nonlinear springs on the peak power and bandwidth of a harvester. As a result, the effects of nonlinear springs on response spectrum analyses were evaluated. Data from instrumented bridges were analyzed assuming Duffing-type nonlinearity for the harvester. The procedure outlined in Section 5.3 was used in developing nonlinear response spectra. Similar to the previous work, peak power and bandwidth are the two key metrics of this study.

Prior to analyzing acquired bridge data, the effects of nonlinear springs on a sinusoidal signal were evaluated. A sine wave with an amplitude of 0.1g and a frequency of 4 Hz was used as the input motion. As demonstrated in Equation 7.1, an extra nonlinear spring force term is added to the governing differential equation of motion for the damped mass. The spring force at any given time is described by a first-order linear term with an initial spring stiffness, k_o, and a third-order nonlinear term with a nonlinear spring stiffness constant, k_1, as shown in Equation 7.2. A positive k_1 term means that the spring stiffens with increasing displacements, and a negative k_1 term means that it softens with increasing displacements (Figure 7.6). As previously discussed, the initial stiffness, k_o, is directly related to the initial harvester frequency, f_o. That means the

natural frequency of a stiffening spring would increase with increasing displacements, and the frequency of a softening spring would decrease with increasing displacements (Figure 7.7). Again, hysteretic behavior of the spring was neglected. All three cases (linear, stiffening, and softening) were examined in the sinusoidal study.

$$m\ddot{z}(t) + c_t\dot{z}(t) + k_0 z(t) + k_1 z(t)^3 = -m\ddot{y}(t) \qquad \textbf{Equation 7.1}$$

$$F_s = k_o z + k_1 z^3 \qquad \textbf{Equation 7.2}$$

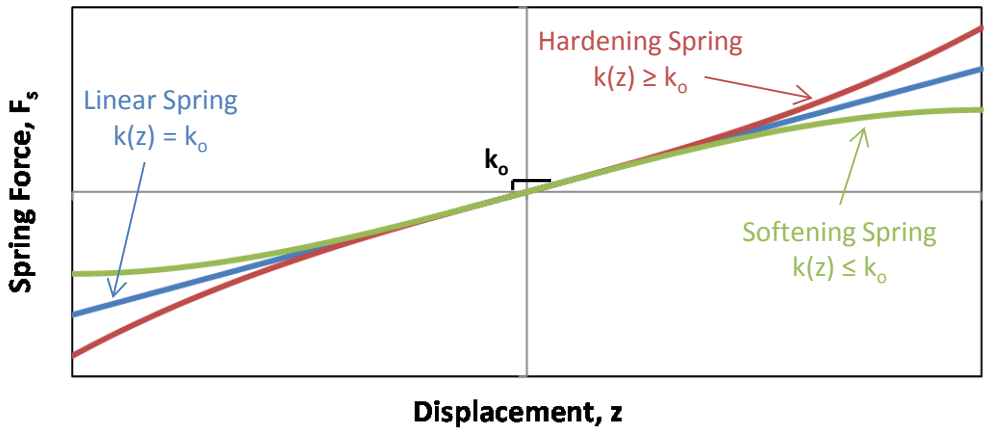

Figure 7.5 Spring force-displacement relationship comparing linear and nonlinear cases.

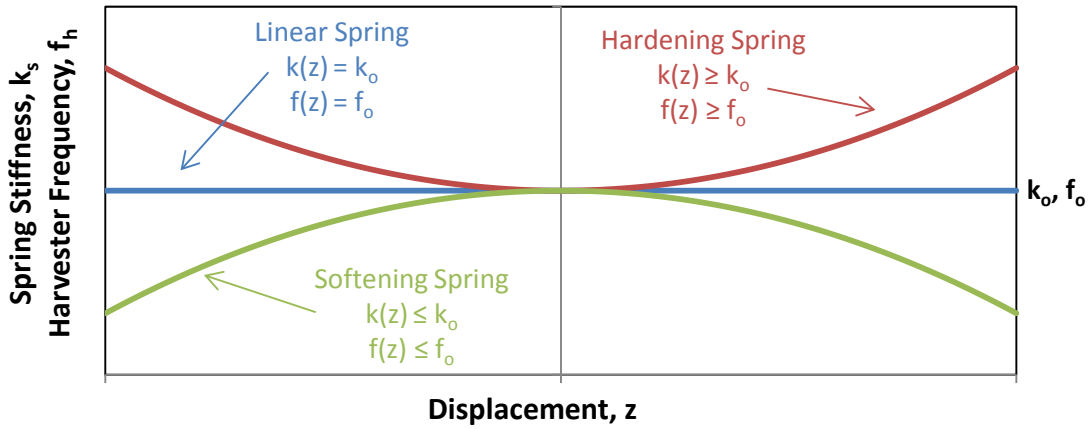

Figure 7.6 Spring stiffness-displacement and harvester frequency-displacement relationships comparing linear and nonlinear cases.

Figure 7.7 shows the results of applying harvester nonlinearity under a 0.1g, 4-Hz sinusoidal motion. Note that the x-axis varies with the initial natural frequency of the harvester, f_o. In other words, the x-axis varies with k_o, and the difference between the individual curves is the nonlinear stiffness constant, k_1.

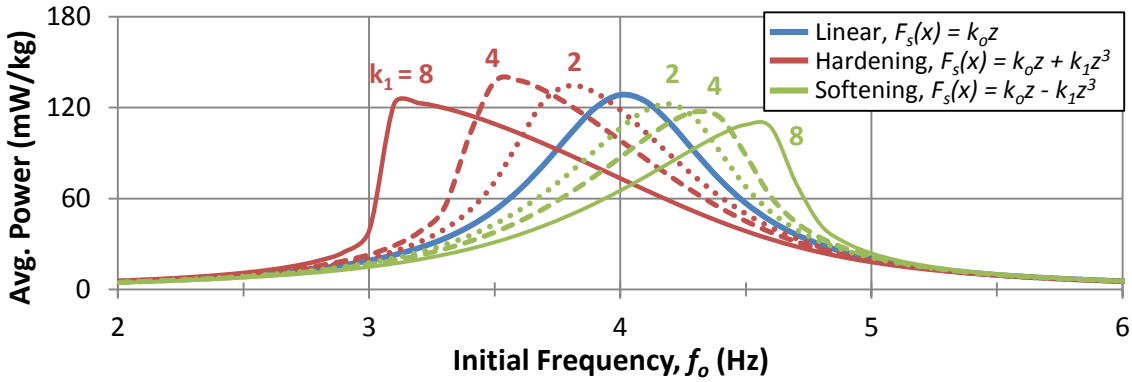

Figure 7.7 Effects of spring nonlinearity on the response spectrum corresponding to a sinusoidal input motion, $\ddot{y}(t) = 0.1 sin\left(\frac{4t}{2\pi}\right)$.

There are a few things to note from this figure. First, the power peaks of the response spectrum shift left for stiffening springs and right for softening springs. At large displacements, the spring stiffens or softens depending on the value of k_1. This, in turn, changes the natural frequency of the harvester. Therefore, the behavior of a spring changes under deformation, leading to a change in the response spectrum. For example, a linear harvester (k_1 = 0) achieves maximum power when its initial frequency is tuned to 4 Hz because the source also vibrates at 4 Hz. But, a nonlinear harvester with a k_1 value of +8 kg/(s^{2}mm^2) achieves its peak power when its initial frequency is tuned to 3.1 Hz. If that same nonlinear harvester were tuned to 4 Hz instead, nearly half of the power production would be lost. That is because under a large, constant-amplitude source like this sinusoidal example, the nonlinear range tends to dominate behavior. And although the nonlinear harvester may have started with an initial frequency the same as the source (4.0 Hz), its deformed frequency is actually stiffer. As described previously, maximum

power occurs when the harvester frequency and source frequency are close, whether the harvester is in an undeformed, initial state or a deformed, stiffened state.

Moreover, stiffening springs proved to outperform linear or softening springs under a sinusoidal vibration. The area underneath the curve and the peak power both increase with stiffening springs, but only for certain levels of nonlinearity. For softening springs, both performance measures decreased in this analytical model. Figure 7.8 illustrates these results.

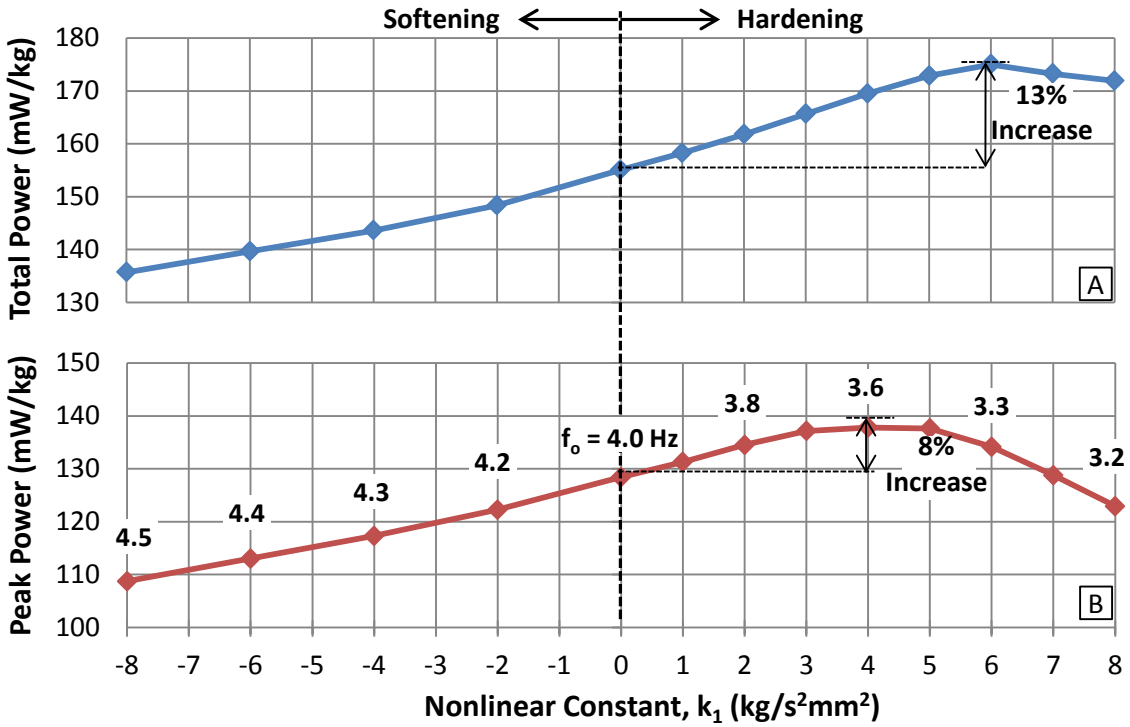

Figure 7.8 Effect of spring nonlinearity on (A) the total power production and (B) peak power of a vibration energy harvester under a sinusoidal motion, $\ddot{y}(t) = 0.1sin\left(\frac{4t}{2\pi}\right)$.

For the linear harvester (k_1 = 0), the total area underneath the response spectrum for the 0.1g, 4-Hz sinusoidal signal is 156 mW/kg, and the peak power, which corresponds to an initial frequency of 4.0 Hz, is 128 mW/kg. Both performance measures decrease as the nonlinear constants becomes more negative. But for k_1 = +6, total power

generated is maximum, and for k_1 = +4, the peak power is maximum when the initial tuning frequency is 3.6 Hz. However, as the spring becomes more nonlinear beyond those maximum points, the performance of the harvester diminishes. From a design standpoint, an initial tuning frequency between 3.3 and 3.6 Hz and a nonlinear constant, k_1, between 4 and 6 kg/s^{2}mm^2 would outperform a linear, 4-Hz harvester and would yield the most efficient results. Both bandwidth and peak power are optimized in these ranges. In summary, the spring parameters can be optimized to achieve 8-13% increase in the two key performance measures, bandwidth and peak power, for a uniform, 0.1g sinusoidal excitation. But when applying the same analysis to ambient excitations such as bridge vibrations, the results are less promising.

Figure 7.9, Figure 7.10, and Figure 7.11 show sample response spectra for a single truck event (5-seconds sample) at the Medina River, US-290, and TX-71E bridges, respectively. Because stiffening springs were found to outperform softening springs, only stiffening types were included in the analysis. Note that two different nonlinear constants (k_1 = 5, 10 kg/(s^{2}mm^2)) were analyzed in the Medina River response spectrum, whereas only one constant (k_1 = 10 kg/(s^{2}mm^2)) was analyzed in US-290 and TX-71E spectra. Note that 10% damping was assumed in these plots.

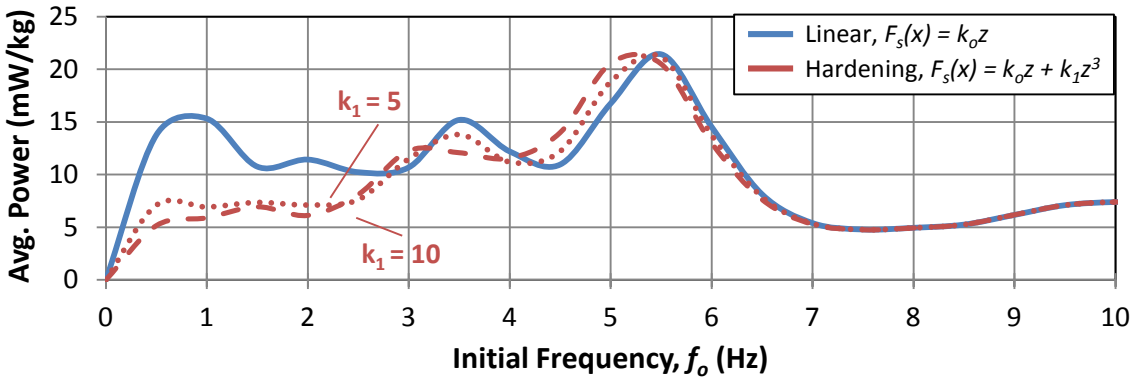

Figure 7.9 Effects of spring nonlinearity on the response spectrum of midspan accelerometer (floor beam 35) at the Medina River Bridge.

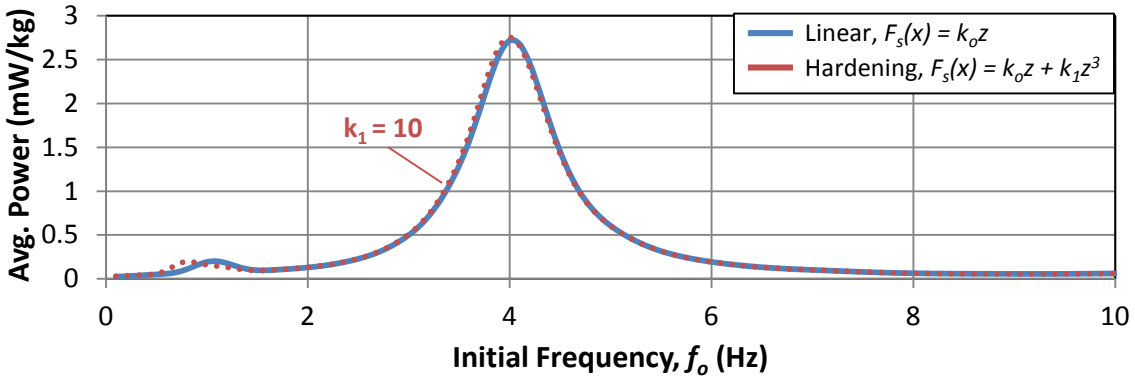

Figure 7.10 Effects of spring nonlinearity on the response spectrum of midspan accelerometer (span 2) at the US-290 Bridge.

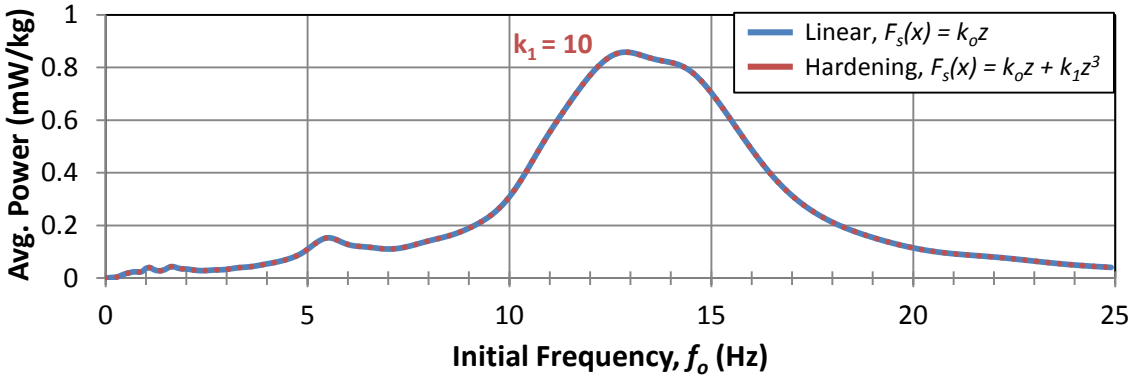

Figure 7.11 Effects of spring nonlinearity on the response spectrum of midspan accelerometer (span 3) at the TX-71E Bridge.

There are two more trends about spring nonlinearity that can be established with these figures. First, spring nonlinearity affects lower frequency harvesters more than higher frequency ones. Referring to Equation 7.2, there is a linear and a nonlinear term that make up the total spring force. When the initial stiffness of the spring, $\boldsymbol{k_o}$, is high, displacements are small, and the system is generally kept in the linear range. Because of this, the first-order linear term tends to dominate the third-order nonlinear one, and the nonlinear harvester response at those frequencies is nearly identical to the linear response. Conversely, an initially flexible spring will displace large amounts under bridge excitations, and, as a result, the cubic term of Equation 7.2 will dominate the linear term.

In this case, the nonlinear response spectrum at lower initial frequencies would be different than the linear response. This behavior is demonstrated in all three response spectra, especially in Figure 7.9 and Figure 7.10. In both cases, the difference between the linear response and the nonlinear response above an initial harvester frequency of 7 Hz is negligible.

Secondly, the benefits of nonlinear springs are dependent on the amplitudes of the signal. If acceleration amplitudes are small, like those at the US-290 and TX-71E bridges, spring deformations will also be small. At small deformations, the spring stiffness and harvester frequency never drift too far from their initial values. Therefore, the response of a nonlinear harvester to a low-amplitude bridge vibration will be nearly identical to a linear harvester, as demonstrated by Figure 7.10 and Figure 7.11. A dramatic change in the response spectra of US-290 and TX-71E would only occur at extremely large and likely unrealistic values of $\boldsymbol{k_1}$. Because acceleration amplitudes at the Medina River Bridge are comparatively high, the effects of nonlinear springs are noticeable. Although noticeable, Figure 7.9 shows no significant improvement in peak power and actually a reduction in bandwidth. Similar to the findings of Barton et al. (2010) and Lee et al. (2010), the performance of a vibration energy harvester is found to be unaffected by nonlinear springs under low-amplitudes excitations such as bridge vibrations.

7.3 CHAPTER SUMMARY

Because of the variable nature of traffic-induced bridge vibrations, the parameters of a vibration energy harvester must be adjusted to maximize power potential and bandwidth. Harvester damping and spring nonlinearity have both been proposed to achieve improved performance. Based on the findings of this research, harvester damping can be adjusted on a case-by-case basis to find the ideal balance between peak power and bandwidth. The level of required damping is dependent on the bandwidth of the excitation source, but 10% damping is generally a good value. Spring nonlinearity

showed great promise for high-amplitude sinusoids, but failed to improve performance significantly from the linear case under ambient bridge excitation.

It is suggested that a linear harvester with around 10% total damping be used for most highway bridge applications. This conclusion is in agreement with the parameters developed by Dierks (2011) and used in all response spectrum analysis in the thesis so far. Chapter 8 applies the information form this chapter to long-term analysis of bridge vibrations. From this, a feasibility assessment of vibration energy harvesting for typical highway bridges can be made.

CHAPTER 8

Assessing Long-Term Harvester Power Potential

As discussed in Chapter 6, the frequency content and amplitudes of bridge vibrations change with time. Consequently, the optimal tuning frequency and power production of a harvester can also change. Because the wireless monitoring system is targeted for a ten-year service life, the performance of the energy harvesting system must supply adequate power over that entire time. Therefore, long-term performance of the harvester is essential and must be understood. So far in this thesis, the response spectrum analyses have focused on short-term results. In order to assess the long-term feasibility of a vibration energy harvester, all the variables discussed (bridge configuration and stiffness, temperature, and truck traffic volume) should be taken into account. This chapter introduces a method to estimate long-term power production with consideration to these vibrational variations. Average weekly response spectra not only consider variability in the data, but also provide an indication of long-term power production and long-term stable frequencies. This analysis is described in this chapter. Long-term response spectra analyses will then be used to compare the response of all five instrumented bridges. Based on these results, the feasibility of a vibration energy harvester at the bridges is discussed.

8.1 Advantages of Long-Term Analysis

In order to assess the feasibility of a vibration harvester, performance must be evaluated over the long term. Basing the design of an energy harvester on a few hours of data is inappropriate. As demonstrated in Figure 6.6, there is a huge disparity between harvested power during rush hour traffic and during the early morning hours. If only rush hour performance results are considered, power production will be severely overestimated. Such a mistake might in fact be the difference between a feasible solution

and an unfeasible solution to power needs. The best technique to handle these fluctuations in power production is computing a weekly average response spectrum.

Procedurally, long-term analysis can be done by computing response spectra at a given location on a bridge and averaging them over different hours of the day. From this, a single response spectrum can become a daily average and even a weekly average. Bridge configuration, temperature effects, and truck traffic patterns are all accounted for when the averaging occurs. The resultant weekly average power spectrum provides two major metrics: long-term, stable frequencies and long-term power production. And because frequency and power production tend to fluctuate more on a day-to-day basis than a week-to-week basis, a weekly average can potentially be extrapolated to a monthly average or even a yearly average. Therefore, the long-term performance of a vibration energy harvester can accurately be predicted by computing a weekly average response spectrum.

8.2 LONG-TERM RESPONSE SPECTRA

Weeks of acceleration data were captured at various locations on five different steel bridges in Texas and Oregon over a two-year period. By utilizing the numerical integration techniques outlined in Chapter 5, harvested power potential was computed directly from acceleration time-histories. Typically, response spectra were computed for 5.5-minute acceleration-history samples. Note that a linear system and 10% damping was used because these parameters yield a good balance between bandwidth and peak power, as shown in Chapter 7. This procedure was then repeated for weeks of data in half-hour intervals. For example, 48 5.5-minute response spectra were developed for a single accelerometer location at the Medina River Bridge for one day. The end result of this analysis was 48 individual spectra per day for every accelerometer location instrumented at all five bridges. These short-term spectra were then further processed and averaged together to form hourly, daily, and weekly spectra. Figure 8.1 shows the process of

developing a weekly average response spectrum from short-term spectra for Medina River girder vibration at floor beam 25.

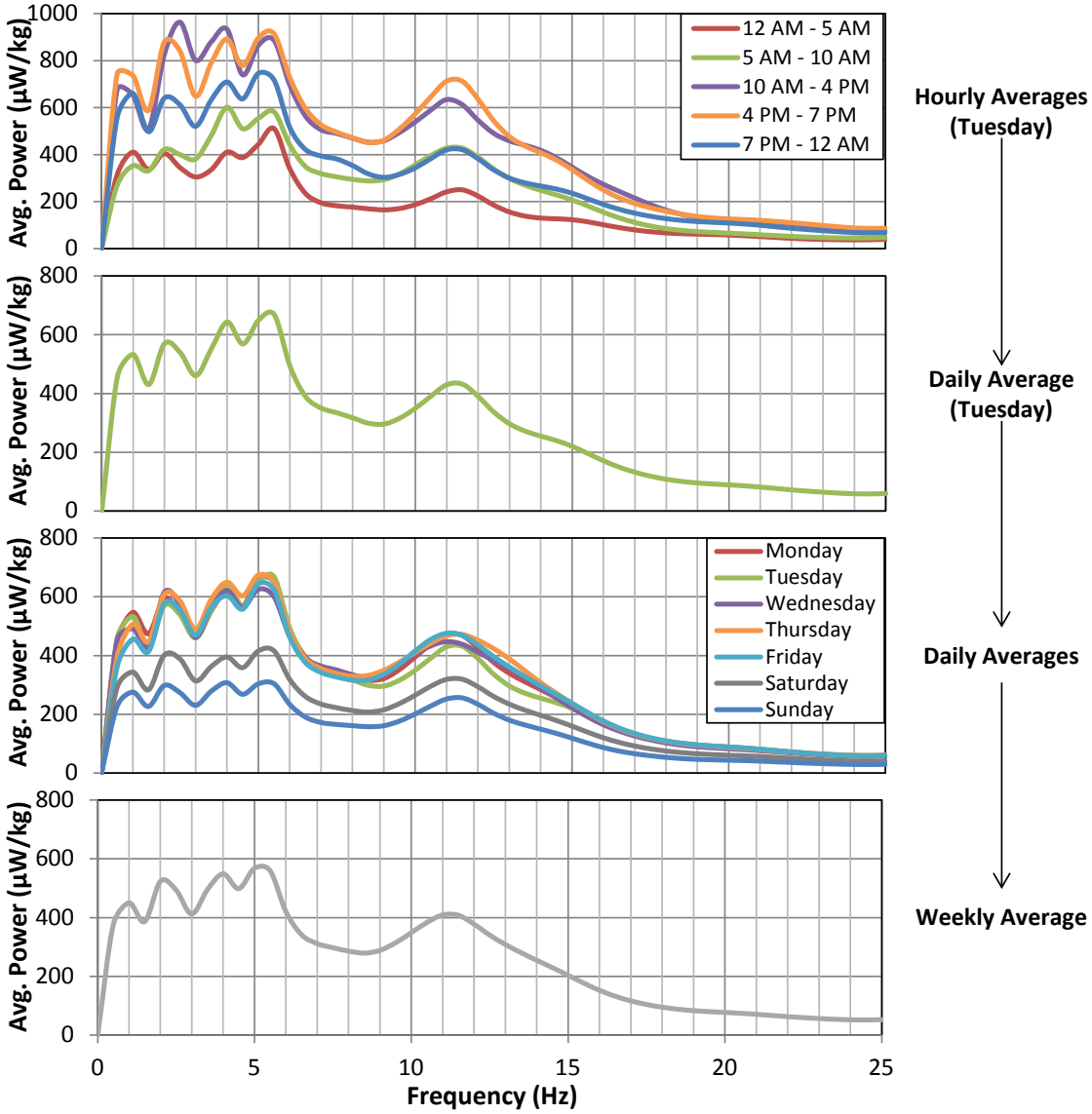

Figure 8.1 Schematic showing development of average weekly response spectrum for east girder vibration at floor beam 25 at the Medina River Bridge.

It can be seen that peak power levels change over a 24-hour day and over a week. During evening rush hour traffic from 4-7 PM, power production at the optimal tuning frequency (5.5 Hz) is nearly double that during 12-5 AM. Moreover, average daily power

for Sunday was significantly less than for the five weekdays. Fortunately for harvester design, the tuning optimal frequencies (2, 4, 5.5 Hz) are the same in all cases. That is because the Medina River Bridge did not show much sensitivity to temperature-induced frequency shifts. Therefore, these three frequencies are very stable in the long-term.

The weekly average results in Figure 8.1 can then be compared to the power requirements of the NI wireless strain node, which is expected to consume a constant 0.5 mW for normal sleep and acquisition activities (Weaver et al., 2011). However, the weekly average response spectrum in Figure 8.1 is in terms of a unit-mass density, and the wireless sensor node power demand is a real, physical value. In order to compare like terms, the estimated input power to the energy harvester (per unit mass) can be scaled according to the mass parameter established by Dierks (2011). These parameters are presented in Table 8.1. Figure 8.2 shows the weekly average power density spectrum developed in Figure 8.1 scaled by 1.454 kg to replicate the harvester fabricated by Dierks. The scaled response spectrum is then compared with the 0.5-mW requirement.

Table 8.1 Key parameters of the UT Austin electromagnetic vibration energy harvester.

Parameter	Value	Unit
Mass	1.454	kg
Frequency	Adjustable	Hz
Mechanical Damping	0.044	-
Electrical Damping	0.0546	-
Total Damping	0.0986	-

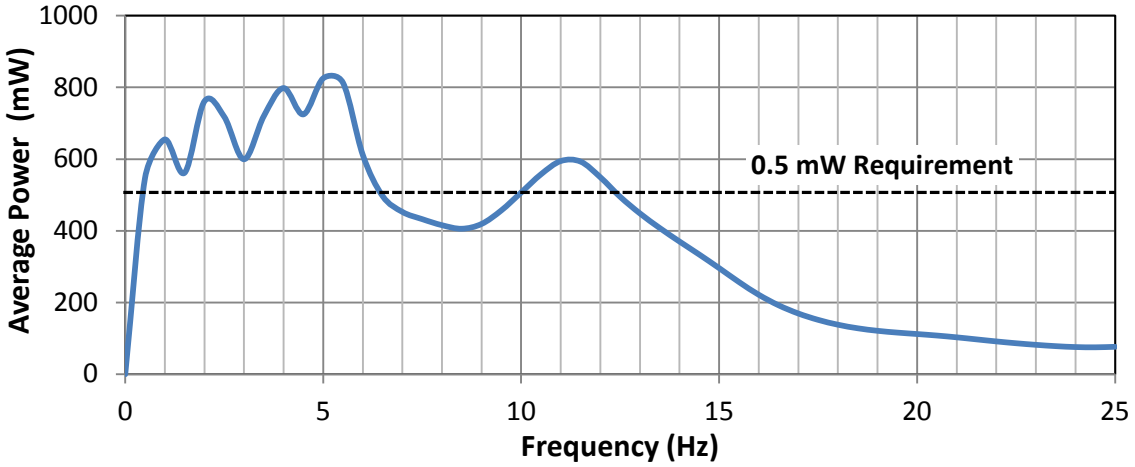

Figure 8.2 Average weekly response spectrum for a vibration energy harvester with a 1.454-kg mass under east girder vibration (floor beam 25) at the Medina River Bridge.

In observing the weekly average response spectrum in Figure 8.2, this location on the bridge (east girder at floor beam 25) supplies sufficient long-term vibrational energy to the node to satisfy its power requirements in a range of tuning frequencies (0.5-6.5 Hz and 10-12.2 Hz). This is still, of course, assuming a perfectly efficient, frictionless system. As discussed in Chapter 1, input power, not output power, is being calculated in this analysis. Therefore, a true comparison of the analytical results and the 0.5-mW power demand of the wireless node requires some knowledge of the harvester efficiency. To estimate the power delivered to the electrical load, some fraction of the input value must be subtracted as frictional losses.

Figure 8.4 shows the same response spectrum in Figure 8.2, but assuming 50% efficiency to account for frictional losses within the harvester. When considering these conversion loss effects, it can be seen that the vibration energy harvester does not output sufficient energy to power a wireless node. However, this is not to say vibration energy harvesting at this bridge is unfeasible for all cases. Given a larger vibrating mass within the harvester, the 0.5-mW demand can be achieved.

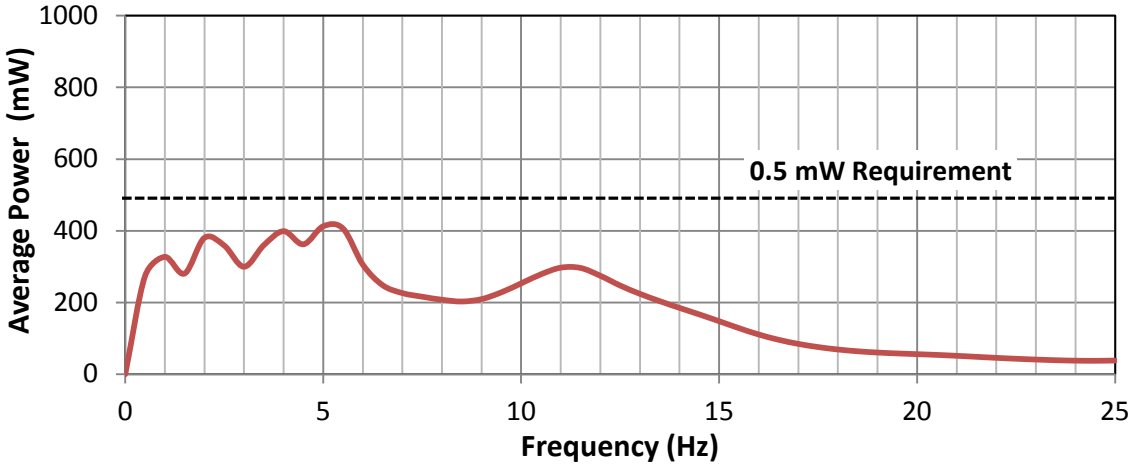

Figure 8.3 Average weekly response spectrum for a 50%-efficient vibration energy harvester with a 1.454-kg mass under east girder vibration (floor beam 25) at the Medina River Bridge.

As previously mentioned, this analysis was performed for every accelerometer location instrumented on each of the five bridges. Figure 8.1, Figure 8.2, and Figure 8.3 just demonstrated one location at the Medina River Bridge. Figure 8.4, on the other hand, compares the long-term results at four representative locations on the Medina River Bridge. Figure 8.4 is plotted in terms of a frictionless, unit mass harvester. Similar calculations can be performed on these acceleration data to match the results of Figure 8.2 and Figure 8.3.

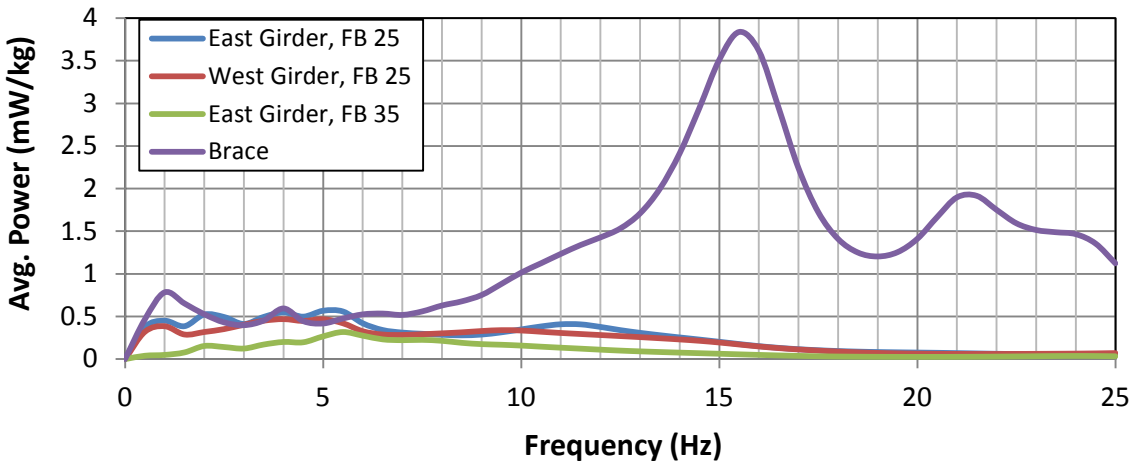

Figure 8.4 Average weekly response spectra for different locations at the Medina River Bridge.

Observe that three of the four locations shown would supply sufficient vibrational power to the node to satisfy the 0.5-mW requirement at one or multiple tuning frequencies. Again, this statement is made assuming a 1-kg moving mass and a frictionless system. Only the east girder at floor beam 35 (in the north anchor span) is below the threshold. But again, this issue can be resolved if a heavier mass is used within the harvester.

Also note that the harvester performs significantly better under brace vibration as opposed to girder vibration, assuming the active damping of the brace caused by the motion of the harvester mass (feedback) is negligible. This is the same result that was shown in Figure 6.10. In summary, Figure 8.1, Figure 8.2, Figure 8.4, and Figure 8.4 show the long-term power predictions for the Medina River Bridge. The subsequent section applies the same analysis so that a comparison between all five bridges can be made.

8.3 Vibration Harvester Feasibility at Instrumented Bridges

The five bridges instrumented in Texas and Oregon are a good representation of typical highway bridges in the United States. By assessing the long-term feasibility of a

vibration energy harvester for these five bridges, general conclusions about its feasibility on most U.S. bridges can be made. Therefore, this section offers long-term power predictions for each of the five bridges studied so that conclusions on harvester feasibility can be made.

8.3.1 Comparison of Instrumented Bridges

For the Medina River, TX-71E, and US-290 bridges, a weekly average response spectrum could be developed because at least seven days of data was acquired there. However, this long-term analysis could not be completed for the Columbia River and I-5/I-205 bridges in Oregon because only a few hours of intermittent data during evening rush hour was collected at each site. Consequently, the results of these two bridges are slightly inflated because the early morning hours are not included. With that in mind, Figure 8.5 shows average response spectra (in terms of a unit-mass density) for midspan girder vibration at each of the five bridges instrumented. Note that the east girder near floor beam 25 was used for the Medina River Bridge data, midspan of the third span for TX-71E, midspan of the second span for US-290, midspan of the fourteenth span for I-5 over the Columbia River, and midspan of the second span for I-5/I-205. Each of these represented the highest energy content for girder vibrations at the five bridges.

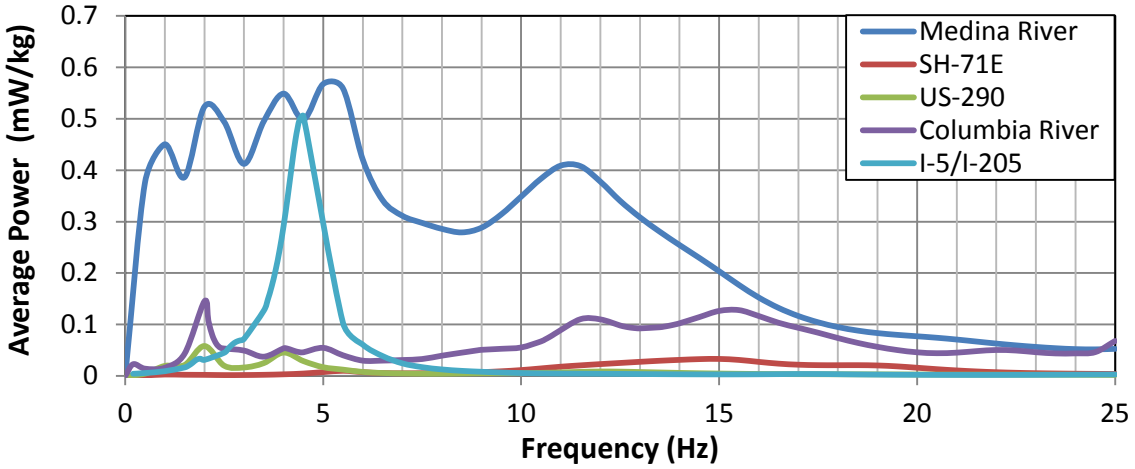

Figure 8.5 Average weekly response spectra for midspan girder vibration at the five different highway bridges.

It can be seen that the Medina River and I-5/I-205 bridges show the most promise. For a frictionless and unit-mass system, both of these bridges supply sufficient vibrational energy to the harvester at one or more tuning frequencies. However, the I-5/I-205 harvester response is extremely narrowband, so any frequency shifts from 4.4 Hz will cause significant power loss. But as discussed in Chapter 7, harvester damping can be adjusted to widen the bandwidth of the response, so that this is less of an issue.

For all five bridges, specifically TX-71E, US-290, and I-5 Columbia River, the harvester could be feasible given a large mass and minimal friction losses. However, both requirements are unlikely given size constraints and physical limits of the harvester. The mass can only be so heavy within the harvester housing, and a totally frictionless system is impossible. Therefore, it can be concluded that the Medina River and I-5/I-205 bridges are the only two feasible bridges for such a harvester.

Figure 8.5 explained the performance under girder vibration, but when the results of the lateral brace analysis at the Medina River and I-5 Columbia River bridges are included, three of the five bridges now appear feasible (Figure 8.6). The Medina River and I-5/I-205 bridges, along with the Columbia River Bridge braces, supply adequate

vibrational energy to the harvester to power a wireless node. In general, the energy content of these brace vibrations are substantially higher than girder vibrations due to the reasons explained in Chapter 6. Note that the long-term response spectra for the braces did consider the weight of the harvester, so that the results are not grossly overestimated.

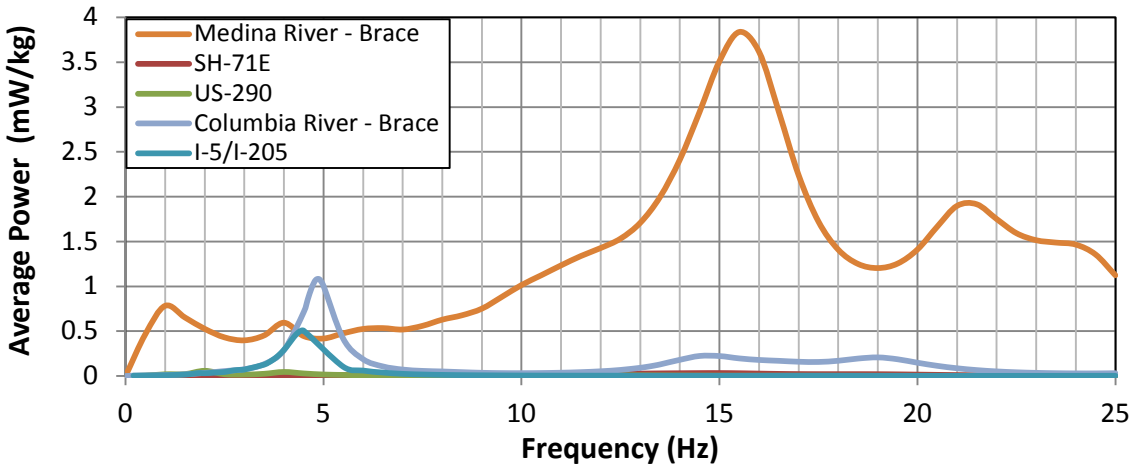

Figure 8.6 Average weekly response spectra for different locations including brace vibration at the five different highway bridges.

8.3.2 Long-Term Feasibility Assessment of Instrumented Bridges

From the power density results provided in Figure 8.6, it can be noted that the TX-71E and US-290 bridges simply do not vibrate enough to supply sufficient energy to a wireless node. The TX-71E Bridge is a short-span, multi-girder bridge that does not carry a large percentage of truck traffic. As a result, vibrational energy is extremely low compared to the other bridges. The only way a harvester would be feasible at this location is to use a very heavy (and probably unrealistic) mass. Unfortunately, many modern highway bridges are similar to this bridge, meaning vibration energy harvesting is likely not feasible for a majority of bridges in the United States.

The US-290 Bridge, on the other hand, has long spans, but high-speed truck traffic volume is low. In other words, a single truck event inputs a substantial amount of energy to a vibration harvester, but high power production is not sustained over long

periods of time. Again, a vibration energy harvester would only be feasible with a high vibrating mass.

The I-5/I-205 Bridge in Oregon, as mentioned in Chapter 3, is a trapezoidal box girder bridge like the US-290. When comparing the response spectra of the bridges, the I-5/I-205 clearly provides more vibrational energy to the harvester than the US-290. This large disparity in energy content can be attributed to age, increased flexibility, more frequent truck traffic, and substructure geometry. For a harvester to be a feasible power solution at this site, the mass would need to be greater than 1 kg to compensate for frictional losses because the 1-kg, frictionless system barely exceeds 0.5 mW as is. Damping could also be increased to widen the bandwidth response of the harvester. Ultimately, the 0.5-mW power requirement could reasonably be met at this site with these few minor adjustments.

The girders of the I-5 Bridge over the Columbia River do not sustain high enough power levels to continuously power a wireless sensor node (Figure 8.5). However, the long, slender braces do provide a potential improved vibration source (Figure 8.6). Truss bridges like the I-5 are not typical highway bridges. Therefore, long lateral braces like those instrumented are not often found in common highway bridge construction. So although the power content of these types of braces may be sufficient to power a wireless node, this does not necessarily apply to most U.S. highway bridges.

Lastly, the I-35 Bridge over Medina River is the ideal candidate for a vibration energy harvester. Both brace vibration and girder vibration, especially near deck discontinuities, supply adequate energy to the harvester to power a wireless node. Bandwidth response of the harvester is also wide because the excitation source is broadband. The increased age, flexibility, and truck traffic of this bridge allows for fairly regular energetic vibrations.

8.3.3 General Conclusions about Harvester Feasibility

Likely candidates for a vibration energy harvester are flexible, long-span bridges that experience heavy truck traffic. Newer, stiffer highway bridges and/or short-span bridges, where vibrations are typically low-amplitude and narrowband, will not likely supply enough energy to power a node. Older bridges such as the Medina River Bridge, on the other hand, are likely candidates. Fortunately, these older bridges are generally the primary targets for wireless sensor network implementation. Although only three (I-35 Medina River, I-5 Columbia River, and I-5/I-205 Interchange) of the five bridges instrumented supply sufficient vibrational energy to power an NI wireless node, these same three bridges are the most likely candidates for an integrated wireless monitoring system. For example, the newer US-290 Bridge in Austin may not vibrate enough to power a wireless sensor node, but such a monitoring system is not likely to be used on the bridge anyway.

Ultimately, feasibility must be assessed on a case-by-case basis. It may be discovered that vibration energy harvesting is not a feasible power solution to the majority of highway steel bridges (short-span and multi-girder) in the U.S. But based on the results of this research, many of the bridges suited for wireless monitoring are the same ones that vibrate excessively to traffic loads. So in the right situation, vibration energy harvesting is feasible.

8.4 CHAPTER SUMMARY

In this chapter, long-term evaluation of steel bridge vibrations was discussed. A consistent evaluation approach, weekly average response spectra, was introduced. From this analysis, the feasibility of vibration energy harvesting at the five instrumented bridges in Texas and Oregon was assessed. It was determined that three of the five bridges studied will likely supply enough long-term vibrational energy to power an NI WSN-3214 node. And because these five bridges represent a large portion of highway steel bridges in the United States, general conclusions about the feasibility of this system

nationwide were made. Chapter 9 provides a summary of the findings and recommendations for future feasibility studies.

CHAPTER 9
Conclusions and Recommendations

Chapter 9 summarizes the results of the research, which was conducted as a part of NIST research project entitled, “Development of Rapid, Reliable and Economic Methods for Inspection and Monitoring of Highway Bridges.” Additionally, the major conclusions from this two-year study will be discussed, as well as final recommendations for future feasibility studies.

9.1 SUMMARY

Many bridges in the US are nearing the end of their intended service life. Following the collapse of the IH35 bridge in Minnesota, the US Legislature is considering proposals aimed at increasing the inspection criteria for many bridges. With the aging infrastructure and potential increased inspection requirements, bridge owners will likely struggle to obtain the necessary funding and resources to maintain its infrastructure. Wireless monitoring techniques are being developed to mitigate the costs and time associated with inspections. Although not completely replacing visual inspections, WSNs will complement the current practice by providing continuous, real-time evaluation of damaged structures to bridge owners. However, for a WSN to be economically feasible, a system with a ten-year service life that is independent of the power grid is envisioned. Therefore, a constant source of energy must be harvested to power the system for 10 years or more.

Traffic-induced vibration energy is a proposed source because it is continuous, as long as truck traffic regularly crosses the bridge. Although typical vibration harvesters have power densities orders of magnitude less than solar panels, these systems are localized such that they can be positioned directly next to a wireless node. However, a major disadvantage to harvesting bridge vibrations as a source of energy is that the dynamic response of a bridge to a crossing truck is highly variable depending on the time

of day, ambient temperature, and traffic conditions. The major focus of this thesis was to determine the feasibility of a vibration energy harvester at a given bridge with strong consideration to the variability in the energy source itself (the bridge). Two fields of expertise, dynamic monitoring of bridges and vibration energy harvesting, were effectively united in this study.

Spectral analysis, which is typically used to describe the modal characteristics of a structure, has limitations. It yields only the relative magnitudes and cannot quantify the energy of bridge vibrations. Consequently, an analytical model was developed to not only determine dominant modes of vibration, but also the amount of mechanical energy generated from those vibrations in the form of a response spectrum. This model, which utilizes Newmark-Beta integration and Newton-Raphson iteration techniques, is able to estimate the harvested power given a sample acceleration history of field data. In other words, the feasibility of bridge vibrations as a source of energy can be evaluated directly from the data acquired from accelerometers.

Five bridges in Texas and Oregon (I-35 over Medina River, US-290 Connector, TX-71E over US-183, I-5 over Columbia River, and I-5/I-205 Overpass) were identified and instrumented with an array of accelerometers. These five bridges are fairly representative of common highway bridges in the U.S. Three are considered fracture-critical, which are of particular interest for wireless monitoring. Therefore, the results of this study can potentially be applied to other structures throughout the world. For example, the conclusions derived for the TX-71E Bridge may apply to a similar bridge that experiences similar truck traffic.

Data from each bridge were processed through the analytical routine. And from this, the variability in the bridge response, namely bridge configuration, temperature, truck traffic volume, and spatial effects, could be quantified in terms of power input to the vibration energy harvester. In particular, the effects of frequency shifts on harvester performance (bandwidth and peak power) were evaluated. It was also seen that the two major performance metrics can also be adjusted at the harvester level as to maximize

efficiency of the system for a given vibration source. Harvester optimization studies were performed using response spectrum analysis, which introduced the effects of damping and Duffing-type nonlinearities to the system.

After characterizing the bridge and harvester vibrations for short-duration acceleration histories, a long-term feasibility assessment was undertaken. Weekly average response spectra were shown to be an effective way to estimate long-term performance of a harvester. In performing these calculations on data for five unique bridges, general conclusions about the feasibility of this technology are made.

The results of this study provide useful insight on the design of an electromagnetic energy harvester, especially the one designed and fabricated by Dierks (2011). Important parameters such as tuning frequency and damping can be adjusted based on response spectrum analysis, and the efficiency of the harvester can also be evaluated given the upper-bound predictions provided by said analysis.

9.2 CONCLUSIONS

The following are general conclusions developed based on the findings of this research. These are the most important takeaways from this thesis:

1. ***Spectral analysis, although important, has certain limitations when analyzing bridge vibrational energy that response spectrum analysis does not.*** Spectral analysis reveals the dominant frequencies of the source and their relative amplitudes. It does not, however, indicate real, physical amplitudes. Response spectrum analyses, on the other hand, can be used to determine the optimal tuning frequencies of a harvester and the estimated vibration energy given a raw acceleration history. It should be noted that spectral analyses are still an extremely useful tool for energy harvesting applications. The tuning frequency can be established based purely on spectral analysis because it is known that the tuning frequency of the harvester and the bridge frequency should be very close as to maximize power production. So verifying the dominant bridge frequencies is

valuable, but no knowledge on vibration energy can be obtained with spectral analysis alone.

2. ***Changing bridge configurations and stiffness can affect the frequency characteristics of the structure.*** Several researchers in the literature have documented significant shifts in frequency due to changes in bridge conditions. Although discrete shifts on frequencies were not observed in the data, broadband excitations due to these effects were. The vibrations at the Medina River Bridge were substantially more wideband than the other four bridges. It is theorized that the increased age and flexibility of the bridge has made it more susceptible to these time-dependent changes.
3. ***Ambient temperature can also affect the frequency characteristics of a bridge.*** A decreasing, linear trend between ambient temperature and the second fundamental frequency was observed for the TX-71E Bridge data. And, in total, there was an 8% difference between maximum and minimum frequencies for that mode of vibration. Similar trends, though, were not seen in the data of the other four bridges. It can be concluded that some frequencies are more affected by temperature fluctuations than others, and the effects vary among bridges. But these effects, even if only minor, should still be considered in the design of a vibration energy harvester.
4. ***Frequency shifts in the vibrating source can result in substantial power losses in the harvester.*** By assuming a maximum 8% variation in bridge frequencies, it was shown that a 35% reduction in harvested peak power at the US-290 Bridge could occur. The US-290 Bridge has very narrowband excitations, so the response of the harvester is also narrowband. This reduction is less severe at the other bridges because the excitations are more broadband, especially at the Medina River Bridge. As a result, only a 5% reduction was estimated at the Medina River Bridge with an 8% variation in bridge frequency. But for newer, stiffer bridges

where vibration frequencies are well-defined and the frequency content is narrowband, these shifts can be a major concern.

5. ***Harvester production is highly dependent on the current truck traffic patterns.*** A roughly 700% difference was estimated between harvester power production during early morning hours and evening rush hour traffic. Because acceleration amplitudes are directly related to the performance of the harvester, more truck-induced excitations means more vibrational power. Therefore, these early morning hours must be considered in the design of a harvester. Otherwise, the analysis will severely overestimate the long-term harvester production at a given bridge.
6. ***The frequencies contributing to the vibration response of a bridge are location-specific.*** Although the modes of vibration are constant across the entire bridge, the magnitude and intensity of each mode varies along the length. In general, displacement is highest at midspan of a beam, so accelerations are expected to be highest there as well. Also, the lower modes generally dominate near midspan and higher modes near the support based on basic vibration theory. These trends were also demonstrated in the Medina River Bridge field data through spatial response spectrum plots.
7. ***The optimal location to position a harvester is likely on a brace or near a deck discontinuity.*** The highest vibrational energy content, especially at the Medina River Bridge, was discovered at the pin-hanger assembly below the deck joint or on long, slender braces. The impact of a truck due to deck discontinuities tends to excite the bridge more. A similar result could be achieved with a rough, unpaved road surface. And braces that tend to be slender with low damping characteristics are more likely to experience larger vibrations than the girder to which they are connected. However, long slender braces are not frequently encountered on all bridges. If neither a deck discontinuity nor a long, slender brace exist on a bridge, the next best location for a harvester would be at midspan of a longitudinal girder.

8. ***The weight of the harvester can significantly affect the vibration of a slender brace, and must be considered in analysis.*** One of the major assumptions made in the development of the analytical, SDOF model was that the motion of the damped mass would not interrupt the motion of the source. The UT harvester weighs approximately 13-lbs. and the weight on a slender brace violates this assumption. It was shown that neglecting the weight of the harvester in response spectrum analysis of brace vibration can overestimate production by a factor of eight and change the natural frequency up to 21%. Therefore, this analysis is only valid if some considerations to the harvester mass are made. In this case, a 13-lb weight was clamped to the brace during instrumentation to simulate the effects of an additional weight. Additionally, it was assumed that feedback caused by the vibration of the harvester mass would not dampen the vibration of the brace substantially. In reality, this could negatively affect the performance of the energy harvester.
9. ***Harvester damping can be designed so that power losses due to frequency shifts (caused by changing bridge conditions and/or ambient temperature fluctuations) are less severe.*** Although minimal damping yields maximum power, bandwidth is an equally important measure of harvester performance. Narrowband peaks should be avoided in energy harvesting applications because the harvester response is too dependent on a limited frequency that may change over time. Increased damping lowers power peaks and widens the bandwidth of a harvester. Ideally, a balance between bandwidth and peak power must be achieved. For narrowband excitations such as those measured on the US-290 Bridge, increased damping should perhaps be used to flatten out the response of the harvester. For broadband excitations like the Medina River Bridge, the response is already sufficiently wide, so damping could potentially be reduced to increase peak power.

10. ***Spring nonlinearity improves harvester performance under sinusoidal excitations, but not under ambient bridge vibrations.*** When response spectrum analysis was performed on a constant-frequency signal with constant amplitude, spring nonlinearity (particularly hardening springs) yielded significant improvement in both harvester metrics: peak power and bandwidth. However, when applied to the ambient field data, the advantages were less noticeable. This is because the large displacements required to push the spring into the nonlinear range were not sustained over time under ambient bridge vibrations. Also, the impact of spring nonlinearity is smaller on stiffer springs, when the bridge frequencies are above 7 Hz, which is the case for several of the bridges studied.
11. ***Overall, a linear harvester designed for 10% total damping is typically a good design.*** Based on the harvester optimization studies, it was determined that on average, a linear system with 10%-damping results in a good combination of bandwidth and peak power. Note that these parameters could be modified more precisely on a case-by-case basis, if desired. But because these parameters proved efficient for all five bridges instrumented, they were used in the long-term assessment of the vibration energy harvester.
12. ***Of the five instrumented bridges, only three show promise for a vibration energy harvester.*** Only the brace vibration at the Medina River and Columbia River bridges and the girder vibration (near deck discontinuities or near midspan) at the Medina River and I-5/I-205 bridges show promise for this vibration energy harvesting technology given realistic mass and damping parameters. Based on the results of the long-term response spectrum analysis, these vibrational sources provided enough energy to continuously power a NI wireless node.
13. ***In the right situation, vibration energy harvesting is a feasible solution.*** Likely candidates for a vibration energy harvester are flexible, long-span bridges that carry heavy truck traffic. Newer, stiffer highway bridges and/or short-span bridges, where vibrations are typically low-amplitude and narrowband, will not

likely supply adequate energy to continuously power a node. Fortunately, the primary target of the wireless sensor network are older bridges for which fatigue or deterioration are a major concern between periodic inspections. Although only three (I-35 Medina River, I-5 Columbia River, and I-5/I-205 Interchange) of the five bridges supply the required 0.5 mW of constant power to a node, these bridges are also the most likely candidate for an integrated wireless monitoring system. It may be discovered that vibration energy harvesting is not a feasible power solution for the majority of highway steel bridges (short-span and multi-girder) in the U.S. But based on the results of this research, many of the bridges suited for wireless monitoring likely experience significant vibrations due to traffic loads.

9.3 RECOMMENDATIONS

Despite the information and knowledge gained from the results of this research, assessing the vibrations of a particular bridge as a feasible source of energy is still a case-by-case exercise. No bridge is exactly the same as the five studied in this thesis, and neither are the traffic patterns. Therefore, if an engineer is seeking to implement vibration energy harvesters on a wireless monitoring system, a few measurements and calculations should be performed. There are two ways to obtain the necessary information on the dynamic response of the bridge: through field instrumentation and through finite element modeling.

The first of the two options was the major focus of this thesis. At a minimum, the bridge of interest should be instrumented with a few accelerometers. Note that a dense array of sensors like that used at the Medina River Bridge is not necessary for a quick, cursory assessment of the bridge vibrations. As previously concluded, those sensors are best suited near deck discontinuities or long, slender braces where most vibrational energy content is concentrated. If neither is present at a bridge, the next best location is at

midspan of the longitudinal girders. It is also important that a few days of data be acquired at the site such that the low-traffic times can be evaluated as well.

Moreover, the dynamic response of a bridge can be modeled in a finite element (FE) program. Like time-domain and frequency-domain analysis of field data, finite element software can predict the modal characteristics and resulting acceleration amplitudes of a bridge to a specified truck excitation. Successful FE models of highway bridges have been documented in the literature, ranging from complex to simple models. Halling et al. (2004), Kwasniewski et al. (2006), Nassif et al. (2003), and Paultre et al. (1995) have all validated FE models with the results of field instrumentation. In particular, Samaras (2012) has modeled the TX-71E and Medina River bridges and the corresponding moving truck loads in SAP2000 and ANSYS, respectively. Initial results of this study have shown good agreement between the field data and the analytical results. In all computer analysis cases though, some field instrumentation is necessary so that the model can be verified.

With the dynamic behavior of the bridge understood, whether through field data only or through FE modeling, there are two methods to predicting harvested vibrational power and to assessing the feasibility of the harvester system. First, if the harvester is already designed and fabricated, it can be physically tested on the bridge or a shaker table that can simulate bridge vibration signals. Rather than analytically assessing the feasibility of the harvester, the output power can be directly computed at different tuning frequencies. If, however, the decision to design or purchase a harvester depends on the analytical results first, the response spectrum approach outlined in this thesis can be used. The performance of the harvester can be estimated from raw acceleration data and compared to the power requirements of the wireless node. In summary, assessing the feasibility of a vibrating bridge as an energy source, at a minimum, requires short-term field instrumentation, some signal processing, and analytical modeling.

References

Alampalli, S., Fu, G., & Dillion, E. (1995). *Measuring bridge vibration for detection of structural damage.* Final Report for Research Project 208-1 of Transportation Research and Development Bureau.

Barton, D., Burrow, S., & Clare, R. (2010). Energy harvesting from vibrations with a nonlinear oscillator. *Journal of Vibration and Acoustics, 132,* 1-7.

Brownjohn, J., Pavic, A., Carden, P., & Middleton, C. (2006). *Modal testing of Tamar suspension bridge.* University of Sheffield Report.

Chowdhury, I., & Dasgupta, S. (2003). Retrieved June 16, 2011, from Computation of Rayleigh damping coefficients for large systems: http://www.ejge.com/2003/Ppr0318/Ppr0318.pdf

Cornwell, P., Farrar, C., Doebling, S., & Sohn, H. (1999). Environmental variability of modal properties. *Experimental Techniques*, 45-48.

Cottone, F. (2007). *Nonlinear piezoelectric generators for vibration energy harvesting.* PhD Dissertation, Universita Degli Studi di Perugia.

Cottone, F. (2011). *Introduction to vibration energy harvesting.* NiPS Energy Harvesting Summer School Lecture.

Crossbow Technology. (2011). *CXL-GP Accelerometer Series Datasheet*. Retrieved January 22, 2011, from http://www.xbow.com/

Crossbow Technology. (2011). *LF Accelerometer Series Datasheet*. Retrieved January 22, 2011, from http://www.xbow.com/

Daqaq, M. (2010). Response of uni-modal doffing-type harvesters to random forced excitations. *Journal of Sound and Vibration, 329,* 3621-3631.

Dierks, E. (2011). *Design of an electromagnetic vibration energy harvester for structural health monitoring of bridges employing wireless sensor networks.* Master's Thesis, The University of Texas at Austin.

Doebling, S., Farrar, C., & Cornwell, P. (1997). Effects of measurement statistics on the detection of damage in the Alamosa Canyon bridge. *15th International Modal Analysis Conference*, (pp. 919-929). Orlando, Florida.

Farrar, C., Doebling, S., Cornwell, P., & Straser, E. (1997). Variability of modal parameters measured on the Alamosa Canyon bridge. *15th International Modal Analysis Conference*, (pp. 1-8). Orlando, Florida.

Fasl, J. (2011). Development of a wireless monitoring system for fracture-critical bridges. *SPIE 7983.* San Diego, CA.

Federal Highway Administration. (2010). *Deficient bridges by state and highway system*. Retrieved February 14, 2011, from http://www.fhwa.dot.gov/bridge/nbi/defbr10.cfm

Galchev, T., Aktakka, E., Kim, H., & Najafi, W. (2010). A piezoelectric frequency-increased power generator for scavenging low-frequency ambient vibrations. *IEEE 23rd International Conference on Micro Electro Mechanical Systems (MEMS)*, (pp. 1203-1206). Wanchai, Hong Kong.

Galchev, T., McCullagh, J., Peterson, R., & Najafi, K. (2011). Harvesting traffic-induced bridge vibrations. *16th International Actuators, Solid-State Sensors and Microsystems Conference (Transducers)*, (pp. 1661-1664). Beijing, China.

Ghanaat, Y., Hall, R., & Redpath, B. (2000). Measurement and computation of dynamic response of arch dams including interaction effects. *Journal of Seismology and Earthquake Engineering, 2*(3), 1-19.

Google Maps. (2011). Retrieved 2011, from http://maps.google.com/

Halling, M., Su, M., & Zeng, Q. (2004). Dynamic health monitoring and modeling of a full-scale bridge. *2004 Structures Congress*, (pp. 1-7). Nashville, Tennessee.

Hrovat, K. (2004). *Analysis techniques for vibratory data.* MEIT-2004 Presentation, Section 13.

Infmetry. (2011). Retrieved December 13, 2011, from Faraday Flashlight: http://www.infmetry.com/home-decor/lighting/forever-last-faraday-shark-flashlight

Kwasniewski, L., Wekenzer, J., Roufa, G., Li, H., Ducher, J., & J, M. (2006). Experimental evaluation of dynamic effects for a selected highway bridge. *Journal of Constructed Facilities, 20*(3), 253-260.

Lauzon, R., & DeWolf, J. (2006). Ambient vibration monitoring of a highway bridge undergoing a destructive test. *Journal of Bridge Engineering, 11*(5), 1-29.

Lee, C., Stamp, D., Kapania, N., & Mur-Miranda, J. (2010). Harvesting vibration energy using nonlinear oscillations of an electromagnetic inductor. *SPIE 7683 Energy Harvesting and Storage: Materials, Devices, and Applications.* Orlando, Florida.

Li, H., & Pillay, P. (2008). A methodology to design linear generators for energy conversion of ambient vibrations. *Industry Application Society Annual Meeting*, (pp. 1-8).

Li, J., Su, M., & Fan, L. (2003). Natural frequency of railway girder bridges under vehicle loads. *Journal of Bridge Engineering, 8*(4), 199-203.

Lloyd, G., Wang, M., & Singh, V. (2003). Observed variations of mode frequencies of a prestressed concrete bridge with temperature. *Proceedings of Condition Monitoring of Materials and Structures*, (pp. 179-189). Austin, TX.

Luscher, D., Brownjohn, J., Sohn, H., & Farrar, C. (2001). Modal parameter extraction of Z24 bridge data. *19th International Modal Analysis Conference*, (pp. 1-7).

Marzencki, M., Defosseux, M., & Basrour, S. (2009). MEMS vibration energy harvesting devices with passive resonance frequency adaptation capability. *Journal of Microelectromechancial Systems, 18*(6), 1444-1453.

Mazurek, D., & DeWolf, G. (1990). Experimental study of bridge monitoring technique. *Journal of Structural Engineering, 16*(9), 2532-2549.

McEvoy, T. (2011). *Wind energy harvesting for bridge health monitoring.* Master's Thesis, University of Texas at Austin.

Minnesota Department of Transportation. (2008). *Economic impacts of the I-35W bridge collapse*. Retrieved October 27, 2011, from http://www.dot.state.mn.us/i35wbridge/rebuild/municipal-consent/economic-impact.pdf

Moore, M., Rolander, D., Graybeal, B., & Phares, B. (2001). *Highway bridge inspection: state-of-the-practice survey*. Federal Highway Administration, Turner-Fairbank Highway Research Center.

Nassif, H., Liu, M., & Ertekin, O. (2003). Model validation of bridge-road-vehicle dynamic interaction system. *Journal of Bridge Engineering, 8*(2), 112-120.

National Bridge Inventory. (2008). *Age distribution of highway bridges in the US*. Retrieved October 27, 2011, from http://nationalbridges.com/

National Instruments. (2011). *NI WSN-3214 (Programmable)*. Retrieved November 3, 2011, from http://sine.ni.com/nips/cds/view/p/lang/en/nid/210012

Nguyen, D., & Halvorsen, E. (2010). Analysis of vibration energy harvesters utilizing a variety of nonlinear springs. *10th International Workshop on Micro and Nanotechnology for Power Generation and Energy Conversion Applications.* Leuven, Belgium.

Olson, D. (2008). *I-35W engineer answers concerns about the new bridge*. Retrieved October 27, 2011, from MPR News: http://minnesota.publicradio.org/display/web/2008/07/30/issues_2004/

Paultre, P., Proulx, J., & Talbot, M. (1995). Dynamic testing procedures for highway bridges using traffic loads. *Journal of Structural Engineering, 121*(2), 1-15.

PCB Piezotronics. (2011). *PCB337A26 Accelerometer Datasheet*. Retrieved November 17, 2011, from http://www.pcb.com/index.php

Peeters, B., Maeck, J., & DeRoeck, G. (2000). Dynamic monitoring of the Z-24 bridge: separating temperature effects from damage. *European COST F3 Conference on System Identification and Structural Health Monitoring*, (pp. 377-386). Madrid, Spain.

Perpetuum. (2011). Retrieved December 13, 2011, from PMG FSH Free Standing Harvester: http://www.perpetuum.com/fsh.asp

Ren, J., Su, M., & Zeng, Q. (2010). Vertical load-carrying natural frequency of railway continuous steel truss bridges. *Seventh International Conference on Traffic and Transportation Studies*, (pp. 1387-1398). Kunming, China.

Roundy, S. (2003). *Energy scavenging for wireless sensor nodes with a focus on vibration to electricity conversion.* PhD Dissertation, University of California, Berkeley.

Roundy, S., Wright, P., & Rabaey, J. (2003). A study of low level vibrations as a power source for wireless sensor nodes. *Computer Communications, 26*, 1131-1144.

Samaras, V. (Expected 2013). *Title TBD.* PhD Dissertation, The University of Texas at Austin.

Sazonov, E., Li, H., Curry, D., & Pillay, P. (2010). Self-powered sensors for monitoring of highway bridges. *IEEE Sensors Journal, 9*(11), 1422-1429.

Sohn, H. (2007). Effects of environmental and operational variability on structural health monitoring. *Philosophical Transactions of the Royal Society A, 365*, 539-560.

Wahab, M., & DeRoeck, G. (1997). Effect of temperature on dynamic system parameters of a highway bridge. *Structural Engineering International, 4*, 266-270.

Weaver, J., Wood, K., & Crawford, R. (2011). Exploring innovation opportunities in energy harvesting using functional modeling approaches. *ASME International Design Engineering Technical Conferences.* Washington, DC.

Wikipedia. (2011). Retrieved 2011, from http://wikipedia.com/

Williams, C. B., & Yates, R. (1995). Analysis of a micro-electric generator for microsystems. *The 8th International Conference on Solid-State Sensors and Actuators, and Eurosensors IX*, (pp. 369-372). Stockholm, Sweden.

Williams, C. B., Pavic, A., Crouch, R., & Woods, R. (1997). Feasibility study of vibration-electric generator for bridge vibration sensors. *IMAC-XVI*, (pp. 1111-1117).

Yun, J., Patel, S., Reynolds, M., & Abowd, G. (2008). A quantitative investigation of inertial power harvesting for human-powered devices. *Tenth International Conference on Ubiquitous Computing*, (pp. 74-83). Seoul, South Korea.

Zhao, J., & DeWolf, J. (2002). Dynamic monitoring of steel girder highway bridge. *Journal of Bridge Engineering, 7*(6), 350-356.